A RATIONALLY-DESIGNED FLUORESCENCE COMPETITIVE BINDING ASSAY FOR CONTINUOUS GLUCOSE MONITORING APPLICATIONS

A Dissertation

by

BRIAN MICHAEL CUMMINS

Submitted to the Office of Graduate and Professional Studies of
Texas A&M University
in partial fulfillment of the requirements for the degree of

DOCTOR OF PHILOSOPHY

Chair of Committee,	Gerard L. Coté
Committee Members,	Michael J. McShane
	Kenith E. Meissner
	Michael V. Pishko
Head of Department,	Gerard L. Coté

May 2014

Major Subject: Biomedical Engineering

ABSTRACT

Improved continuous glucose monitoring devices have the potential to increase patient compliance and improve the management of diabetes. One type of sensing chemistry that has been recognized as having significant amount of potential is based on the protein, Concanavalin A. However, to date, this assay has continually shown problems with sensitivity, stability, and reversibility in free solution. This work uses rational design to generate a new version of the competitive binding assay that can allow for its full potential to be shown.

The first part of this work uses a glycosylated dendrimer as the competing ligand in the assay. This assay is optimized with regards to its fluorescence response and encapsulated within microporated microspheres to allow for the glucose-dependent aggregative response to occur. The exact mechanism of this assay was explored, and the stability issues were identified to be a direct result of the electrostatic interactions and multivalent presentation of sugar residues.

The second part of this work generated a model for the unique recognition and transduction mechanisms of the ConA-based assay, in an attempt to generate maps to identify desirable qualities to generate an optimized assay. This model was validated with experimental data, and used to optimize a ConA-based assay to track glucose concentrations with anisotropy. They were also used to explain the problems with previous ConA-based approaches. The core trimannose of N-linked glycans was recognized as a high-affinity ligand that achieved the required affinities without leading

to the aggregation that has caused previous assays to fail. A smartly-designed fluorescent ligand was generated based on this core trimannose to achieve the desired qualities as defined by the previous models, and it was used in a ConA-based assay to track glucose concentrations with anisotropy and Förster Resonance Energy Transfer (FRET). Finally, in an attempt to generate a cost-effective smartly-designed fluorescent ligand that could be encapsulated with a size exclusion membrane, the glycated fraction of ovalbumin was fluorescently labeled and used in a ConA-based assay. This work proves that the smartly-designed fluorescent ligand concept can overcome the problems of previous ConA-based assays, and such an assay is expected to be capable of translation to practical applications.

DEDICATION

In memory and honor of my cousin Derrick

ACKNOWLEDGEMENTS

First and foremost, I would like to thank my committee chair, Dr. Gerard Coté, for his guidance and support throughout the course of this research. Thank you for the opportunity to grow as an individual and a researcher. I could not have asked for a better mentor and advisor over the last several years.

Thanks to my committee members, Dr. Michael McShane, Dr. Michael Pishko, and Dr. Kenith Meissner, for their support and counsel along the way.

To Dr. Gyula Vigh – thanks for your willingness to work with me to help me get where I wanted to go and showing me the power of a good analogy along the way.

Thanks to the Whitaker Foundation and the University of Strathclyde for the incredible international summer research experience. Dr. Birch & Dr. Graham – thank you for letting me join your labs and experience a summer in Glasgow.

Thanks to Texas A&M University for being a home away from home, for the resources all across campus, and for the spirit that makes this university great.

To my friends in the Optical Biosensing Lab and the Biomedical Engineering Department as a whole, thank you for making graduate school such a great experience. Specifically, I'd like to acknowledge Matt, Tony, Bilal, Dustin, and Ryan – I am so glad that I got to go through graduate school with you guys.

Finally, I would like to thank my wife, Kelley, and our families for their unconditional love and support. Thanks for always being there.

NOMENCLATURE

%CLB	Percent of the Competing Ligand Bound to ConA
ADOTA	Azadioxatriangulenium
ADOTA-OVA	ADOTA-Labeled Glycated Ovalbumin
AF	Alexa Fluor
APTS	8-Aminopyrene-1,3,6-Trisulfonic Acid
APTS-MT	APTS-Labeled Mannotetraose
CGM	Continuous Glucose Monitoring
CL	Competing Ligand
ConA	Concanavalin A
FA	Fluorescence Anisotropy
FITC	Fluorescein Isothiocyanate
FRET	Förster Resonance Energy Transfer
G2	Generation Two
G4	Generation Four
MARD	Mean Absolute Relative Difference
MT	Mannotetraose
MW	Molecular Weight
NTA	Nanosight Tracking Analysis
PEG	Poly(Ethylene Glycol)
PET	Photoinduced Electron Transfer

PLL	Poly-L-Lysine
RQY	Relative Quantum Yield
SFL	Smartly-Designed Fluorescent Ligand
TRITC	Tetramethylrhodamine Isothiocyanate

TABLE OF CONTENTS

Page

LIST OF FIGURES

LIST OF TABLES

Page

CHAPTER I

INTRODUCTION AND BACKGROUND[*]

Glucose Metabolism

Glucose is a simple 6-carbon sugar that is used as an energy source for most organisms.[1] Glucose is an ideal reducing monosaccharide for this role due to its lower tendency to react non-enzymatically with the amino groups that are commonly found on proteins. In solution, glucose primarily exists in cyclic form with less than 0.1% of the glucose molecules in open chain form. Other monosaccharides exist in the acyclic form at a higher percentage and would lead to increased levels of glycation. Reducing monosaccharides either have an aldehyde or are capable of forming an aldehyde in the open chain. These aldehydes can form Schiff-bases with primary amines and then rearrange to form permanent, advanced glycated end-products (AGEs). AGEs irreversibly change the properties of the protein and are the source of the secondary complications associated with the widely-known disease Diabetes Mellitus.[2]

In a healthy individual, the blood glucose concentration is held relatively constant even under high loads and demands of glucose. These steady-state concentrations are at levels that are high enough to meet the continuous demand of the tissue without being in excess. The hormones insulin and glucagon constantly provide

[*] Part of this chapter is reprinted from B. M. Cummins, J. Lim, E. E. Simanek *et al.*, "Encapsulation of a concanavalin A/dendrimer glucose sensing assay within microporated poly (ethylene glycol) microspheres," Biomedical Optics Express, 2(5), 1243-1257 (2011) with kind permission of OSA,

feedback control to maintain normal levels.[1,3] Insulin is released in hyperglycemia conditions, and glucagon is released in hypoglycemia conditions.

Insulin is a 5.8 kDa peptide hormone that is produced by the beta cells of the pancreas and stored in secretory vesicles that respond to glucose concentrations. The body responds to high glucose concentrations by releasing insulin to stimulate the cells in the liver, muscles and fat to absorb glucose. This absorbed glucose is then converted to the energy storage unit known as glycogen. A single glycogen molecule can store thousands of glucose molecules. While each glucose molecule has a reducing terminus capable of forming AGEs with an amine-bearing protein, once it is stored in the glycogen molecule, it does not.[1,3]

Glucagon is a 3.5 kDa peptide hormone that is generated in the alpha cells of the pancreas. In hypoglycemia conditions, glucagon binds to the glucagon receptors of hepatocytes, stimulating the conversion of stored glycogen into individual glucose molecules to be released to meet the energy demand of the body.[3]

Overview of Diabetes Mellitus

Diabetes is a disease where the body is unable to enact the normal feedback mechanism to convert excess glucose into glycogen, and it is characterized by elevated blood glucose concentrations.[4-6] As a result, the patient is more likely to form AGEs which can cause complications in tissues/organs with relatively long-lived proteins/cells. There are two primary types of diabetes. Types 1 diabetes is an autoimmune disorder that results in the destruction of the beta cells in the pancreas and is often referred to as

juvenile diabetes or insulin-dependent diabetes. This type results in an absolute insulin deficiency where insulin is no longer released at concentrations that can help control the concentrations of glucose.[7-9] Type 2 diabetes is characterized by insulin resistance due to lifestyle and genetic factors. Lifestyle factors that increase the risk of developing Type 2 diabetes include obesity, lack of physical activity, poor diet, and stress.[10,11] Of the total number of diabetes cases, approximately 10% have Type 1 and 90% have Type 2.[12]

This disease is currently at epidemic proportions in the United States and worldwide. In the United States, approximately 25.8 million people have diabetes.[13] Worldwide, the World Health Organization (WHO) estimates there to be 346 million people with the disease, where more than 80% of the people with diabetes live in low- and middle-income countries.[14,15] In 2012, the direct and indirect expenditures associated with diabetes totaled 548 billion U.S. dollars.[12] These numbers are expected to continue to rise. Half of the adult population in the U.S. is expected to have pre-diabetes or diabetes in 2020.[16] By the year 2035, there are estimates that diabetes will affect 592 million people worldwide.[12]

The original diagnosis of diabetes can be made with several different methods: the A1C test, the fasting plasma glucose (FPG) test, and the oral glucose tolerance test (OGTT). The A1C value is effectively the percentage of the hemoglobin that is glycated. Since hemoglobin is a relatively long-lived protein, it can give an average of the blood glucose values over the last month. The FPG measures the blood glucose concentrations of an individual that hasn't had any caloric intake for 8 hours. The

OGTT is a two-hour test that tests how your body responds to a certain amount of glucose. Healthy individuals display an A1C value of less than 5.7%, a FPG of less than 100 mg/dL, and an OGTT of less than 140 mg/dL. Diabetes is often diagnosed with an A1C value of higher than 6.5%, FPG of higher than 126 mg/dL, and an OGTT of higher than 200 mg/dL. Prediabetes is diagnosed with test results that are in between those identified by diabetes and normal. It has been shown that the onset of diabetes can be delayed if the proper lifestyle changes are made.[4]

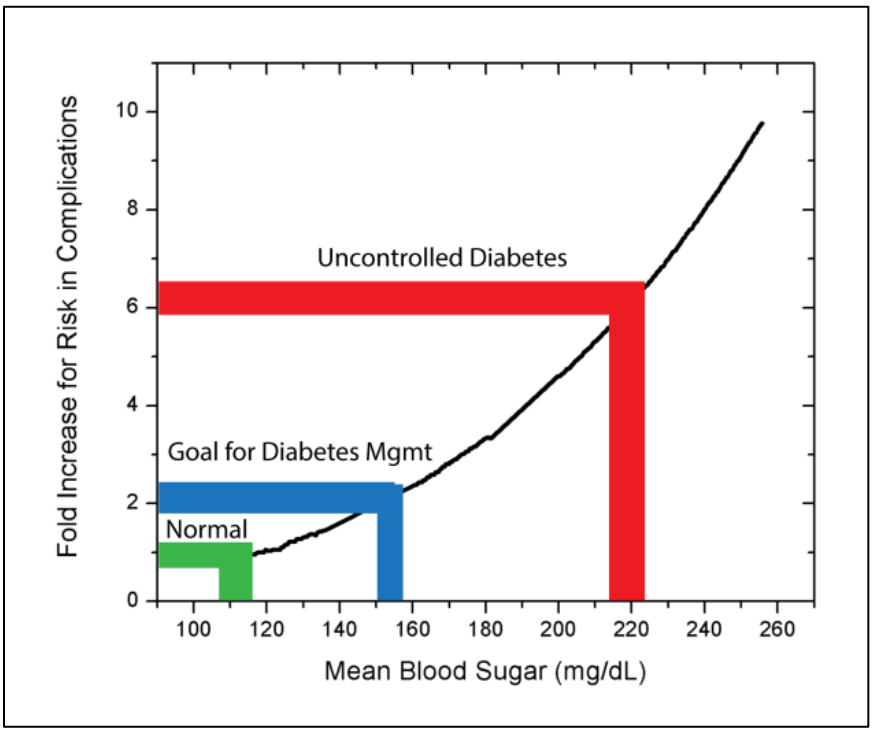

Figure 1: Increase in the risk of complications according to the mean blood sugar. This exponential curve was fit to the data from the 1993 trial.

In 1993, the Diabetes Control and Complications Trial published 10 years of data from multiple centers that showed improved glycemic control (maintaining blood glucose values within normal ranges) decreased secondary complications associated with diabetes.[17] Figure 1 shows the risk in complications as a function of the patient's mean blood sugar as a fitted exponential to the data from the 1993 trial. Typical mean blood sugar values that are seen for normal and uncontrolled diabetes are shown, as well as the goal for diabetes management.

This trial also showed that the strict management of glucose also increased the risk of time spent in hypoglycemia.[17] Hypoglycemia is the result of delivering too much insulin for the glucose levels present in the system, and it can result in coma and even death. The high residual insulin concentrations continue to convert glucose into glycogen even though the amount of glucose in the blood is dangerously low.

Therefore, the management of blood glucose concentrations is a balance between minimizing the average blood glucose concentrations and avoiding hypoglycemic events. The target A1C value for diabetic management (7%) is typically higher than what is normal for a healthy individual (less than 5.6%).[4] Upon diagnosis, physicians typically instruct interventions such as exercise, diet, delivery of exogenous insulin, and medication. There are many different types of insulin that can be delivered: rapid-acting, short-acting, intermediate-acting, and long-acting.[18] There are as many different medications that try to improve the response to insulin or the production of insulin in various ways.[19] Because of the numerous possibilities for management plans, it is imperative that the patient meets with his/her physician and follows the management

plan that is chosen. Each management plan depends on the blood glucose information; however some plans require more frequent information than others. For those plans that require current information, the patients are instructed to perform frequent blood glucose measurements.[4]

Glucose Monitoring

Commercial Glucose Sensors

The blood glucose meter is the primary tool to perform these measurements, and it is widely considered the most successful commercial biosensor to date.[20] Briefly, the device requires a drop of blood to be applied to an enzyme-coated paper strip that is then inserted in a handheld device to be measured. The enzymes on the paper strip consume the glucose, converting it into byproducts that are typically measured electrochemically. The device uses an algorithm to convert this signal into an expected blood glucose concentration, and these readings typically show an error that is less than 20%. Possible sources of increased error include the denaturation of the enzymes on the paper strip, inadequate blood volumes, and variations due to temperature.[21]

Physicians typically instruct patients that use insulin to make 5-7 measurements per day (before and after meals) to get a true picture of the daily profile and allow one to minimize the time outside of normal levels. However, the majority of patients display low compliance to this instructed frequency of measurement – which has been attributed to inconvenience (pain, time, etc.). In fact, 60% of the patients that rely on insulin

average less than a single measurement per day. That number increases to 95% for patients who do not use insulin.[22]

Continuous glucose monitoring (CGM) has been identified as a technique that can improve diabetes management by placing less of a demand on the patient and giving the user more information.[23] The current CGM devices on the market are marketed for trending information, and they display the current glucose levels and historical trends on the monitor. They also notify the patient before they reach levels previously defined limits (low and high). As a result, this technique has been shown to result in fewer highs and fewer lows, improving diabetes management.[24,25] These current CGM sensors are based on a similar electrochemical-enzymatic approach to the paper strips, and this chemistry is placed on the tip of an electrode in a diffusion-limiting matrix. This sensor is placed just underneath the skin in the interstitial fluid, and the matrix allows glucose, oxygen, and other small molecules to reach the sensing chemistry. The enzymatic chemistry consumes glucose, and the byproducts undergo redox reactions with an electrode to generate a current that is glucose-dependent.[26]

The primary problem facing current CGM devices is the foreign body response.[27-29] Because the reorganization of the tissue changes the absolute and relative glucose and oxygen transport, several calibrations are required each day to maintain accurate glucose predictions. Eventually, the limited transport prevents the sensors from displaying sufficient accuracy and requires replacement after 3-7 days. It is important to note that the sensors continue to work once they are removed and cleaned, indicating that it is truly a transport problem.[30]

Research towards Improved Glucose Sensors

An extensive amount of research is being done to improve the accuracy and lifetime of CGM devices. One approach is to minimize the foreign body response to the percutaneous sensor for current CGM devices. Modeling has been performed to identify the specific characteristics of this foreign body response that disrupt the sensor predictions. The changes in transport are not only due to the lag time due to the increased diffusion barrier, but they are also due to the increased consumption by the metabolically active cells in the area.[31] Research groups have devised numerous strategies to minimize this response, including the release of drugs and the design of the surface of the membrane.[32-34] It is also possible that this response can be minimized by fully-implanting the device.[35]

In addition to the electrochemical-enzymatic sensing scheme, there are many alternative approaches that have been explored in research labs. Techniques based on microdialysis, near-infrared (NIR) absorption, Raman spectroscopy, and polarimetry all show considerable potential, and groups are currently pursuing them in research labs.[36] One particularly attractive sensing approach is a fluorescent affinity-based assay, in which the sensor employs a glucose-receptor for the specificity.[37,38] Instead of measuring the rate of consumption with an electrode, the equilibrium binding can be interrogated with an optode. This type of approach has recently received significant amount of interest by major medical device companies. Becton Dickinson has pursued a fluorescent affinity-based sensor based on the glucose-binding protein for many years.[39] In addition, Medtronic has recently acquired the fluorescent competitive binding

affinity-based technology from PreciSense.[40] In 2012, they were awarded $20 million from the Juvenile Diabetes Research Foundation (JDRF) to combine this approach with their traditional CGM approach to create an orthogonally redundant glucose sensor in an attempt to improve the accuracy and stability of the sensor. This recent activity indicates that large medical device companies recognize the many advantages that optical affinity-based chemistries can offer to generate an improved CGM device.

Outlook

Current glucose sensing strategies already offer the user information that can allow for improved diabetes management, but they place a significant burden on the user and display low patient compliance. This low compliance could be due to the requirements placed on the user to perform either the measurement or the intervention components required for proper management. For both of these issues, an improved CGM device has the potential of improving patient compliance. A CGM device that requires fewer calibrations and fewer replacements could minimize the requirements placed on the user to collect blood glucose concentration data. In addition, an improved CGM device could minimize the burden on the user by allowing for the realization of the artificial pancreas.

The artificial pancreas is a device that connects a CGM device with an insulin pump to continuously deliver the insulin required to keep the blood glucose concentrations within normal values.[41] The delivery of insulin must be carefully administered; delivering too much can result in severe hypoglycemia. To mitigate this

risk, this strategy has started to include a glucagon pump to allow the system to increase glucose levels as well.[42] This type of system could function for long periods of time without input by the user. As a result, this concept requires accurate CGM readings for it to become a reality. JDRF has identified the Artificial Pancreas Project to transform the lives of people with Type 1 diabetes. In 2013, the top priority area of JDRF's Artificial Pancreas Project is the development of differentiated glucose sensing technologies to improve reliability and accuracy of continuous glucose monitors.

Concanavalin A-Based Glucose Sensors

One glucose sensing technology that has generated interest over the last three decades is the fluorescent affinity-based assay using Concanavalin A (ConA) as the receptor. ConA is a c-type lectin that is a tetramer at physiological pH with a molecular weight of 104 kDa . Lectins are a set of proteins that reversibly and non-enzymatically bind specific carbohydrates, and ConA binds glucose and mannose in the presence of certain divalent cations.[43,44] Unlike proteins such as hexokinase and glucose-binding protein, ConA does not undergo a measurable conformational change upon its binding to glucose.[45,46] Instead, ConA-based sensors typically employ a competing ligand and track the glucose concentration with the amount of competing ligand is bound to ConA. As the assay is exposed to increasing glucose concentrations, the amount of the competing ligand bound to ConA decreases, which can be transduced via fluorescence.[47-50]

Dr. Irwin Goldstein performed a significant amount of work with ConA in the 1960s and 1970s that paved the way for much of the understanding of the lectin.[51-57] His quantitation precipitation studies showed a significant percentage of the lectin fell out of solution when it was paired with certain various polysaccharides, such as dextrans and glycogens. This precipitation was prevented to varying degrees with certain monosaccharides, and as a result he identified the requirements for a monosaccharide to bind to the primary binding site of ConA. These have been coined as the "Goldstein Rules." Each monomeric subunit of ConA contains a single primary binding site capable of binding glucose and mannose monosaccharides with unmodified hydroxyls at positions C3, C4, and C6.[52,58,59] Dextrans are polysaccharides of glucose and are primarily comprised of α-1,6 glycosidic linkages with branches formed by α-1,3 linkages.[60] Due to this branching, dextrans can have many non-reducing termini to which ConA can bind. As a result, dextrans can display a higher affinity to ConA than their monomeric subunit D-glucose and this affinity increases for larger molecular weight dextrans.[61]

The cell membrane displays certain glycoproteins to the external environment that can be recognized by ConA.[44] Native, tetrameric ConA displays binding sites that are approximately 6.5 nm apart from one another and could potentially cluster the glycoproteins upon binding. However, the biotoxicity of ConA has been extensively studied, and has been shown to pose little to no adverse health risk in use for in vivo sensing at low concentrations.[62]

As a result, ConA-based competitive binding assays have been developed as potential solutions for *in vivo* continuous glucose monitoring applications. This was first introduced by Dr. Schultz, Dr. Mansouri, and Dr. Goldstein in 1982.[48] In this work, ConA was paired with FITC-labeled dextran in a microdialysis membrane that was fit at the end of an optical fiber. While the FITC-dextran was left free in solution, ConA was tethered to the inner wall of the membrane. Glucose could equilibrate across the membrane, but FITC-dextran was large enough to be held inside.

This significant potential of this scheme has led to many variations in the design of the fluorescent competing ligands, optical transduction mechanisms, and encapsulation techniques used with this assay.[47,49,63-69] Fluorescence assays have been proposed to be encapsulated inside microspheres or fibers, embedded within the dermis, and optically interrogated from the surface of the skin. However, to date, they have continued to display sub-optimal sensing performance when both assay components were left in free solution.

Problems with irreversibility and precipitation in free solution have consistently been reported by research groups. Specifically, Dr. Joseph Lakowicz's group stated that "the success of a glucose sensor using ConA as the glucose-binding protein depends on being able to eliminate agglutination."[70] In addition, Dr. Birch's group stated that "the main obstacle to developing this assay for in vivo use is the tendency for ConA complexes to precipitate after extended incubation periods, particularly at low glucose concentrations."[71]

The objective of the work presented in this dissertation is to show the full potential of the fluorescent affinity-based assay using Concanavalin A (ConA) for continuous glucose monitoring applications.

CHAPTER II

ASSAY BASED ON CONCANAVALIN A AND GLYCOSYLATED DENDRIMER[*]

Introduction

In an attempt to decrease the irreversible binding associated with the ConA/dextran system, our group has previously employed the use of glycosylated dendrimers as the competing ligand.[72] Dendrimers are tree-shaped, globular macromolecules that have been explored for potential uses in chemotherapeutics,[73,74] anti-viral pharmaceuticals,[75-79] and scaffolds for tissue repair due to their biocompatibility.[80,81] By adjusting the size and altering the functional end-groups of the dendrimers, the effective diameter, molecular weight, and hydrophilicity can be varied.[82-84] Using specifically tailored glycosylated dendrimers that can bind to ConA, our group has generated a competitive binding assay that has been shown to be sensitive to glucose concentrations. The assay components have been shown to remain functional for several days after being held at body temperature (37 °C) when they were separate and paired together.[85] A schematic of the ConA/glycosylated dendrimer glucose response is shown in Figure 2.

---

[*] Part of this chapter is reprinted from B. M. Cummins, J. Lim, E. E. Simanek *et al.*, "Encapsulation of a concanavalin A/dendrimer glucose sensing assay within microporated poly (ethylene glycol) microspheres," Biomedical Optics Express, 2(5), 1243-1257 (2011) with kind permission of OSA, Copyright 2014 by The Optical Society; and from B. M. Cummins, J. Lim, E. E. Simanek *et al.*, "Understanding the mechanism and optimizing a competitive binding fluorescent glucose sensor." 7906. (2011) with kind permission of SPIE, Copyright 2014.

This chapter further explores the ConA-based glucose sensing assay that employs these glycosylated dendrimers. A set of glycosylated dendrimers with unique characteristics were paired with ConA in assays to determine which assay maximized the fluorescence response to physiologically relevant glucose concentrations. One of these assays was encapsulated using a microporated microsphere approach to allow glucose diffusion to occur and the assay to respond. The stability issues that have continued to plague this type of assay in free solution were then explored further.

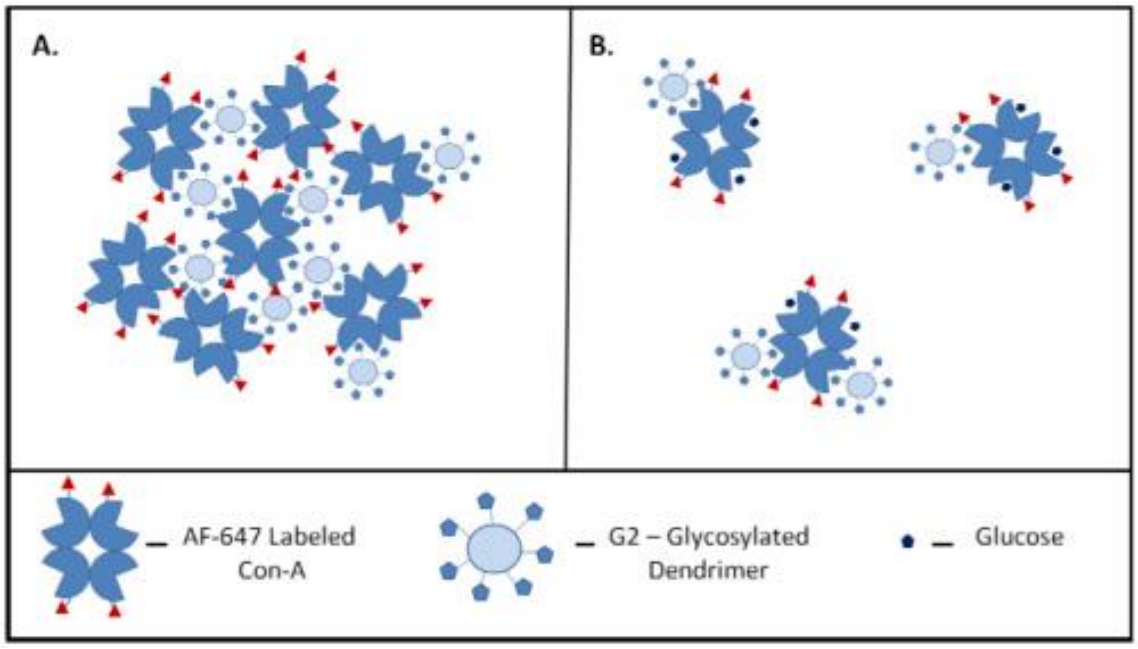

Figure 2: Schematic representation of the aggregative nature of the ConA/glycosylated dendrimer assay. In (a) low glucose concentrations, the assay emits lower fluorescence than (B) in high glucose concentrations.

Optimization Studies

Traditional ConA-based sensors typically shown a ~30% increase in the fluorescence of the donor fluorophore across physiological glucose concentrations in free solution.[47,86,87] Previous versions of this ConA/glycosylated dendrimer assay have shown significantly larger changes across these same glucose concentrations.[67,88] However, while this assay was originally engineered to display a typical Förster Resonance Energy Transfer (FRET) response, it did not show such a response. In a competitive binding assay that uses FRET to transduce the binding, low concentrations of the analyte of interest (glucose) should allow for a large amount of binding to occur between the fluorescent receptor and the fluorescent ligand. This binding can allow for energy transfer to occur, decreasing the steady-state fluorescence intensity from the donor. Upon the addition of the analyte of interest, there should be a decrease in the amount of fluorescent receptor that is bound to the fluorescent ligand, and the donor fluorescence should increase. For the work with the glycosylated dendrimer, the opposite response was seen. The fluorophore that should have acted as the acceptor increased with the addition of the glucose.

This ConA/glycosylated dendrimer assay also generated a fluorescence response to glucose concentrations when the glycosylated dendrimer was unlabeled.[89] This suggested that part of the fluorescence response stemmed from the glucose-dependent aggregation of the Alexa Fluor 647 labeled ConA (AF647-ConA). This aggregation could decrease the fluorescence through several pathways, including: (1) homo-FRET (where the fluorophore on ConA could transfer energy to an unexcited fluorophore on a

neighboring ConA), (2) increased scattering of the solution (shielding), and (3) the fluorescent material falling out of solution due to precipitation.

To examine whether the dynamic range of this assay based on AF647-ConA could be extended even further by combining the aggregation effects with energy transfer, a set of different glycosylated dendrimers were designed to be capable of undergoing energy transfer with the AF647 fluorophore. Instead of being labeled with the donor-fluorophore of the FRET-assay, these dendrimers were labeled with chromophores that could serve as the acceptor-fluorophore with AF647-ConA. To this end, a set of glycosylated dendrimers were synthesized and provided by Dr. Eric Simanek and used as received. Generation two (G2) triazine dendrimers (MW ~9kDa & ~1.5 nm diameter) were provided with 12 glucose groups and 12 amine groups in unlabeled, QSY-21-labeled, and Alexa Fluor 750 (AF750) labeled versions. Generation four (G4) triazine dendrimers (MW ~36 kDa & ~2.5 nm diameter) were provided with 48 glucose groups and 48 amine groups in unlabeled, QSY-21-labeled, and AF750-labeled versions. The degree of labeling was expected to be 1 label per glycosylated dendrimer. Accordingly, the expected number of amines for the labeled versions was one less than the unlabeled version of the same size.

The QSY-21 label is a non-fluorescent diarylrhodamine chromophore that can serve as a FRET-acceptor with AF 647. The donor/acceptor FRET pair has an expected Förster radius of 6.9 nm. The AF 750 label is a fluorophore with similar fluorescent properties to Cy7. The Alexa Fluor set of dyes are typically sulfonated versions of other

dyes – resulting in a fluorophore that is brighter, more stable, and less sensitive to pH. Several of the key properties of these fluorophores are listed in Table 1.

Table 1: Properties of the fluorophores used in the ConA/glycosylated dendrimer assay.

Fluorophores	***Maximum Absorbance (nm)***	***Extinction Coefficient ($cm^{-1}M^{-1}$)***	***Quantum Yield***
AF 647	650	239,000	0.33
AF 750	749	240,000	0.12
QSY-21	661	90,000	0

ConA was fluorescently labeled with AF647 via the following method. Briefly, 10 mg of ConA was dissolved in 1 mL of 0.1 M sodium bicarbonate buffer (pH ~8.3) and 1 mg of AF647 succinimidyl ester was added to 100 µL DMSO. The dye solution was then added drop-wise to the protein solution while it was being stirred, and allowed to react for one hour in the dark.[90] The solution was then loaded onto a G75 Sephadex column that had been pre-swelled and equilibrated with TRIS buffer (with the required divalent cations). Inactive ConA and free AF647 dye eluted from the column with TRIS, and the active, AF647-ConA was eluted with a 200 mg/mL glucose solution in TRIS. This fraction was collected and dialyzed against TRIS buffer to remove the glucose in the solution. After centrifugation, the concentration and labeling ratio were then determined by measuring the absorption spectra. These measurements were performed by UV-VIS spectrometry indicating a labeling ratio of 4.7 dye molecules per ConA tetramer. This sample was used for subsequent studies. Samples that were not to be used immediately were added to centrifuge tubes and frozen for a later date. The

comparison of excitation and emission fluorescent spectra of AF647 with QSY-21 and AF647 with AF 750 are shown in Figure 3.

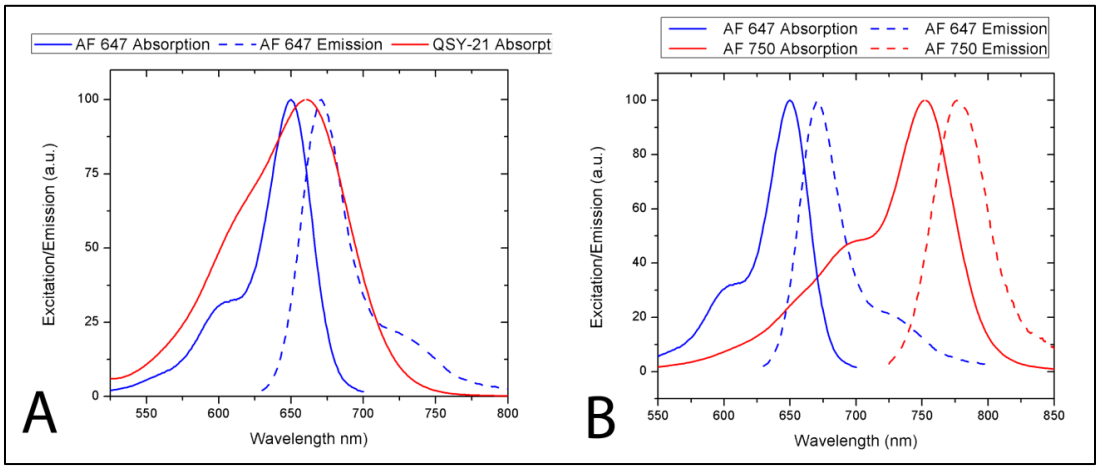

Figure 3: Excitation/emission properties of the chromophores within the ConA/glycosylated dendrimer optimization studies. (A) AF647 and QSY-21, and (B) AF647 and AF 750.

To be able to quickly judge the effectiveness of these ConA/glycosylated dendrimer assays, fluorescence measurements were performed on a microplate reader. Each ConA and glycosylated dendrimer combination was loaded to the microplate at a set of different assay configurations with a final volume of 300 µL. These six assay configurations are shown in Table 2. Each of these configurations were loaded in triplicate in the absence and presence of 500 mg/dL glucose concentrations, allowed at least 15 minutes to equilibrate prior to measurements.

Table 2: Assay configurations tested for each ConA/glycosylated dendrimer assay.

Assay Configuration	*[ConA] (nM)*	*[Dendrimer] (nM)*
1	500	500
2	250	250
3	500	250
4	250	500
5	1000	500
6	1000	250

Measurements were performed on the monochromator-based Tecan microplate reader from a top-reading, fluorescence approach. The excitation wavelength was set to 620 nm with a bandwidth of 10 nm. The fluorescence emission was scanned from 650 nm to 820 nm in 5 nm increments. This emission had a bandwidth of 20 nm. The gain was set to 94, and the integration time was 20 µs. The z-position was 20126 µm. The relative increase in the peak of AF647-ConA's fluorescence from 0 mg/dL glucose to 500 mg/dL glucose was determined and shown in Figure 4. The absolute increase (counts) in the peak of AF647-ConA's fluorescence from 0 mg/dL glucose to 500 mg/dL glucose was determined and shown in Figure 5. Each well had the same experimental set up, allowing the absolute counts to be comparable. The figure of merit was determined to be the product of the absolute increase and the relative increase, and this value is shown in Figure 6. The absolute increase was included in the figure of merit because the signal-to-noise associated with fluorescence measurements is proportional to the square root of the number of counts measured (Poisson Distribution).

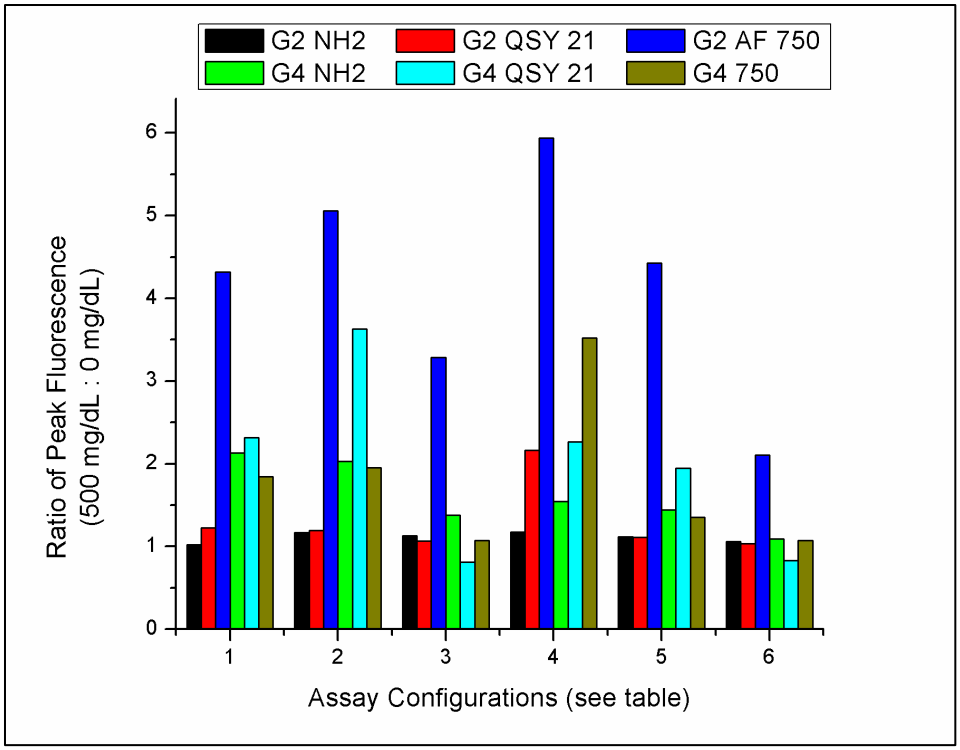

Figure 4: Relative increase in the peak of AF647-ConA's fluorescence from 0 mg/dL glucose to 500 mg/dL glucose for each assay configuration.

The relative changes in Figure 4 show that the largest relative changes are typically associated with the lowest initial AF647-ConA concentrations. In addition, higher changes were typically seen when the ConA concentration was either equal to or lower than the glycosylated dendrimer concentrations. The QSY-21 and unlabeled versions of the G4 dendrimer showed higher responses than for its G2 counterparts, but the opposite is true for the AF750-labeled version. The QSY-21 labeled dendrimers showed mixed results when compared with the unlabeled dendrimers. However, the AF750-labeled dendrimers were better than the unlabeled versions of both G2 and G4.

The highest responses were with the AF750-labeled G2 glycosylated dendrimer. It is also important to note that each configuration with the G2-NH2 dendrimer showed small changes across physiologically relevant glucose concentrations. This is different than what has been seen in cuvette based studies.

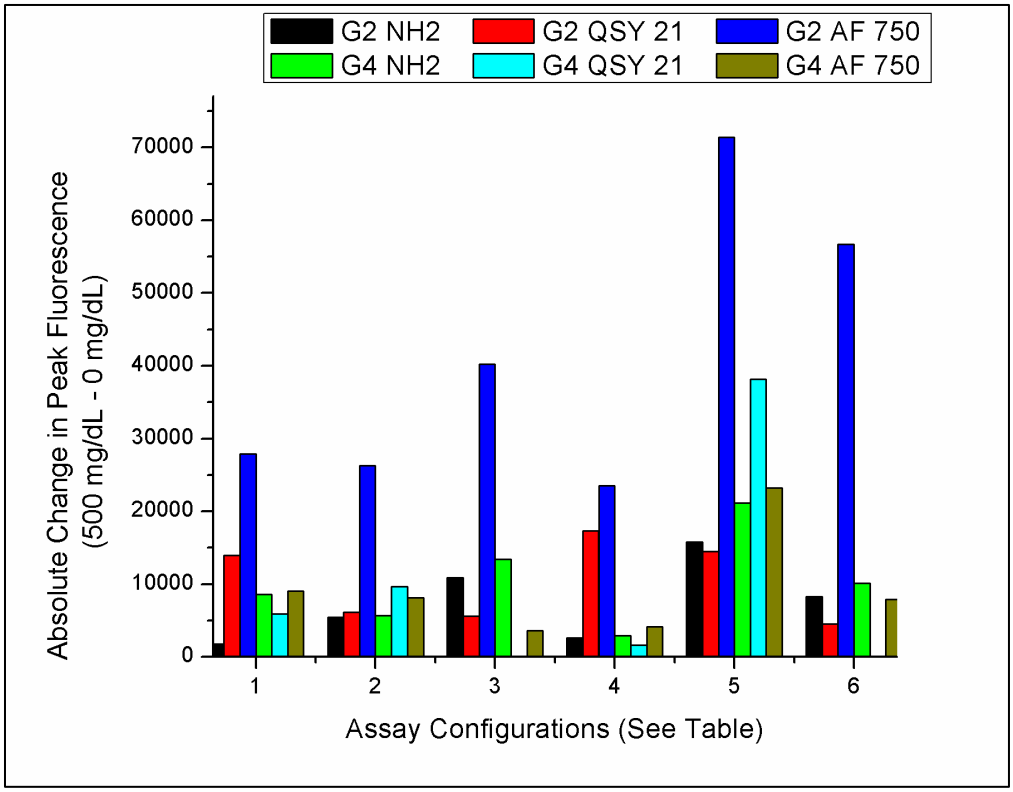

Figure 5: Absolute increase (counts) in the peak of AF647-ConA's fluorescence from 0 mg/dL glucose to 500 mg/dL glucose.

For most cases, the absolute changes in Figure 5 seem to increase the most in assays that showed higher concentrations of AF647-ConA. The highest ConA concentrations (1 µM) showed a higher change in absolute fluorescence counts than the

other samples. These samples have the most AF647 in the solution, and can allow for large changes in absolute count even with smaller ratiometric responses. Again, in each assay configuration the G2-AF750 glycosylated dendrimer showed the highest responses.

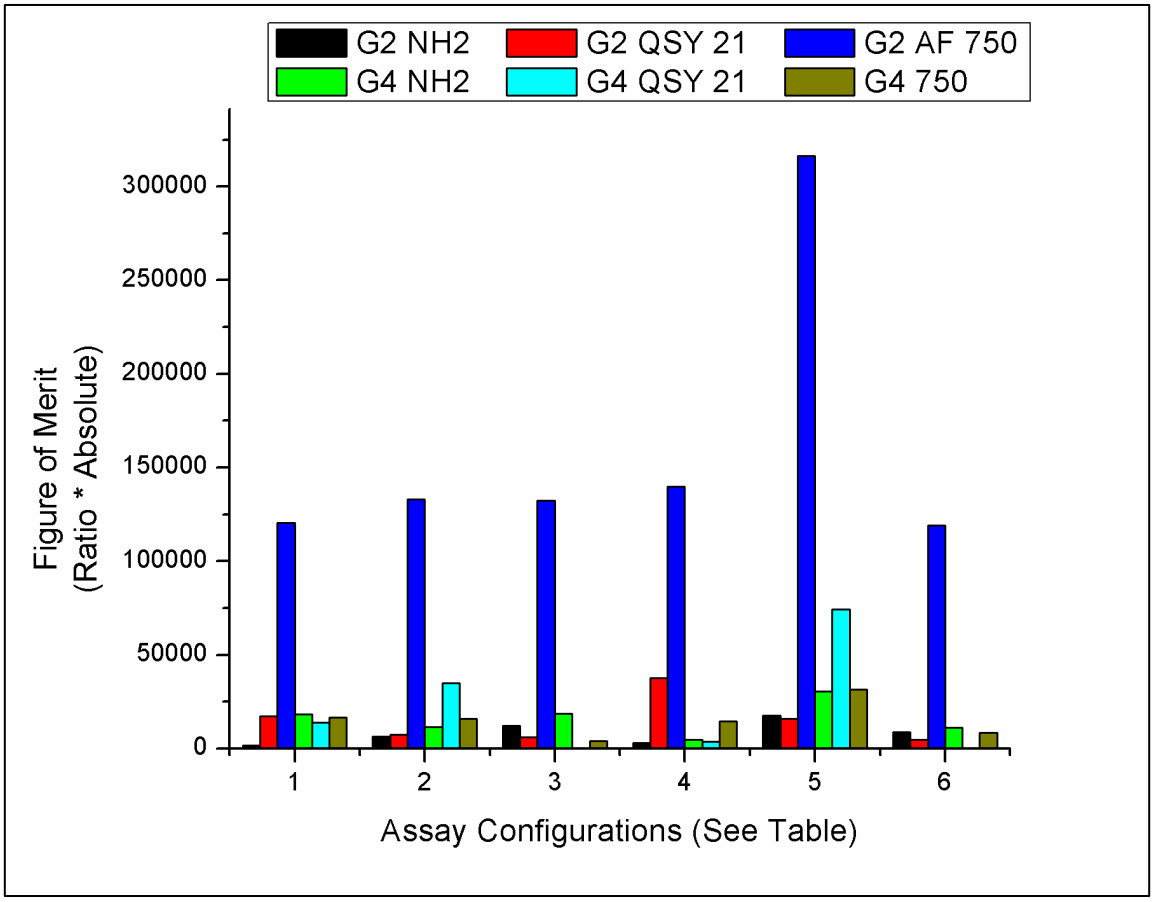

Figure 6: Figure of merit (ratio*absolute) increase for each assay configuration.

According to the figure of merits (Figure 6), the optimized assay configuration is composed of 1 µM AF647-ConA with 500 nM AF750-G2 dendrimer. The G2 AF 750

dendrimer's figure of merit was consistently better than the unlabeled G2 dendrimer in each assay configuration. This could indicate that the additional pathway of energy transfer can further increase the dynamics of the assay. However, the G4 AF 750 dendrimer showed similar responses to the unlabeled G4 dendrimer. This could be due to the difference in diameters between G2 and G4 dendrimers, where the smaller dendrimers display a higher FRET-efficiency. The dendrimers labeled with QSY-21 should show a similar trend as the dendrimers labeled with AF750. However, both the G2 and G4 versions of the QSY-21 labeled dendrimers showed similar responses to the unlabeled versions.

A full study of the glucose response of the assay of 1 μM AF647-ConA with 500 nM AF750-G2 dendrimer was run in a similar configuration as to the previous study. Glucose concentrations ranged from 0 mg/dL glucose to 1000 mg/dL. This response is shown in Figure 7. This response shows the highest change in response across physiological glucose concentrations, increasing its fluorescence by ~250% from 0 mg/dL to 400 mg/dL.

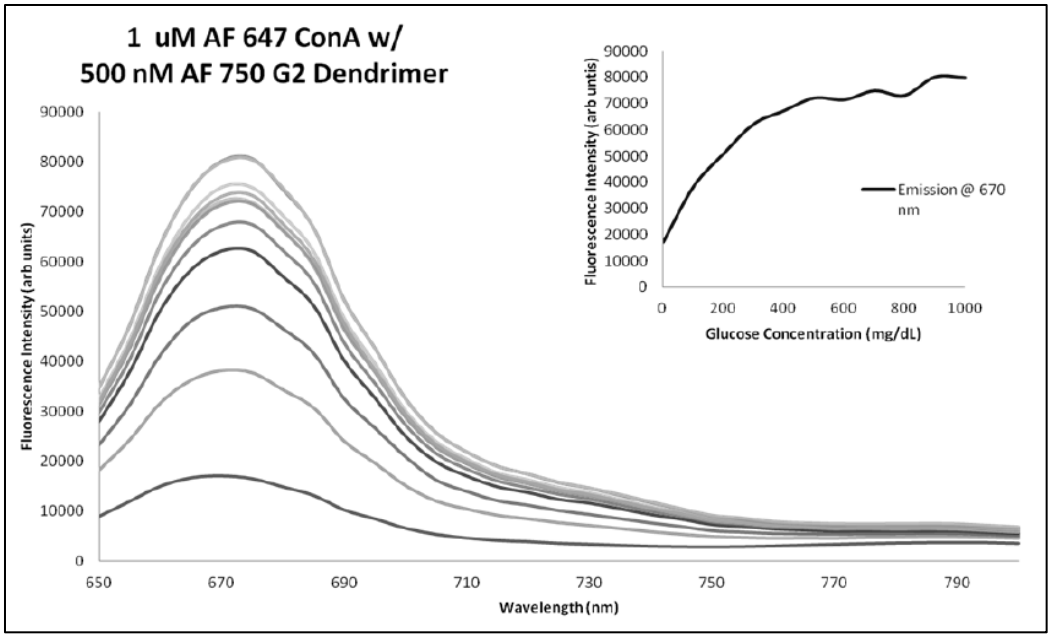

Figure 7: Glucose response of the 1 µM AF647-ConA and 500 nM AF750-G2 dendrimer assay.

In summary, the systematic evaluation of the various glycosylated dendrimers and assay configurations generated a specific fluorescence assay that displays a high sensitivity to physiological glucose concentrations. However, the introduction of a FRET acceptor to the glycosylated dendrimer should have increased the number of quenching/transfer pathways possible for the AF647 fluorophore on ConA in each assay. While that was seen for the AF 750-G2 vs. the unlabeled G2, it was not consistently seen for any other dendrimer. This is probably due to different complex binding interactions between ConA and the various dendrimers, especially upon aggregation. Observing significant variations like this could indicate problems with stability and repeatability like previous versions of this assay. The aggregative interaction between ConA and the

glycosylated dendrimer appears to be complex, and it calls for a further exploration to assure a stable, optimized assay. One potential method that was explored in an attempt to stabilize this assay was encapsulating it in microspheres.

Encapsulation within Microporated Microspheres

For functioning aggregative assays to be translated from cuvettes and microplate wells to implantable sensors, specifically tailored encapsulation methods which maintain the chemistry's binding kinetics must be employed. Requirements for such a strategy must prevent the leaching of assay components while allowing for the diffusion of the targeted analyte and response of the sensing chemistry to the analyte. Much work in the field of encapsulation has been focused on the extension of drug delivery profiles. Concepts such as polymeric microspheres and layer-by-layer (LbL) approaches have been used and reported.[91-96] These microencapsulation techniques have begun to be altered for general sensing purposes in attempt to meet the aforementioned requirements.[97] For example, several groups have loaded sacrificial spherical templates (i.e. melamine formaldehyde and calcium carbonate) with proteins and sensing chemistry that can then be exposed to alternating layers of poly-electrolytes which coat the template.[98-100] These cores can then be dissolved freeing the chemistry within the micron-sized LbL capsule that can then serve as a semi-permeable membrane for sensing purposes. Advantages of this technique include the fine level of control for the mesh size of the capsule and the high synthetic reproducibility. However, future work must be done to minimize the effects of electrostatic binding of the sensing chemistry to

the charged interior wall of the capsule.[101] Additionally, groups have embedded sensing chemistries within a dense matrix in an attempt to maintain long-term functionality. Poly-(ethylene glycol) (PEG) has been employed in this manner due to its proven biocompatibility and hydrophilic nature.[102] Microspheres can be created using PEG by crosslinking the individual chains via thermo-chemical or photo-chemical initiation, resulting in a mesh of PEG chains in which chemistry can be embedded. The effective pore size of this mesh can be altered by varying the average molecular weight of the PEG and/or changing the water content within the precursor solution prior to crosslinking.[103,104] With these variations, the mesh size for PEG can be tailored to be suitable for sensing purposes. However, the sensing response of assays embedded within this mesh has been limited in its reversibility due to the consistent mesh within these spheres without attachment of the assay to the polymeric backbone.[105]

Until now, the successful encapsulation of the ConA/glycosylated dendrimer sensing assay has not been reported. Previously, our group has proposed and presented an encapsulation strategy combining a water-in-oil emulsion technique with the addition of sugar crystals to the precursor PEG solution to form assay-filled pores within the hydrogel matrix of the microspheres. This microporation technique was shown to be functional with the ConA/Dextran glucose sensitive assay – displaying a reversible response over several days.[105] Since microporated PEG spheres allowed competitive binding within the larger pores while providing for diffusion of smaller analytes due to the selectively permeable mesh, it was believed that similar biocompatible microporated microspheres may be candidates for housing the aggregative ConA/glycosylated

dendrimer sensing assay. Work presented here explores the effectiveness of this technique in encapsulating the sensing chemistry with respect to its dynamic range, sensitivity, and reversibility. The assay that was encapsulated was the AF647-ConA and unlabeled G2-NH2 glycosylated dendrimer.

Synthesis of Loaded Microspheres

Two groups of microspheres, hereafter called microporated-PEG and PEG-50, were created to display the functionality of the microporated microspheres. PEG-50 spheres are created with 50% water and 50% PEG, and microporated microspheres are created with pores within a 100% PEG solution. For comparison, schematic renditions of these are displayed in Figure 8 as well as that of 100% PEG solution. PEG-50 spheres have shown to be effective in allowing the assay to respond with limited reversibility while PEG-100 spheres have been shown to have limited response but high reversibility. Therefore, the microporation technique aims to capture the advantages of both by creating larger assay-filled pores within the tighter mesh of the PEG-100 spheres.

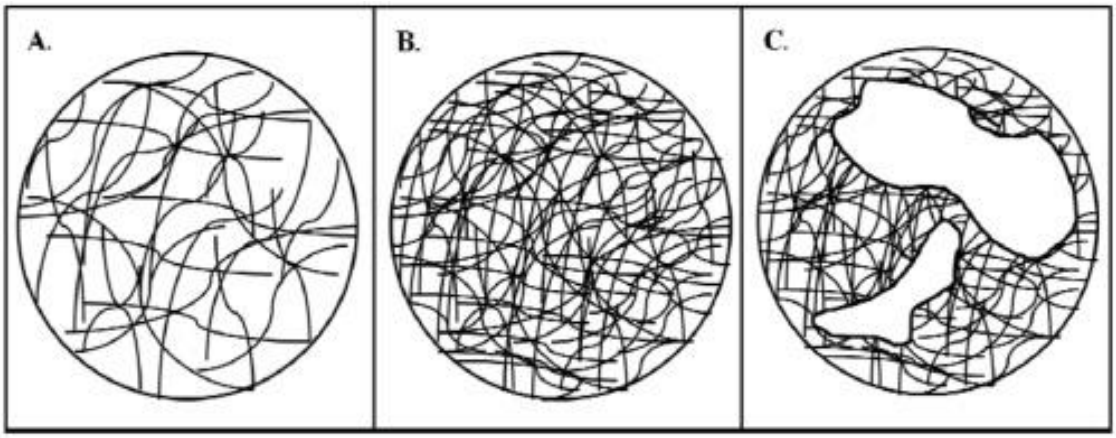

Figure 8: Schematic representation of the mesh/pore sizes of the various spheres described: (A) PEG50 spheres (B) PEG100 spheres and (C) Microporated spheres.

The spheres were synthesized in the following way using AF647-ConA and G2-Dendrimer stock solutions of 1 mg/mL. To create the porogen for the microporated PEG microspheres, 200 µL of AF647-ConA stock solution, 100 µL of G2-Dendrimer stock solution, 300 µL of PBS, and 20 mg of mannitol were added together. This precursor solution was mixed well, and then lyophilized overnight. In order to make the precursor polymeric solution for the microporation technique, 10 mg of the lyophilized sample was added to 1 mL PEG-DA (MW 575) and 10 µL Darocur. This solution was stirred to break up the lyophilized crystals into smaller particles. To make the polymeric precursor for the PEG-50 microspheres, 500 µL PEG-DA (MW 575), 100 µL ConA, 50 µL G2 Dendrimer, 350 µL TRIS buffer, and 10 µL Darocur were added together and mixed well.

A water-in-oil emulsion technique was implemented by adding 50 mL of light mineral oil to a 100 mL beaker. This solution was stirred via a magnetic stir plate,

rotating at approximately 500 rpm. Under these conditions, the polymeric precursor was pipette into the beaker and allowed to spin for 15 seconds to create a fairly homogenous set of spheres. An ultraviolet light source (EFOS Ultracure 100SS Plus) at a wavelength of 365 nm was shone incident upon the beaker from a probe at 20 W/cm2 for 2.5 seconds to sufficiently cause the cross-linking via free-radical photo-initiation. Spheres were removed from the oil bath and vigorously rinsed with TRIS buffer via several buffer exchanges, and then added to a final solution of TRIS buffer. Spheres were stored at 4℃ after synthesis.

Characterization of Loaded Microspheres

To examine the average size of these particles, a bright-field microscopy technique was performed using a Leica DMLM microscope by adding a small volume of spheres on the surface of a microscope slide. To calculate the average diameter for each group of microspheres, ten images were captured by randomly translating the x-y motorized stage and focusing on the spheres within the image plane via a 10x objective. The diameters were calculated for each in-focus sphere that was taken, and the average diameter and standard deviation for each set was found.

The poration within the PEG microspheres was examined through the use of a confocal fluorescence microscope by taking slices of the collected fluorescence through the depth of the sphere. This was performed using a Leica TCS SP5 Confocal Microscope. For these experiments, a HeNe 632.8 nm laser was used at 4.5 mW with a 73.7 μm pinhole and a 10x, 0.3 NA, dry objective. Images were taken without averaging

and the resulting Z-step size was 2.383 μm with a 512 x 512 pixel resolution for the frame. This procedure was performed for both groups of the synthesized microspheres. Since these microspheres were comprised of a hydrogel material that largely consists of water, the refractive index of these spheres was approximately 1.37.[106] These spheres were immersed in TRIS buffer (n = 1.33) for confocal scans. Therefore, the shape of the sphere did not display a significant distortion of the image as the index was somewhat matched.

Fluorescent measurements with regards to leaching were performed on a commercially available spectrofluorometer system (Make: Photon Technology International, Model: Model L-201M Source, MP-1 Sample Compartment, and Model 814 Analog/Photon-Counting Photomultiplier Detector). In emission scan mode, the incident light was set to 633 nm and the emission monochromator was scanned from 650 nm to 710 nm with 1 nm steps and 1 second integration times. Fluorescent measurements of the sensing spheres with regard to response and long-term reversibility were taken with a custom-designed 90 degree fluorescence optical set up (Figure 9).

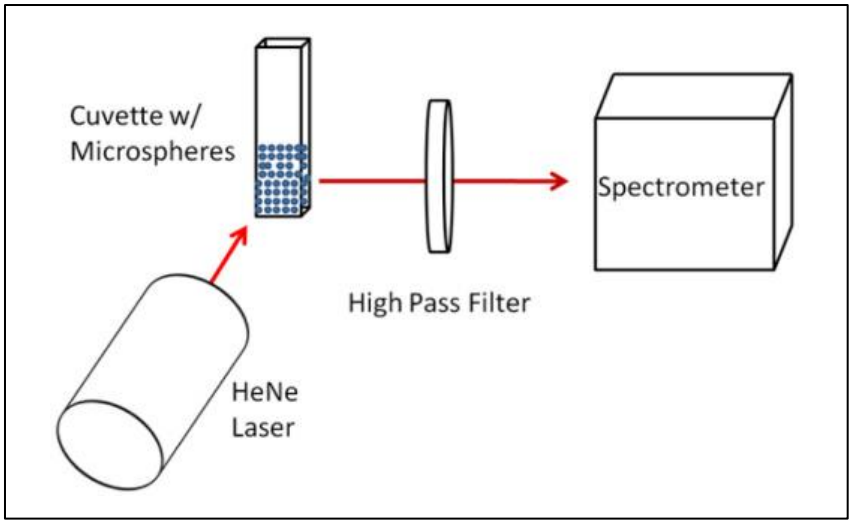

Figure 9: Schematic representation of the optical set up for the fluorescence measurements of the microspheres.

A cuvette holder held the micro-cuvette containing the sensing spheres, and a 5 mW, HeNe 632.8 nm laser was made incident normal to its face. Due to the slight mismatch of refractive index between the spheres (1.37) and the buffer (1.33), there were multiple scattering events. Given the 1 cm path length of the cuvette, a 1 mm beam width, and scatter due to the packed spheres, the sampling volume is approximately 25 µL. This corresponded to approximately 250 spheres within that sampling volume. At 90 degrees, a Roper Scientific SpectraPro 150 spectrometer was placed with a fixed slit width, and a 650 nm long-pass, emission filter was used to eliminate stray laser light. The integration time of the system was 500 milliseconds to avoid saturation of the signal, and the grating had a blaze wavelength at 750 nm with 1200 grooves/mm. For collection purposes, the spectrometer was centered at 690 nm, collecting counts from 647 nm to 727 nm. This was performed to further minimize saturating the detector with

scattered light from the source and in order to sufficiently measure the peak of the AF647 emission at approximately 670 nm. The fluorescent intensity value used in all subsequent data analysis was the maximum value of the fluorophore emission for each spectrum collected.

For titration measurements, 500 µL of microporated microspheres were packed within a microcuvette and 2 mL of TRIS buffer were added. These microcuvettes were used to minimize the amount of spheres used. Highly concentrated, low volume aliquots of glucose were then added to the cuvette to make the surrounding solution increase in glucose concentration. This addition was performed without perturbing the settled spheres to assure adequate comparison. Sufficient time was given to allow for the diffusion of varying glucose concentrations into the spheres and for the response of the assay to achieve steady state. Three runs were performed for the microporated spheres and triplicate data was recorded for each run. The refractive index change between 0 mg/dL and 6000 mg/dL glucose levels have been shown to increase from 1.333 to 1.34.[107] As the physiological glucose concentration are an order of magnitude less than this step change, the change in refractive index should be negligible when compared to the fluorescent response from the competitive binding chemistry.

In addition, the titration was performed on free assay in solution. A sensing assay was formulated in an attempt to mimic those concentrations and ratios seen within the microporated spheres for proper comparison. Specifically, 2 mL of TRIS buffer and 100 µL of 1 mg/mL ConA were added to the cuvette. 50 µL of glycosylated dendrimer was then added and given 1 hour to equilibrate and fluorescent measurements were taken

resulting in an assay with 450 nM ConA & 2.3 μM dendrimer. Aliquots of glucose were added to the system making glucose concentrations in step-wise fashion up to 1000 mg/dL. Steady state measurements were taken upon each addition after giving time for the system to equilibrate. Three runs were performed for the titration in free solution and triplicate data was recorded for each run.

For the leaching experiments, 500 μL of both groups of microspheres that had not been exposed to glucose were packed in microcuvettes with the addition of 2 mL of TRIS buffer and given time to settle. Triplicate fluorescence spectra were then taken for baseline, 0 mg/dL glucose, measurements. Equivalent dilution factors were performed on each cuvette by adding 60 μL aliquots of 200 mg/mL glucose solutions to the settled spheres without perturbation to achieve glucose saturated solutions (600 mg/dL). To allow for the maximum response and any subsequent leaching, the spheres were given twenty-four hours upon the addition of glucose prior to triplicate fluorescence spectra being taken. Supernatant was then collected from the microcuvette and triplicate fluorescent spectra were taken to quantify the amount of leaching, if any, of the fluorescently labeled ConA from within the microspheres.

The reversibility of the system was tested by packing 500 μL of microporated-PEG into a microcuvette and adding 2 mL of TRIS buffer. These spheres were allowed to settle, and triplicate baseline fluorescent readings were taken for each. A highly concentrated aliquot of glucose was then added to make the resulting solution 300 mg/dL. Fluorescent readings were taken again six hours after the glucose was added to the cuvette to be assured the system was at steady-state. The remaining buffer in the

microcuvette was then exchanged 4 times that evening, and exchanged 3 times the following morning to assure that the glucose concentration was effectively zero. This entire process was repeated for fourteen consecutive days.

Per the technique previously described, the average diameter of the microporated spheres was determined to be 545 µm with a standard deviation of 242 µm. In comparison, the average diameter of the PEG-50 spheres was determined to be 476 µm with a standard deviation of 174 µm. As the ultimate application for these spheres is to be minimally invasive subcutaneous interstitial glucose sensors, they must be capable of being embedded interstitially. Therefore, future work will focus on reducing the average diameter by decreasing the size of the emulsified PEG droplets. However, for comparison purposes in this study the two sets of spheres were roughly the same size on average.

The crux of this work depends on the ability for pockets to be created that allow the ConA/glycosylated dendrimer sensing assay to be held within a tight polymeric mesh but also allow for diffusion of the glucose analyte and room for the aggregative assay to respond to the glucose concentration. From the fluorescence confocal microscopy images, the differences between PEG-50 spheres and microporated spheres are visualized. With a step size in the Z direction of 2.38 µm, these images show a slice through the interior of the spheres which display the fluorescent ConA particles. For the microporated microspheres, the fluorescence is localized within striated pockets which are the residual imprint of sugar crystals that had since been dissolved. The average volume fraction of these pores is approximately 1% when accounting for the v/v% ratio

between mannitol within the PEG precursor. In comparison, there is no such localization for PEG-50 spheres Figure 10. PEG-50 spheres do show a relatively homogenous distribution of fluorescence; however, this distribution is a result of the non-localized withholding of sensing chemistry. Ultimately, it may be beneficial for the microporated microspheres to have a more homogenous distribution of size and distribution of pockets since a disperse population of sensing spheres with regard to these variables could result in a response that is dependent on which spheres are being interrogated. Future work will be done to minimize the variability by increasing the porogen to PEG ratio, increasing the speed of the homogenizer, adding surfactant to the precursor, and using a centrifugation/filtration system to retrieve the desired sphere-size.

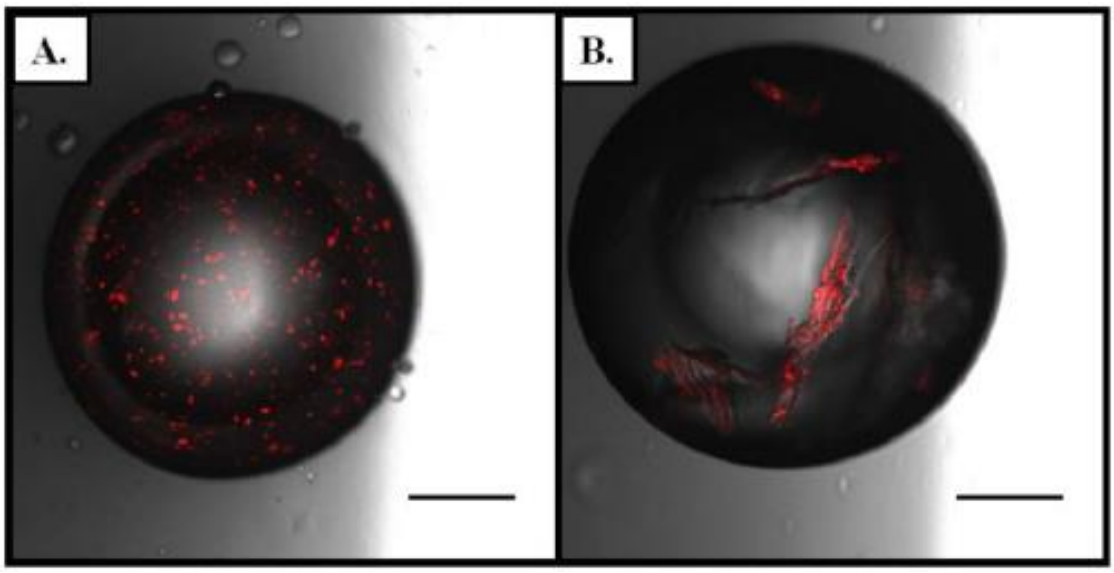

Figure 10: Hybrid fluorescence and bright-field images of the (A) PEG50 microspheres and (B) microporated microspheres. (Reference bar is 100 µm)

Typically, the sensing response for an assay is inhibited by the specific attachment strategy due to the manipulation of the free binding kinetics. For an aggregative assay like the ConA/glycosylated dendrimer system described here, such strategies would result in prohibiting any response by preventing the mechanism, aggregation, to take place. Since this strategy does not purposely employ the use of a covalent/ionic attachment, and instead allows the chemistry to remain free within pores it was hoped that the sensing response would be present and similar to that seen in solution. Figure 11 displays the titration response to monotonic increasing concentrations of glucose for microporated microspheres.

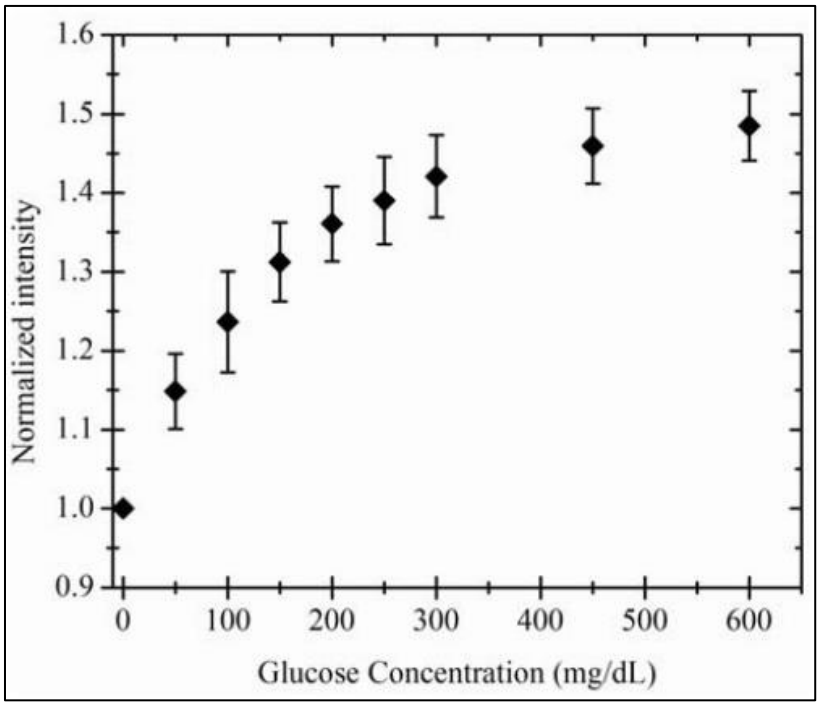

Figure 11: Fluorescence response of the assay containing microporated microspheres to glucose concentrations.

The microporated response is relatively linear from 50 to 200 mg/dL with a sensitivity of 1.3% per 10 mg/dL, and the response at 200 mg/dL is at 75% of the total response of the sensor. For comparison, Figure 12 displays the fluorescent response for the sensing assay in solution across physiological concentrations of glucose as compared to the microporated response – displaying a linear response through 500 mg/dL of glucose and a sensitivity of 1.8% per 10 mg/dL. Above 500 mg/dL, the sensitivity decreases to approximately 0.4% per 10 mg/dL. In free solution, the sensing chemistry is at approximately 35% of the linear dynamic response at 200 mg/dL. The microporated sensing spheres do show a slightly greater sensitivity through the hypoglycemic range (0-100 mg/dL); however, there is an overall decrease in the dynamic range and fluorescent signal. A possible explanation for this decrease includes the variable loading of sensing components since the ratio of free/bound competing ligand is dependent on the concentration of the receptor and competing ligand for steady-state glucose concentrations. Therefore, any change in either the ConA or glycosylated dendrimer concentration within the pores will shift the response in a manner similar to that observed. This shift can also be attributed to the confinement of the aggregative sensing assay within pores, a process that can theoretically shift the distribution of aggregates to favor smaller particles in comparison to free solution with a given glucose concentration because of entropy requirements and steric hindrances presented by the pores. As the fluorescent response is dependent on the extent of competitive binding, this shift in aggregation can shift the response to mimic that seen at higher glucose concentrations of the assay in free solution.

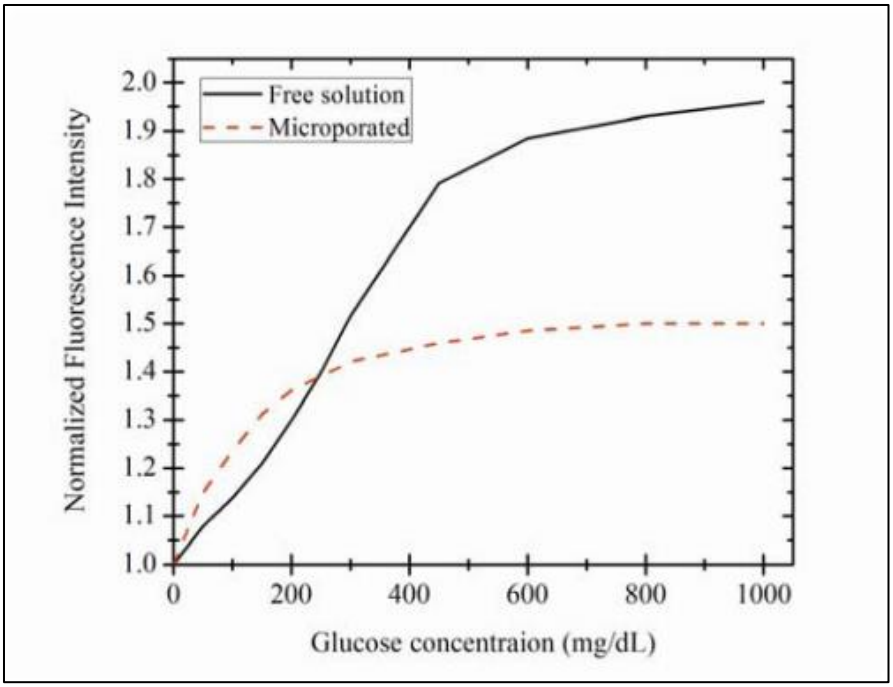

Figure 12: Comparison of the normalized fluorescence response of the assay in solution and microporated microspheres.

The standard deviation seen in the titration response of the microporated spheres was also higher than that for the free assay. This can be attributed to the variation which was seen in the poration of the spheres. The rinsing of spheres required to eliminate the glucose within the buffer between runs may have resulted in a different subset of spheres being interrogated each time that ultimately could add noise to the system. As previously mentioned, the dynamic range of the assay is a function of the aggregation associated with competitive binding between the ConA and glycosylated dendrimer. Therefore, the fluorescent response it is primarily dependent on the equilibrated glucose concentration. However, since the sensing chemistry is aggregative is nature, the dynamic range would

be dependent on the size of the pores that contain the assay if they limited the extent of aggregation. The dynamic range of the sphere size should be independent of the individual sphere size and porosity, given that they allow for the appropriate size for individual pores.

The response time of the sensing chemistry within the spheres is primarily dependent on the diffusivity of hydrogel, the size of the spheres, and the porosity (volume fraction) of the spheres for whatever system they are placed in. Specifically, higher diffusivities should decrease response time for equilibrium, larger spheres should increase diffusion distances and increase response time, and higher porosity should decrease diffusion distances and decrease response time.

The quantification of the leaching from within the microporated microspheres and PEG-50 microspheres is displayed by Figure 13. Upon 24 hours of exposure to highly concentrated volumes of glucose (600 mg/dL), the supernatant showed insignificant values of fluorescence from the fluorescently labeled ConA for microporated microspheres indicating that no leaching had occurred. In comparison, the plot of the fluorescence from the supernatant for the PEG-50 microspheres shows approximately 20% of the original fluorescence signal from the fluorescently labeled ConA and confirms the problematic leaching associated with the PEG-50 polymeric mesh for encapsulation purposes. For these PEG-50 microspheres, the aggregates are sufficiently large to remain entrapped within the polymeric crosslinks at low concentrations of glucose. However, upon the addition of glucose, ConA competitively binds to the analyte rather than the glycosylated dendrimer – decreasing the size of the

aggregates. The fluorescently labeled ConA chemistry attached to the glucose as well as the free glycosylated dendrimer is then capable of diffusing outwardly, into the supernatant. In contrast, the 100% PEG around the pores of the microporated microspheres seen via confocal microscopy is capable of withholding the assay throughout physiological concentrations of glucose due to the tighter mesh. As previously described, the long-term application of any sensing scheme requires an effective encapsulation/attachment method which disallows the undesirable release of key chemistry components. This leaching is effectively eliminated via the microporation technique and provides long-term functionality for the aggregative assay.

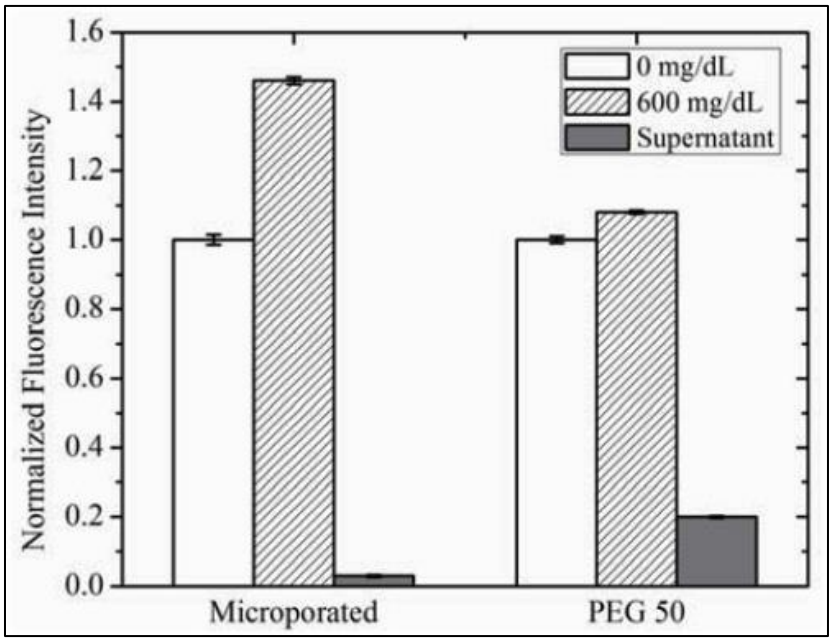

Figure 13: Fluorescence leaching studies from the microporated and PEG50 sensing spheres.

Fluorescent opto-chemical sensors often lose their functionality as a result of irreversible binding of the sensing components, photobleaching of the fluorophore, leaching of the chemistry, and/or the denaturing of the tertiary structure for the binding receptor.[37,108] In an attempt to address part of this potential problem with reversibility, glycosylated dendrimer was used in this system to avoid the increased binding affinity from a tetrameric unit of ConA binding to multiple sites, such as what may occur for a long chain like dextran, and by using AF 647 which is more resistant than other fluorophores, such as the rhodamine dyes, to photobleaching. As displayed in Figure 14, the microporated microsphere sensor is shown to respond to cycling from 0 to 300 mg/dL glucose concentration over fourteen days. The key result is that there is reversibility with no drop off toward the end of the two weeks, a result that has not been previously displayed. In terms of absolute count, the signal from the microporated spheres shows a declining trend. The majority of the aforementioned reasons for such a loss in functionality should be exponential in nature, but this absolute response does not appear to have a true exponential decay. This could be due to the combination of the effects on the aggregative assay. However, the relative increase from 0 mg/dL to 300 mg/dL each day shows no such trend. Therefore, a ratiometric sensing scheme using two fluorophores could be employed to maintain long-term functionality and reversibility. The relative results do show fluctuations in the response from day to day; however, as previously mentioned, we believe the variability in the relative readings between days is a result of polydispersity of the spheres in both the size and poration. Nonetheless, the data convincingly shows that microporated microspheres can effectively allow the

sensing assay to remain functional and reversible to varying glucose concentrations through fourteen days at ambient conditions.

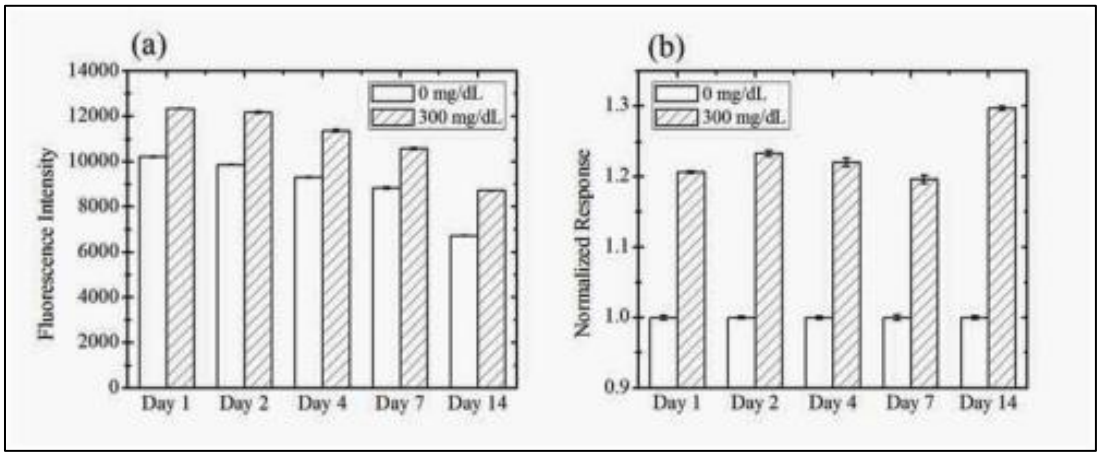

Figure 14: Reversibility studies for the glucose response of the microporated microspheres.

In this work, the ConA/glycosylated dendrimer glucose sensitive assay is shown, for the first time, to remain functional to varying glucose concentrations within polymeric microspheres. A microporation technique is used in which assay-filled pores are created within a polymeric mesh that allows the diffusion of glucose to the interior pockets while withholding the chemistry from outwardly diffusing throughout the competitive binding response. In addition, the microporation synthesis was shown to be advantageous for the aggregative sensing chemistry for several reasons: (1) it does not require the addition of powerful solvents to dissolve the porogen that could disrupt the tertiary structure of the protein, (2) the PEG hydrogel is hydrophilic and biocompatible

which allows it to ultimately be implanted within the dermal layers of the tissue, and (3) the cross-linking between PEG chains is covalent which is not susceptible to electrostatic binding of the sensing chemistry to the inner surface. As a result, the sensing spheres were shown to be responsive to glucose with a sensitivity of 1.3% per 10 mg/dL glucose from 50 to 200 mg/dL. In addition, because of the tight mesh surrounding the pores, there was shown to be effectively no leaching of the fluorescently labeled ConA from within the microporated microspheres.

Determining the Mechanism of the Sensing Assay

As the exact mechanism behind the sensor based on ConA and the glycosylated dendrimer is not well understood, a more thorough exploration into the dynamics was performed. Because ConA is a multivalent receptor and glycosylated dendrimers present multiple ligands, it is possible that the competitive binding that occurs is no longer simply a monovalent interaction. After ConA binds to a single glycosylated dendrimer, it can continue to bind to additional glucose moieties if given the appropriate binding conditions. Many groups have shown the extensive crosslinking that occurs between receptors that have multiple binding sites and ligands that have multiple moieties capable of being bound.[51,109,110] Therefore, this ConA/glycosylated dendrimer competitive binding chemistry could continue to crosslink over time. This extensive crosslinking could result in multiple pathways that decrease the fluorescence intensity of the AF647-ConA. This work attempts to measure how much (if any) aggregation is

actually displayed in a solution of ConA and glycosylated dendrimer by using Nanoparticle Tracking Analysis (NTA).

This NTA technique uses Stokes-Einstein equation to compare the motion of particles to the Brownian motion of spherical particles. Therefore, a histogram of particle sizes can be created from following the particle's motion. This was performed with Nanosight's LM10 instrument. Briefly, a 65 mW, 488 nm laser line was projected horizontally across a sample solution of 500 microliters. The particles that scatter this light within this plane are imaged using a 20X objective to focus the scattered light onto the EMCCD. Frames are taken over time and image processing is performed to follow the movement of individual particles. By following individual particles, this technique has been shown to be more effective than Dynamic Light Scattering (DLS) in determining the size distribution of a sample containing particles of mixed sizes.[111]

For this experimental set up, two sensing assays were created with 250 nM AF-647 Concanavalin A and 2 μM G2-NH2 glycosylated dendrimer in TRIS buffer. TRIS buffer was composed of 0.15 M NaCl, 0.01 M TRIS base, 1 mM CaCl2, and 1 mM MnCl2 at pH 7.4. One assay had no glucose added (A), and the other had glucose added at a final concentration of 100 mg/dL. The solution was given ten minutes to equilibrate. The solution was then added into the sample chamber of Nanosight's instrument and measurements were performed.

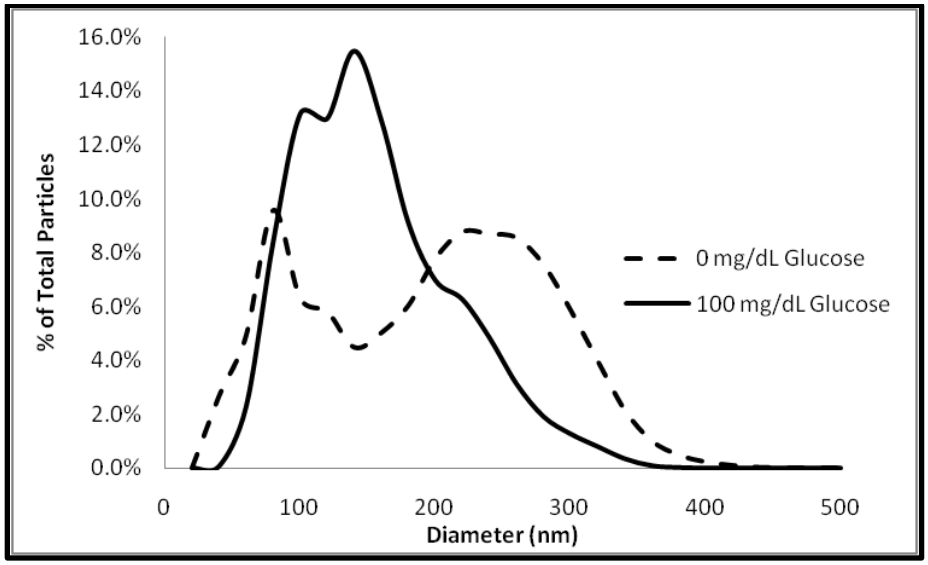

Figure 15: Glucose-dependent aggregate distribution for the ConA/glycosylated dendrimer assay.

Figure 15 shows the size distribution profile for these assays. The original sizes of the ConA and glycosylated dendrimer are 8 nm and 1.5 nm, suggesting that monovalent complexes between the ConA and dendrimer would be 10 nm. However, these results show that an assay that pairs ConA with this glycosylated dendrimer can form aggregates that are larger than 300 nm in diameter, indicating that a significant amount of aggregation is occurring. The distribution profiles of the two glucose concentrations suggest the addition of glucose shifts the aggregates to smaller sizes. It is expected that this trend would continue for increasing concentrations of glucose.

The aggregate distribution was expected to be broad, but it was expected to have a single maximum value with monotonic decays to both sides. The distribution for the 100 mg/dL glucose concentration resembles that expectation, but the distribution for 0

mg/dL does not have that characteristic shape. The leftmost peak for the 0 mg/dL distribution curve could be an example of an unreactive or damaged portion of the Concanavalin A where that mode is generated from aggregates reaching an ideal size. Other possible explanations could be related to the time response of the sensing chemistry – either we did not wait long enough for full aggregation to occur or the assay was actually falling out of solution.

Table 3: Results from NTA of ConA-based assay with glycosylated dendrimer.

Assay Response	***0 mg/dL glucose***	***100 mg/dL glucose***
Average Diameter (nm)	194	156
# Particles (*10^8/mL)	3.06	8.32

Table 3 shows the average particle diameter and number of particles in each solution. From these preliminary results, it appears that glucose decreases the mean size of aggregation and increases the number of particles within the system. This agrees with the concept that the aggregation is glucose dependent. The binding events to glucose would decrease the total number of receptors available for crosslinking to the glycosylated dendrimer. As the particle size decreases, the number of aggregates found in the system increases because the total dendrimer and receptor concentration remains constant.

Additional studies were attempted to explore this idea further, but showed limited success. Tracking the profile of aggregate size proves difficult because as aggregates grow larger, they have the propensity to fall out of solution. Figure 16 shows an example of an assay that had been prepared for NTA analysis, but had been left in solution for 2 hrs. This falling out of solution could explain the extreme changes in fluorescence that had been seen from labeled ConA, even when it was intended to be the FRET-acceptor. When the assay was loaded into similar cuvettes and tested using a traditional spectrofluorometer, the fluorescent material could have just fallen out of solution.

Figure 16: Visual precipitation of ConA-based assay paired with G2-NH2 dendrimer in the absence of glucose.

This type of aggregation cannot be tracked with NTA, because the technique requires the particles to be suspended in solution. Stirring the solution could potentially keep the aggregates in solution, but it would induce a particle motion that would be difficult to subtract for in the NTA program, and the kinetics of the assay would be different. As a result, the aggregation-studies using NTA were postponed and the design of the glycosylated dendrimer was examined further.

The glycosylated dendrimers that have traditionally been paired with ConA by our group have presented glucose moieties and amine functional groups at the surface of the molecule. Originally, this was a consequence of using the amine-reactive chemistry to attach glucose molecules (using either glucosyloxyethyl methacrylate or isothiocyanatophenyl β-D-glucopyranoside).[67,88,89] In those glycosylated dendrimers, a percentage of the primary amines were left unconjugated and left on the dendrimer. Each of the dendrimers tested from Dr. Simanek had also presented primary amines at the surface of the glycosylated dendrimer with the addition of 4-aminomethyl piperidine (4-AMP) as the last step of the triazine chemistry.[66,112,113] To explore the role that these primary amines have on the response of the glycosylated dendrimer, an alternative version of the glycosylated dendrimer was generated by Dr. Simanek that presented hydroxyl groups in their place (using 4-piperidinemethanol (4-PPM) instead of 4-AMP). Generation two dendrimers with 12 glucose groups and 12 hydroxyls (G2-OH) were compared to the generation two dendrimers with 12 glucose groups and 12 primary amines (G2-NH2).

In separate microplate wells, three solutions were made that each had a final volume of 300 µL. Each solution was in TRIS buffer (pH 7.4) and had 500 nM AF647-ConA. One of the solutions had no dendrimer. One had 500 nM G2-OH dendrimer, and the other had 500 nM G2-NH2 dendrimer. The peak fluorescence intensity of the AF647-ConA was measured, and these fluorescence intensities are shown in Figure 17.

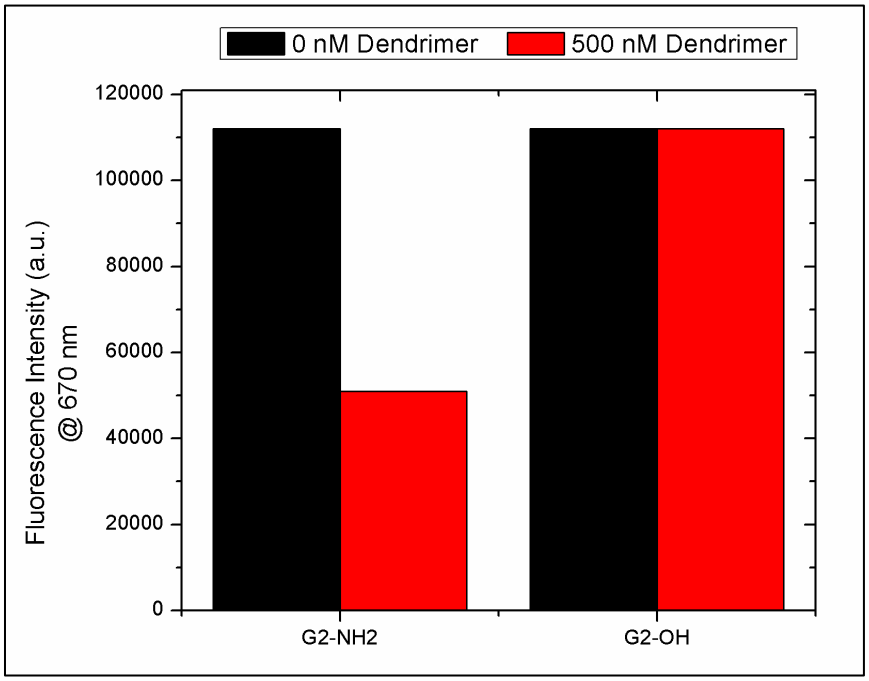

Figure 17: Fluorescence intensity of 500 nM AF647-ConA in the absence and presence of two different dendrimers (G2-NH2 and G2-OH).

This shows that the G2-OH dendrimer does not decrease the fluorescence in the same way that the G2-NH2 dendrimer does. This could be due to the G2-OH dendrimer not binding to ConA at the same affinity, possibly due to a decreased amount of non-

specific electrostatic interactions. A primary amine typically has a pKa around pH 9 and ConA's isoelectric point is ~5. Therefore at pH 7.4 in TRIS buffer, the dendrimers should display a net positive charge with multiple positive charges while ConA should display a net negative charge with multiple negative charges. The multiple charges on each molecule can allow for non-specific interactions to cause the cross-linking. In addition, this could be why the AF647-ConA that is labeled in our lab has generally displayed a more dynamic response than that which is purchased. The higher degree of labeling could make the ConA more negatively charged which would presumably increase the electrostatic interactions. It is also important to identify the conformation of the glucose moieties that are presented on the surface as ConA is shown to bind to the alpha-conformation of glucose much stronger than the beta-conformation.[52]

The decrease in quenching efficiency for the G2-OH dendrimer could also be that the quenching of the fluorescence actually has something to do with the amines. Deprotonated amines have been shown to undergo photo-induced electron transfer (PET) with various fluorophores.[114] AF647 is a cyanine based dye, and it is very likely that there are several deprotonated primary amines on the surface of the dendrimer at physiological pH due to the high level of crowding on a single dendrimer.[115] Upon aggregation, it is likely that fluorophores would be in close proximity to deprotonated primary amines. This could allow PET to occur.

Visual Precipitation

To have a qualitative understanding of the binding affinity, precipitation experiments were performed by pairing ConA with various ligands. Separate centrifuge tubes were loaded with 500 µL of 500 nM AF647-ConA and 500 nM of one of the following: (a) 500 nM G2-NH2 dendrimer, (b) .005 w/v% poly-l-lysine (PLL), or (c) 500 nM G2-OH dendrimer. The PLL is a polypeptide that has no glucose residues but displays many primary amines and is expected to be positively charged at physiological. A centrifuge tube of 500 nM AF 647-ConA was used as a control. Each of these solutions was in TRIS buffer. These solutions were allowed to interact with each other for 30 minutes, and then were centrifuged to force aggregates to fall out of solution. These centrifuge tubes were then examined for visual precipitation.

These experiments showed that the solutions with G2-NH2 dendrimer and PLL show visual precipitation (blue dot at the bottom from the AF647). The AF647-ConA control and the solution with G2-OH dendrimer do not show precipitation. This suggests that a good portion of the binding is due to the electrostatic interactions between ConA and the G2-NH2 dendrimer.

Glucose Response with PLL

To examine this more closely, an assay based on AF647-ConA and PLL was generated and exposed to glucose. Three microplate wells were loaded (final volume 300 µL) with a final concentration of 500 nM AF647-ConA in TRIS buffer. Two of these wells were loaded with a final concentration of 0.005 w/v% PLL. Finally, one of

those was loaded with a final concentration of 1000 mg/dL glucose. The wells were excited with 620 nm light and emission was collected from 650 nm to 720 nm to look at the emission from the AF647-ConA. This response is shown in Figure 18.

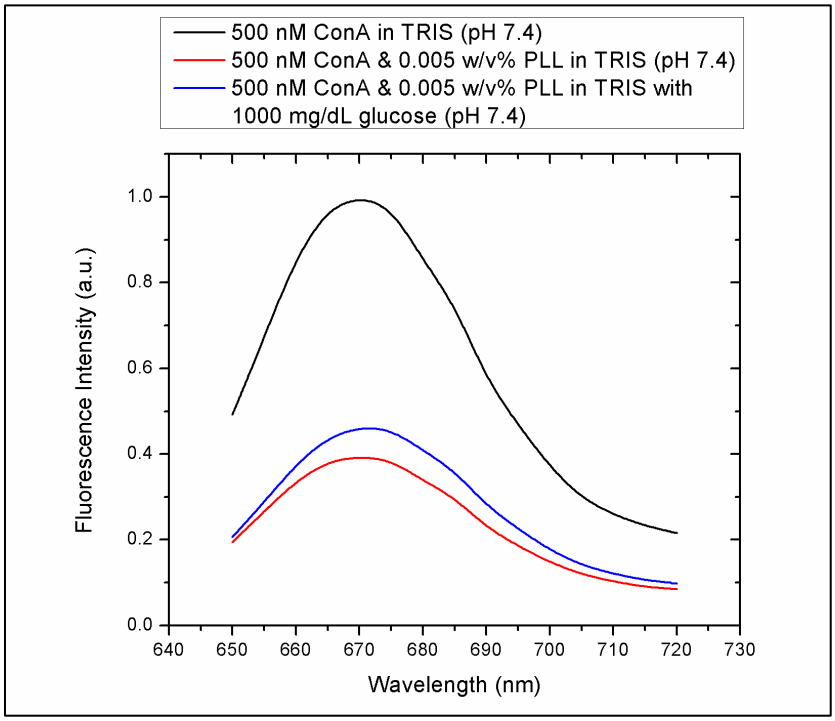

Figure 18: Fluorescence of 500 nM AF647-ConA in TRIS buffer (pH 7.4) (black), paired with PLL without glucose (red) and paired with PLL with glucose (blue).

Figure 18 shows that the fluorescence significantly decreases with the addition of the positively-charged PLL, in a very similar manner to the G2-NH2 glycosylated dendrimers. This could be attributed to aggregation induced by electrostatic interactions. The decrease in fluorescence could be due to scatter from the aggregation, falling out of solution due to the aggregation, PET from the aggregation, and energy transfer from the

aggregation. Upon addition of glucose, there is an 18% increase in the fluorescence intensity. While this isn't as large as the increases that have been seen with the G2-NH2 glycosylated dendrimer, it seems higher than error of the microplate reader and/or loading of the microplate. This indicates that the addition of glucose changes the electrostatic interactions between ConA and the PLL in some way. It could be due to glucose's ability to form Schiff bases with the amines on the PLL. This could potentially decrease the net charge of the PLL and could increase steric hindrances due to the open-chain glucose molecules extending from the PLL. These changes would decrease the electrostatic interactions and potentially break up the aggregation between the PLL and the AF647-ConA to allow fluorescence to be regained.

The same experiment was performed in bicarbonate buffer at pH 10.25 in an attempt to decrease the overall net charge on the PLL. This pH is above the pKa of lysine's primary amines and should cause the majority to be deprotonated. The results are shown in Figure 19. The addition of PLL displays less of a decrease to the fluorescence in comparison to the decrease seen in TRIS buffer. This suggests that the electrostatics play a significant role in the binding between G2-NH2 glycosylated dendrimers and ConA. The addition of the glucose again shows an increase in the fluorescence.

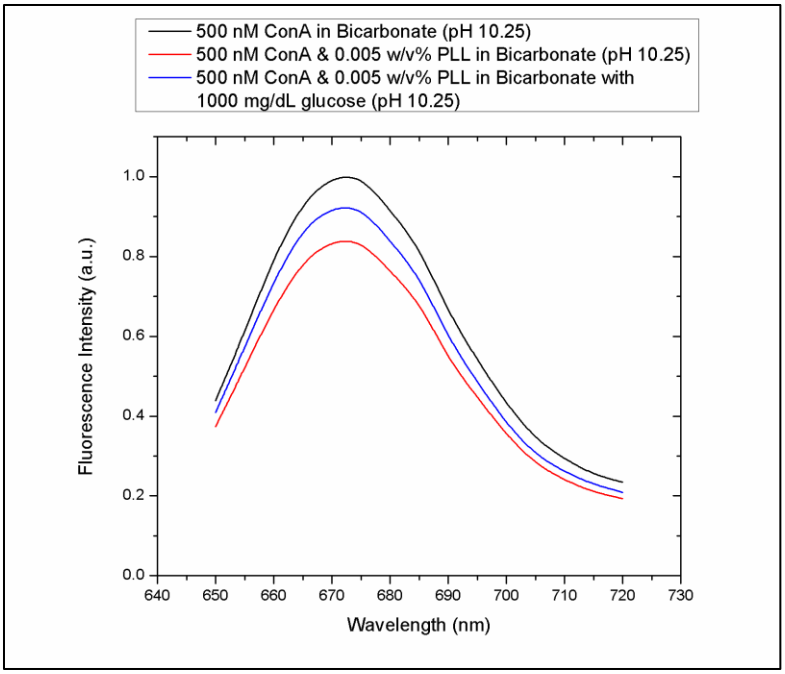

Figure 19: Fluorescence of 500 nM AF647-ConA in bicarbonate buffer (pH 10.25) (black), paired with PLL without glucose (red) and paired with PLL with glucose (blue).

This combination of results indicates that a net positive molecule without glucose residues can cause a decrease in the fluorescence of the AF647-ConA. In addition, it shows preliminary results that the fluorescence from such an assay can be increased upon the addition of glucose. This ConA/PLL assay does not have any specificity, because the PLL does not display moieties that can attach to the glucose binding site on ConA.

This exploration into the mechanism of the ConA/glycosylated dendrimer assay indicates that it is very complex sensing assay. It shows that the glycosylated dendrimer approach has used a combination of specific binding and electrostatic interactions to cause the binding to ConA. In addition, it has multiple possible pathways that can cause

decreases in measured fluorescence intensity. Since both assay components display multiple specific and nonspecific sources of interaction, it is not surprising that the assay shows a significant amount of aggregation in free solution. These aggregates were measured to reach several hundred nanometers in size, and were even visible to the eye after a fairly short amount of time. This aggregation can cause fluorescence responses in a myriad of different ways. It could significantly decrease the fluorescence intensity of an assay in a cuvette by just falling out of the beam-path - which is not expected to translate into a percutaneous or fully implanted sensor. The portion of the amines on the glycosylated dendrimer that are deprotonated could also undergo photo-induced electron with the fluorophore. To allow an assay to remains stable in free solution, it is essential to use a fluorescent ligand that simplifies the binding and fluorescence mechanisms.

Conclusions

For a sensor to be useful, it must be capable of responding in a predictable manner. To date, the ConA-based glucose sensor that uses the glycosylated dendrimer has shown problems with repeatability, and preliminary experiments suggest that a large portion of the quenching is due to aggregation that can cause the complexes to completely fall out of solution. This aggregation requires a unique strategy for encapsulation purposes. At its very best, this type of assay is a complex system that (1) does not follow typical competitive binding theory, (2) relies on non-specific electrostatic interactions, (3) and employs an aggregation mechanism that can allow the entire assay to fall out of solution. Receptors are used in binding assays to give it

specificity. The electrostatic interactions are seen with the primary amines on the glycosylated dendrimers are non-specific and decrease the specificity of the assay. The fluorescent competing ligand paired with ConA could eventually use a glycosylated dendrimer approach, but the dendrimers would need to be redesigned to cause a specific, predictable binding response to ConA.

CHAPTER III

MATHEMATICAL MODEL OF CONA-BASED GLUCOSE SENSOR BASED ON COMPETITIVE BINDING WITH FLUORESCENCE ANISOTROPY[*]

Introduction

Because the glycosylated dendrimer approach displayed problems with repeatability, reversibility, and specificity, a mathematical model was generated to guide the design of an optimized assay. Instead of allowing the recognition and transduction mechanisms to be dependent on each other, the goal is to design this assay to have them independent. Accordingly, these mechanisms are modeled independently to identify specific characteristics for the assay that maximize the fluorescence response to physiological glucose concentrations.

Fluorescent ConA-based sensors have typically used FRET to transduce the equilibrium binding with changes to either the fluorescence intensity or fluorescence lifetime. For a ConA-based assay with given association constants for the CL and glucose, there exists an ideal set of concentrations of ConA and CL at which the greatest change in binding will occur across the physiologically-relevant glucose range. However, the typical transduction mechanism of FRET requires the concentrations of

[*] Part of this chapter is reprinted from B. M. Cummins, and G. L. Coté, "A fluorescence polarization based assay for glucose sensing." 8229 (2012), with kind permission of SPIE, Copyright 2014; from B. M. Cummins, J. T. Garza, and G. L. Coté, "Optimization of a concanavalin A-based glucose sensor using fluorescence anisotropy," Analytical Chemistry, 85(11), 5397-5404 (2013), with kind permission of ACS, Copyright 2014.; and from B. M. Cummins, J. T. Garza, and G. L. Coté, "Limitations of current fluorescent glucose sensing assays based on competitive binding." 8591 (2013), with kind permission of SPIE, Copyright 2014.

the fluorescently labeled ConA and the fluorescently labeled CL to be on the same order to avoid significant amounts of non-specific absorption/quenching and spectral bleed-through by the FRET acceptor. This coupling of the transduction and recognition mechanism makes FRET a non-ideal technique to study the binding profile at the full range of assay concentrations. Therefore, unless the association constant between ConA and the CL is already tuned, the experimentally observed FRET response will not display the full-potential of the assay at the configuration that maximizes binding. Ideally, the binding would first be optimized for concentrations that can work for FRET, and the assay components would then be labeled with appropriate fluorophores to allow FRET to occur. A brief schematic of a FRET-based assay is shown in Figure 20.

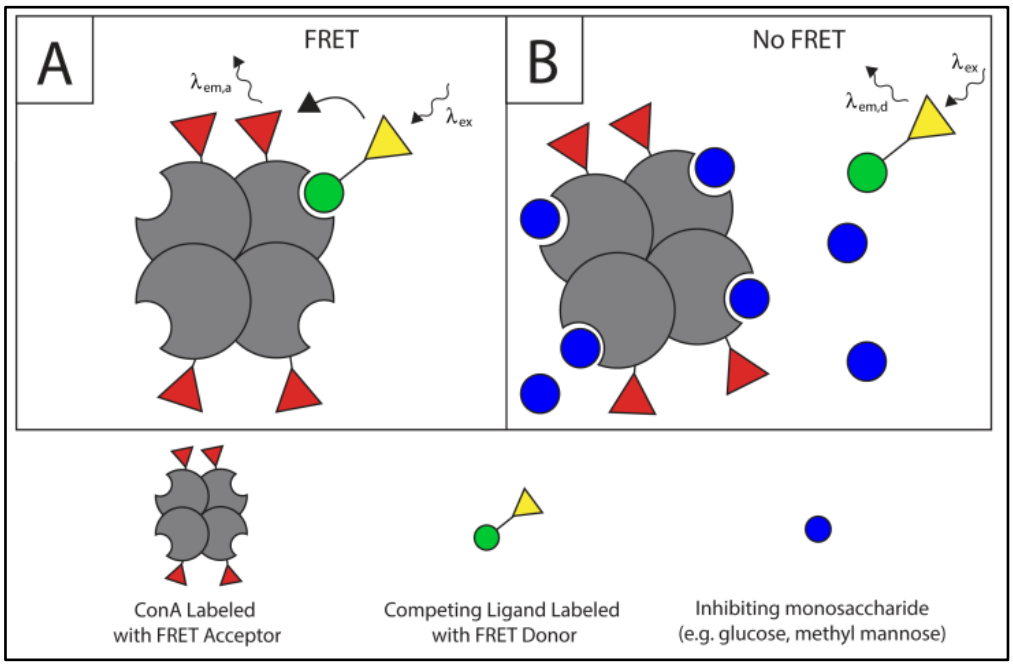

Figure 20: Schematic representation of a FRET assay based on competitive binding with ConA.

ConA-based assays have typically been generated by developing a unique CL and recording the FRET response of various ConA and CL concentrations against physiological concentrations of glucose. The concentration pair that elicits the greatest change in the measurable signal is identified as the optimized sensing assay. Because this measured signal is effectively the convolution of the recognition and transduction mechanisms, the sensor's response can misrepresent the full potential ConA has towards continuous glucose monitoring applications if both mechanisms are not optimized for the final assay configuration.

Unlike FRET-based approaches that track intensity or lifetime, fluorescence anisotropy (FA) is a polarization-based approach. While it would likely be unsuitable to be used in an implantable ConA glucose-sensor because of the highly depolarizing scatter from the tissue, it can be used as a transduction mechanism to characterize the capability of a ConA-based glucose sensor as long as the environment is low in scattering and the size of the CL is relatively small. Specifically, because FA requires only one labeled population, it can allow for both mechanisms to be fully optimized for a given assay configuration. Thus, the technique offers the user the capability of exploring a wider range of concentrations for a given set of association constants without the aforementioned transduction/recognition coupling concerns. By decoupling and independently optimizing these two mechanisms, it is possible for the sensitivity of the assay towards glucose to be enhanced and the true capability of ConA to be realized.

This chapter introduces a mathematical model for the recognition mechanism (competitive binding) and the transduction mechanism (fluorescence anisotropy) to

identify characteristics of an optimized fluorescence anisotropy competitive binding assay to track physiologically relevant glucose concentrations. Various assay-configurations based on the 4-kDa FITC-dextran fluorescent ligand are shown to validate the model. The results of this model are then presented in 2D sensitivity maps to clearly display the regions that are ideal for such an assay, and specific qualities are identified to optimize the anisotropy assay and other assays based on FRET. This description is then used in an attempt to describe the historical problems with ConA-based glucose sensors.

Mathematical Model

The ultimate goal for a fluorescence competitive binding assay is to be able to track the concentration of an analyte of interest with the fluorescence from that sample. The competing ligand is chosen to be the fluorescent ligand that is tracked in this assay because it gives us more control and avoids potential problems with protein denaturation. Here, we introduce a model for a fluorescence anisotropy competitive binding assay based on ConA for glucose sensing that tracks the fluorescence from the competing ligand.

Background and Theory

Fluorescence anisotropy (FA) has been extensively used within the field of biochemistry to explore molecular interactions.[116] More specifically to this work, FA has been used as a transduction technique in the field of glycobiology to determine

association and inhibition constants for various sugars.[117-119] These assays have recently been complemented with high throughput glycan arrays to allow for the quick determination of interactions between a receptor and a diverse set of glycans.[120-122] FA remains a powerful spectroscopic technique to transduce events occurring on the molecular level.

Briefly, FA is a homogeneous and reproducible method that can be used to explore the average rotational diffusion rate of the fluorescently labeled molecules in a given system. By interrogating the system with plane polarized excitation light, information can be retrieved about the rotational speed of the fluorescent molecules from the polarization of the fluorescence. In an FA measurement, vertically polarized excitation light selectively excites the fluorophores in the solution that have the appropriately oriented excitation dipoles. During the period of time that the fluorophore is in the excited state, the molecule is free to rotate in solution. Because larger molecules tumble more slowly than smaller molecules, they could display a higher FA even if they are labeled with the same fluorophore. In a binding assay, the portion of the fluorescently labeled ligands that are bound can display a higher FA than the portion that is free. This typically requires the receptor to be larger than the fluorescent ligand and the appropriate fluorophore to be used. The schematic in Figure 21 shows an optimized assay in which the bound population (bottom) displays a higher FA than the free population (top).

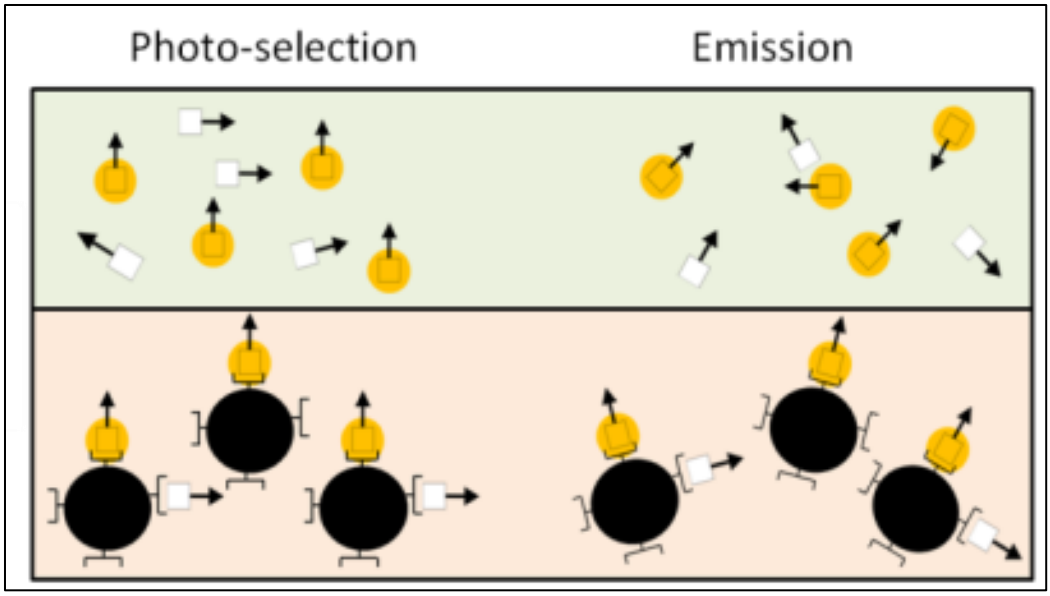

Figure 21: Schematic representation of the change in rotational speed of fluorescent ligands upon binding. (White square: fluorescent ligand, arrow: dipole of fluorophore, yellow circle: excited fluorophore, dark circle: receptor)

Theoretically, FA (r) can exist from -0.5 to 1, but these limits are only reached when all dipoles are aligned upon photo-selection. In free solution, the dipoles are randomly oriented when photo-selection occurs, and the limits of FA are -0.2 to 0.4. In practice, the polarized fluorescence intensity is measured in the parallel ($F_{\parallel}$) and perpendicular ($F_{\perp}$) directions (defined by the polarization of the excitation light), and the FA of a sample is calculated as shown in Equation 1.

$$r = \frac{F_{\parallel} - F_{\perp}}{F_{\parallel} + 2F_{\perp}} \quad (1)$$

In a FA competitive binding assay, the FA will effectively track the average rotational speed of the fluorescent ligands in the sample. As seen in Equation 2, the experimentally observed FA (<r>) corresponds to the linear summation of fluorescent populations with unique FA values (r_i) with regard to their fractional contributions of the total intensity measured (f_i). Because our competitive binding assay will be engineered to only display two fluorescent populations within the sample – a bound population and a free population – this can be written as Equation 3.

$$< r >= \sum_{i=1}^{n} f_i \, r_i \tag{2}$$

$$< r >= f_b r_b + f_f r_f \tag{3}$$

The glucose-dependent competitive binding changes the fractional fluorescence intensity that comes from the bound and free populations. If we assume that the quantum yield of the fluorescent ligand does not change upon being bound, the fractional fluorescence intensity that comes from the bound can be described with the percent of the fluorescent competing ligand that is bound (%CLB) and Equation 3 can be written as Equation 4. The sensitivity of this assay (the change in the anisotropy across a certain glucose range) can then defined by Equation 5.

$$< r >= \%CLB_{(G)} r_b + \left(1 - \%CLB_{(G)}\right) r_f \quad (4)$$

$$\frac{\Delta < r >}{\Delta G} = (r_b - r_f) \frac{\Delta \%CLB}{\Delta G} \quad (5)$$

This explicitly defines the sensitivity of the assay as a function of the two mechanisms involved: the transduction mechanism and the recognition mechanism. In order to maximize the assay's sensitivity and generate the ideal sensor, both mechanisms need to be optimized. To optimize the transduction mechanism of the assay, the goal is to maximize the change in steady-state anisotropy between the bound and free populations ($r_b - r_f$). The recognition mechanism can be optimized by maximizing the change in the %CLB across the glucose range of interest ($\frac{\Delta \%CLB}{\Delta G}$).

Transduction Mechanism: Fluorescence Anisotropy

To identify characteristics of a competitivve binding assay that can maximize the sensitivity associated with the transduction mechanism, the fluorescence anisotropy was modeled. Figure 22 shows a schematic where the fluorescence anisotropy is higher in the bound state than the free state. By using a labeled CL with a low molecular weight and a receptor with a high molecular weight, the degree of binding can effectively be tracked via FA.

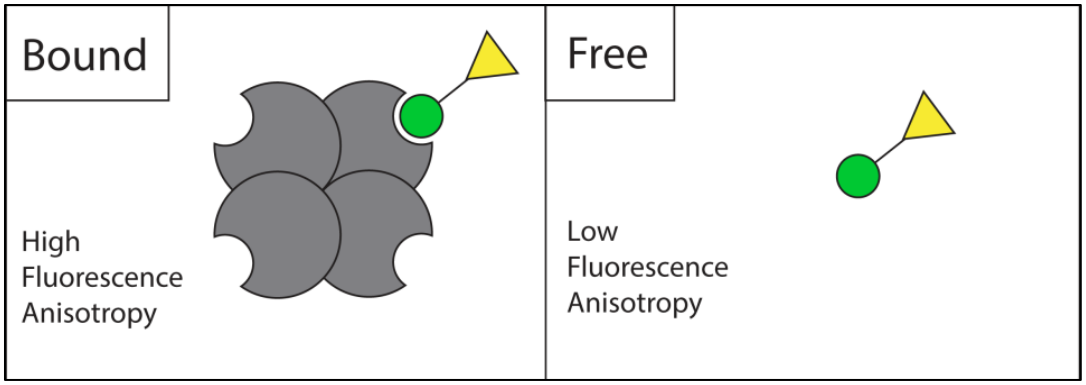

Figure 22: Schematic representation of the transduction mechanism for a fluorescence anisotropy assay based on competitive binding with ConA.

The fluorescence anisotropy of a given population is the relationship between the average time that the fluorophore is in the excited state (fluorescence lifetime) and the average time that takes the molecule to tumble (rotational correlation lifetime). This relationship has been described using Perrin's equation (Equation 6). The value r_o is the intrinsic anisotropy value for a given fluorophore, τ is the fluorescence lifetime of the fluorophore, and φ is the rotational correlation lifetime of the fluorophore. For a spherical particle, the rotational correlation lifetime is defined in Equation 7 (M: molecular weight, T: temperature in Kelvin, R: universal gas constant, η: viscosity, v: partial specific volume, h: degree of hydration).

$$r = r_o / \left(1 + \frac{\tau}{\varphi}\right) \tag{6}$$

$$\varphi = \frac{\eta M(\upsilon + h)}{RT} \tag{7}$$

This allows the FA to be predicted for various fluorescent ligands according to their molecular weight and fluorescence lifetime by modeling Perrin's equation (Eq. 6) for spherical particles (r_o = 0.4, T = 293 K, η = 0.01 cP, υ = 0.73 cm^3/g, h = 1.17 ml/mg, and R = 8.321*10^7 erg/K·mol). To generate an expected FA for the fluorescent ligands when they are bound to ConA, the same spherical particle assumption was made and the MW used in Perrin's equation was increased by 104 kDa (the size of ConA). These predictions assume that (1) the local mobility of the fluorophore is negligible, (2) the CL is effectively spherical, and (3) the CL/ConA complex is effectively rigid and spherical. The change in FA upon binding to ConA was determined for each theoretical fluorescent competing ligand (defined by a fluorescent lifetime and a MW), and these results are plotted in Figure 23. The set of fluorescent competing ligands in Table 4 are identified on this 2D sensitivity plot.

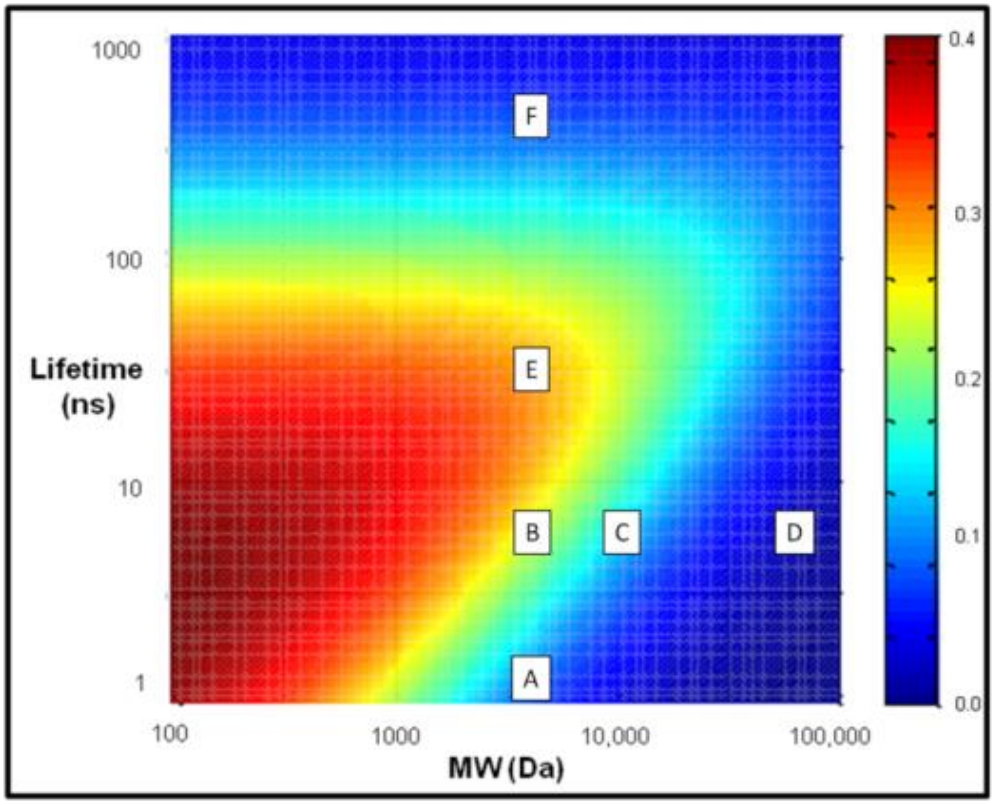

Figure 23: Modeled change in anisotropy upon binding to ConA for various fluorescent ligand properties. Boxes represent the fluorescent ligands in Table 4.

Table 4 shows that the FA of 4 kDa AF 647-dextran is relatively constant at the high end of the possible FA range, suggesting that its lifetime is too short to allow the glucose-response to be observable via FA. The fluorophore is expected to fluoresce prior to significant rotation of the ligand in both the bound and unbound states. The ruthenium-based fluorescent ligand also appears to be unsuitable to track the competitive binding; it appears to lose most of the anisotropy information before it fluoresces regardless of whether it is bound.

Table 4: Modeled bound and unbound FA values at 293 K in water.

	Competitive Ligand (CL)	$FA_{unbound}$	$FA_{bound\ to\ ConA}$
A	4 kDa AF 647-dextran	0.303	0.395
B	4 kDa FITC-dextran	0.175	0.382
C	10 kDa FITC-dextran	0.264	0.383
D	70 kDa FITC-dextran	0.373	0.389
E	4 kDa Dansyl Chloride-dextran	0.054	0.323
F	4 kDa Ruthenium-dextran	0.004	0.088

Dextrans with increasing molecular weights were also explored, but the difference in FA upon binding is shown to decrease with increasing size of the CL. Ligands smaller than 4kDa dextran would increase the predicted difference further; however, the association constant would decrease to a level that is unsuitable for competitive binding.

The 4 kDa FITC-dextran and the 4 kDa dansyl chloride dextran appear suitable, showing an FA difference of 0.207 and 0.269 between bound/unbound states, respectively. However, dansyl chloride is an environmentally sensitive fluorophore that could increase its fluorescence intensity when brought close to hydrophobic residues upon dextran's binding to ConA. FITC is insensitive to the environment's polarity, but is known to be pH sensitive due to its carboxyl and phenol groups. Fluctuations in pH can be minimized by using TRIS buffer at pH 7.4. Thus, 4 kDa FITC-dextran was

chosen as the fluorescent competitor to be used in experimental studies as it should generate a suitable change in FA and is commercially available. The competitive binding was then modeled for this specific ligand to predict glucose responses of various assays.

Recognition Mechanism: Competitive Binding

For the modeling of the competitive binding, we make the assumptions that (1) the interaction between ConA and the fluorescent ligand can be defined with an association constant and that (2) the interaction is monovalent. This means that if ConA and the fluorescent ligand were placed in solution, there would only be two populations for each component in existence (bound and free). We make the same assumptions for ConA's interaction with glucose. In addition, we make the assumption that the binding of glucose and the fluorescent ligand to ConA is directly competitive. If ConA's binding site is bound to glucose, it cannot bind the fluorescent ligand and vice versa. With those assumptions, the following equations can be used. A schematic representation of the competitive binding (the recognition mechanism) is shown in Figure 24.

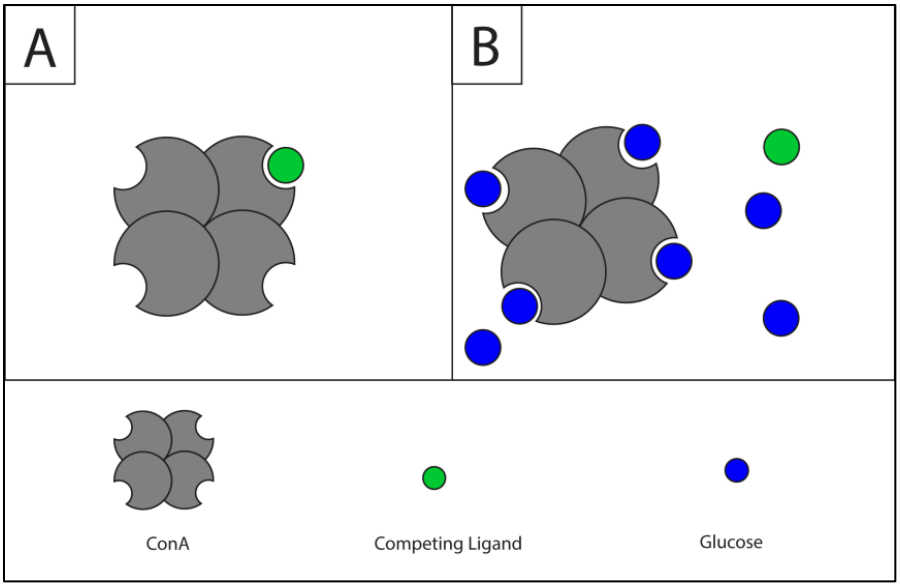

Figure 24: Schematic representation of the recognition mechanism of the fluorescent anisotropy assay based on competitive binding with ConA

$$[C_t] = [C-G] + [C_f] + [C-L] \quad (8)$$

$$[L_t] = [C-L] + [L_f] \quad (9)$$

$$[G_t] = [C-G] + [G_f] \quad (10)$$

$$K_{CL} = [C-L]/([C_f] * [L_f]) \quad (11)$$

$$K_{CL} = [C-G]/([C_f] * [G_f]) \quad (12)$$

In these equations, [C_t], [C-G], [C_f], [C-L], [L_t], [L_f], [G_t], and [G_f] are defined as the concentrations of total ConA, ConA bound to glucose, free ConA, ConA bound to the competing ligand, total competing ligand, free competing ligand, total glucose, and

free glucose, respectively. The association constant K_{CL} is the affinity of ConA to the competing ligand and K_{CG} is the affinity of ConA to glucose. The association constant of tetrameric ConA to glucose and methyl alpha-mannose has been shown to be 400 M^{-1} and 8,200 M^{-1}, respectively.[48,123] The association constant of the tetrameric ConA to the competing ligand can be varied by the choice of the competing ligand.

The exact solution to Equations 5-7, as described by *Wang*, can be used to determine the expected concentrations of each population at equilibrium. This is a function of the total concentrations of the competing ligand, ConA, and glucose as well as the association constants of ConA to the glucose and the competing ligand.[124] Therefore, a competitive binding assay can be fully defined by the total ConA and total competing ligand in the assay as well as ConA's association constants to the competing ligand and glucose. Keeping each of those quantities fixed, the equilibrium binding can be solved for a specific glucose concentration. This solution to the equilibrium binding describes the concentration of each of the populations that are found in the solution. Multiple glucose concentrations can be solved for to determine the glucose response for that 'assay.'

For a competitive binding assay that fluorescently labels the competing ligand, the amount of competing ligand in the bound population needs to change as a function of the glucose concentration. Because we defined the fluorescent competing ligand to only be capable of being in two states, this population can be tracked by calculating the %CLB. For a molecule that does not change its quantum yield upon binding to ConA, the %CLB is equivalent to the fractional fluorescence intensity that comes from the

bound population. Figure 25 shows the effect that physiological glucose concentrations have on the %CLB of three different assays.

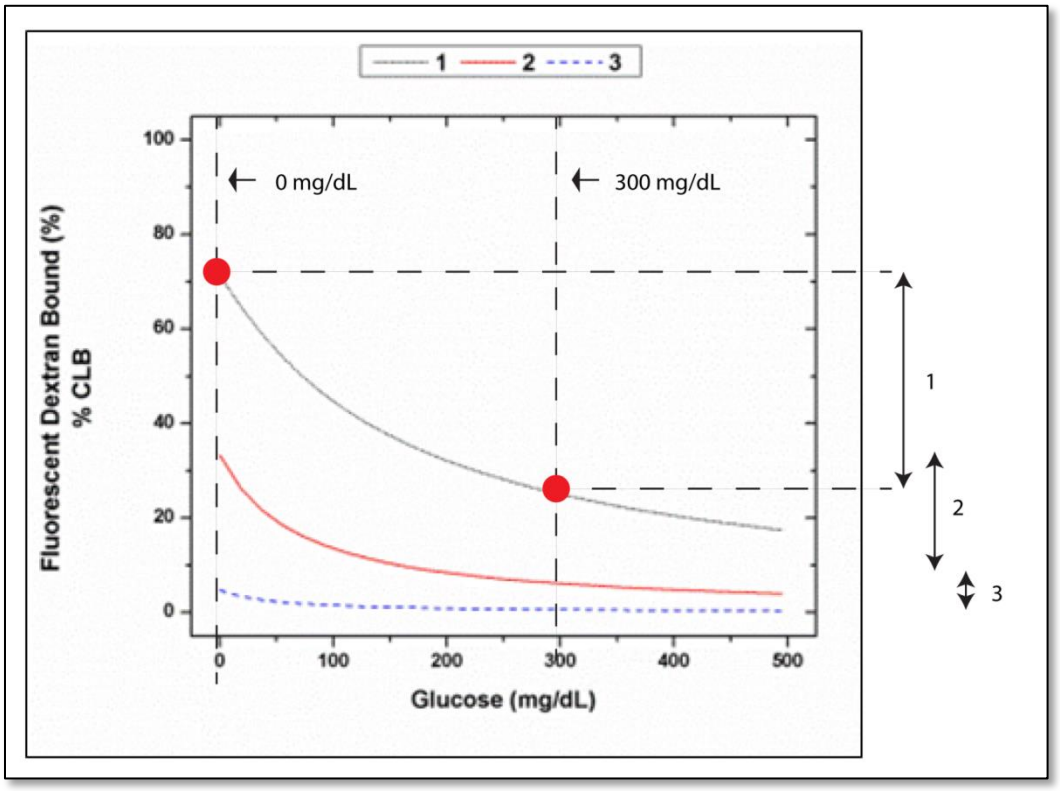

Figure 25: Modeled responses of fluorescent dextran bound (% CLB) vs. glucose for different assay configurations: The change in % CLB from 0 mg/dL to 300 mg/dL for 1, 2, and 3 is 45%, 27%, and 4%, respectively.

The goal of a specific assay is to maximize the absolute change in the %CLB across the desired concentration range for the analyte of interest (i.e. glucose). An assay that generates a higher change in the %CLB across this range would be identified as a more sensitive assay. In this set of assays, Assay 1 is identified as being the most

sensitive because it has the greatest change across the range of interest. To identify that sensitivity with a figure of merit, this work identifies the range of interest for glucose to be 0 mg/dL glucose to 300 mg/dL. For the %CLB vs. glucose curve for a given assay, the difference in the %CLB at these two glucose concentrations is proportional to the sensitivity of the assay. Assay configurations that display similar changes in the %CLB across this range should display similar changes in the measured anisotropy across that range.

For a ConA-based assay that has already chosen its competing ligand (effectively fixing the K_{CL}), this model can be used to identify the optimal concentrations for the competing ligand and ConA that maximize the sensitivity of the assay. The model sweeps through all possible concentrations for ConA and the competing ligand and can generate a map of the change in %CLB for all the configurations. Figure 26 is an example where the competing ligand is chosen to be 4 kDa dextran. Assuming typical branching seen in dextrans, 4 kDa dextran should have ~3 non-reducing termini per dextran molecule and the effective affinity of ConA to the 4 kDa dextran should be ~5000 M^{-1}.[61] Using association constants for ConA to glucose and 4 kDa dextran to be 400 M^{-1} and 5000 M^{-1} (respectively), this shows that the maximum recognition sensitivity (~45% change in %CLB) of this assay is expected to be seen for an assay composed of ~500 µM ConA with a dextran concentration less than 100 µM.

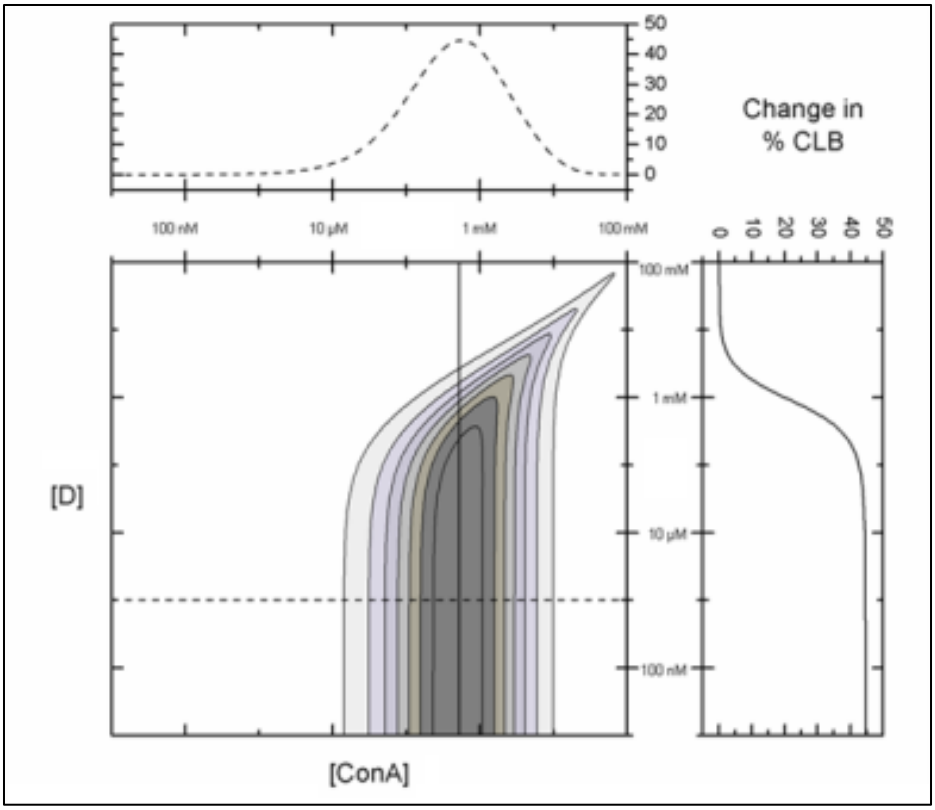

Figure 26: Change in % dextran bound to ConA (% CLB) from 0 mg/dL to 300 mg/dL glucose for various ConA and dextran (D) combinations. Top inset: Change in % CLB vs. [ConA] with [D] fixed at 1 µM (dotted line). Right inset: Change in % CLB vs. [D] with [ConA] fixed at 500 µM (solid line).

Dextran concentrations higher than 100 µM (for a fixed concentration of ConA at 500 µM) begin to show a decreased response to glucose because the % CLB at 0 mg/dL glucose begins to decrease. A similar response is observed using an optimized dextran concentration (1 µM with concentrations of ConA significantly below 500 µM. For concentrations of ConA that are significantly higher than 500 µM ([dextran] at 1 µM), the addition of glucose to physiologically-relevant concentrations has little effect on the

% CLB. Even after the binding of glucose, there is sufficient ConA available to bind the majority of the fluorescent dextran at these ConA concentrations.

The full %CLB vs. glucose responses of various assay configurations are shown in Figure 27 and Figure 28. Figure 27 shows the responses of assays with various ConA concentrations (5 µM-100 mM) for a fixed dextran concentration (100 nM). Figure 28 shows the responses of assays with various dextran concentrations (100 nM-10 mM) for a fixed ConA concentration at 500 µM.

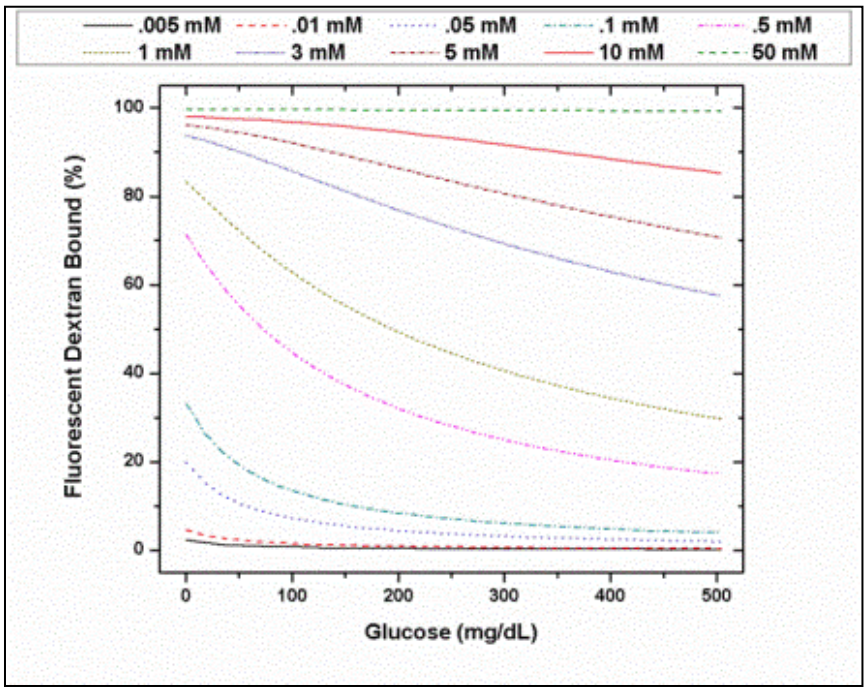

Figure 27: Modeled %CLB vs. [glucose] for competitive binding assays based on 1 µM dextran and varying [ConA].

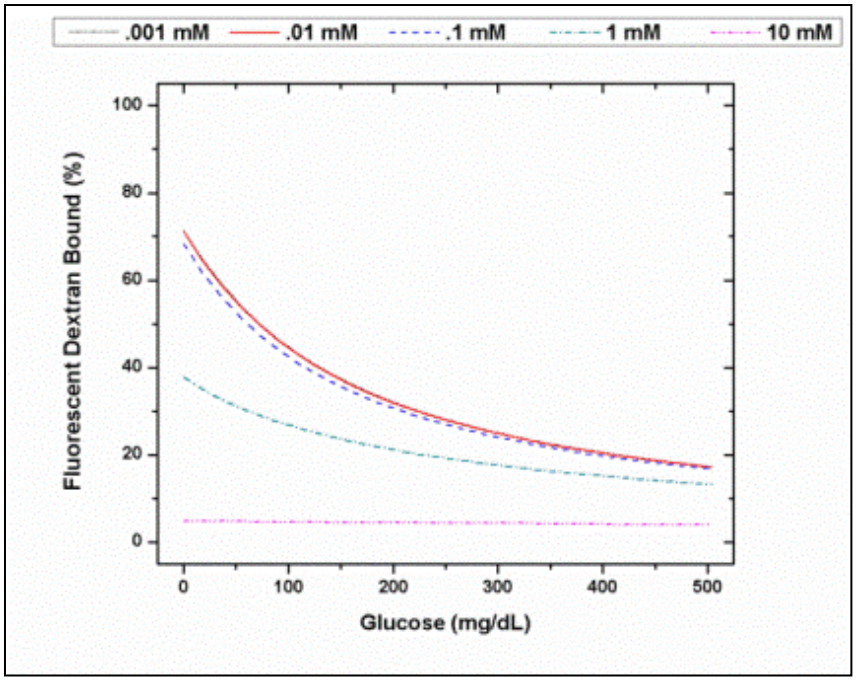

Figure 28: Modeled % CLB vs. [glucose] for competitive binding assays based on 500 µM ConA and varying [dextran].

In reality, an assay that uses 4-kDa dextran as the competing ligand cannot achieve the maximum sensitivity of the assay (as defined by change in %CLB). The solubility limit of native ConA in a physiologically relevant buffer has been shown to be ~100 µM. Therefore, ConA concentrations cannot be higher than this in a stable assay in free solution.

While we have shown that this model can identify the ideal concentrations of ConA and competing ligand for a given competing ligand, this model can also be used to help identify an ideal competing ligand to optimize the assay binding. By fixing the concentration of the fluorescent ligand in the solution, one can predict the glucose

responses for a given K_{CL} and [ConA]. In real fluorescence measurements, it is often desirable to limit the concentration of the fluorophore in the solution to avoid inner-filter effects.[125] According to the degree of labeling of the fluorescent ligand, this fixes the concentration of the fluorescent ligand. Figure 29 is a log-log plot that shows a 2D sensitivity plot for a fluorescent competing ligand concentration of 500 nM. The recognition sensitivity is plotted as a function of the ConA concentration and the K_{CL}.

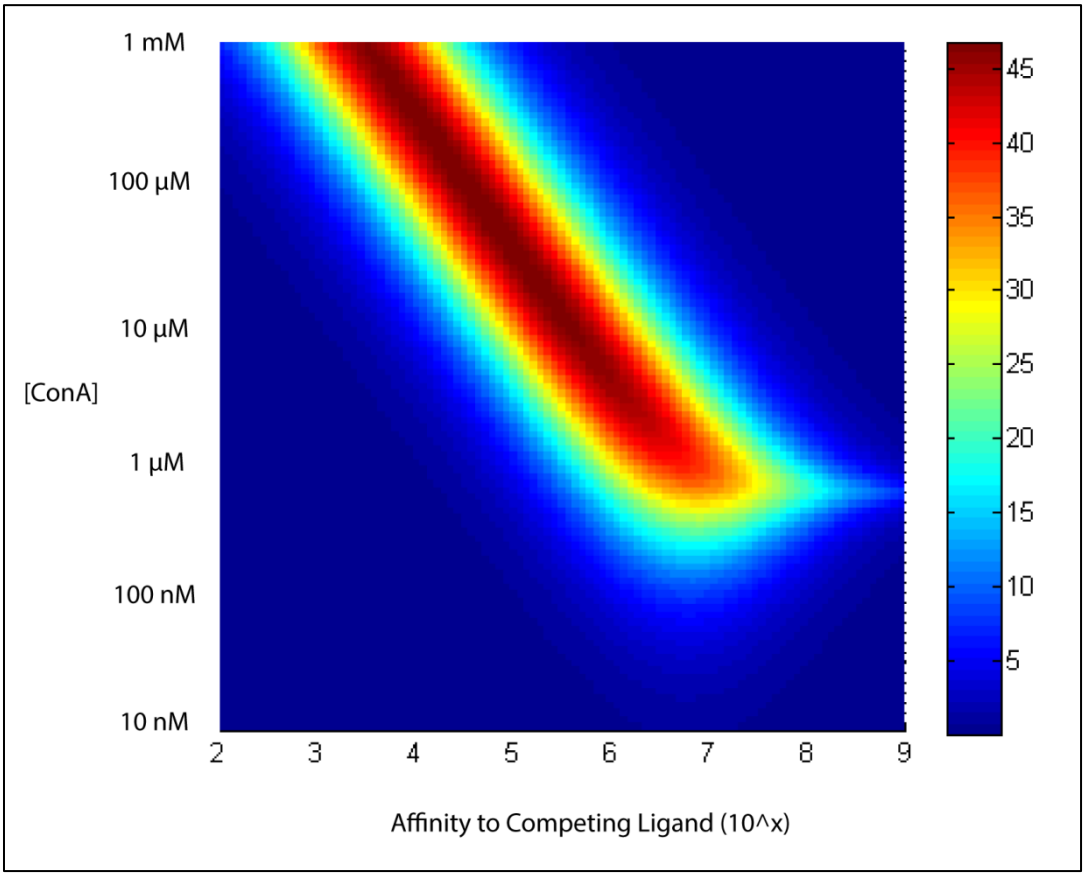

Figure 29: Change in %CLB across physiological glucose concentrations (recognition sensitivity) for 500 nM fluorescent ligand (CL) as a function of the [ConA] and K_{CL}.

In this figure, the blue regions show very little change in the %CLB across the previously identified glucose concentration range. The red portions of the graph indicate the largest possible changes in the %CLB across this range. The maximum value for this change is approximately 45% and is a result of the association constant between ConA and glucose. For the glucose concentration range of interest (0 mg/dL-300 mg/dL), it is not possible to have a larger change in %CLB with native ConA.

This 2D plot shows that by increasing the apparent affinity between ConA and the competing ligand, you require a lower concentration of ConA to track the binding to glucose. This provides some insight as to why groups have typically used multivalent competing ligands in ConA-based assays. The affinity to monosaccharides is typically low (~10^3 M^{-1}), and would require ConA concentrations that are above the solubility limit of ConA.[126] By increasing the affinity to ConA with multivalent competing ligands, the maximum sensitivity can be achieved with the appropriate ConA concentration.

It is important to note that the concentration of the competing ligand that is chosen only changes where the sensitivity trails off at the lower-right portion of the graph. This trail-off point happens at a ConA concentration that is roughly 2 times the chosen competing ligand concentration. At ConA concentrations lower than this, there is not enough ConA to bind a considerable portion of the competing ligand. By choosing a higher competing ligand concentration, the trailing off region would happen along this diagonal at higher concentrations of ConA. Lower competing ligand

concentrations would allow lower ConA concentrations (and higher affinity ligands) to be used and still achieve maximum sensitivity for the recognition mechanism.

Validation of Model

This model was then validated with experiments with the 4 kDa FITC-dextran competing ligand. For the assay configurations listed in Table 5, the expected FA vs. glucose responses were modeled for physiologically relevant glucose concentrations (0-500 mg/dL) with Equation 2. These responses were calculated by using the FA_i and f_i values that were previously predicted for 4k-FITC-dextran. The FA_i from Equation 2 was replaced by the FA_{bound} and $FA_{unbound}$ for 4 kDa FITC-dextran populations from Table 4. The f_i in Equation 2 was replaced by the appropriate % CLB value as predicted by the competitive binding modeling. Again, this can be done by assuming the quantum yield to stay constant upon binding. Because the % CLB is a function of glucose, the observed FA is dependent on glucose concentration in the system.

Table 5: List of assay configurations tested in the validation of model.

Assay Configuration	***[4 kDa FITC-Dextran] (nM)***	***[ConA] (μM)***
1	100	100
2	1000	100
3	100	10
4	100	1
5	100	0.1

The assay configurations were chosen to display a range of predicted sensitivities to demonstrate the effectiveness of the FA-competitive binding model. Unfortunately, the assay configuration that showed the maximum sensitivity was not able to be generated due to the solubility limit of ConA, but some assay configurations were chosen to achieve the maximum possible sensitivity for this competing ligand. All assays are assumed to have the same FA values for the bound and unbound dextran populations because the same fluorescent competing ligand was used. The differences in the different assay configurations should be a result of differences in the binding at equilibrium.

Glucose-Dependent Fluorescence Responses

The actual FA response to glucose concentrations (0-500 mg/dL, 50 mg/dL steps) for each of these assay configurations was determined experimentally. All fluorescence measurements were obtained using black, flat-bottom, 96-well plates on a microplate reader (Tecan model F200) equipped with bandpass excitation filters (483 ± 15.5 nm), emission filters (540 ± 25 nm) and polarizers (Tecan). The G-factor was calculated using a known FA value for 1 nM fluorescein (0.018), and all subsequent runs used this adjustment factor to yield corrected data.

Highly concentrated stock solutions of the individual assay components were prepared using TRIS. Plates were quadruplicate loaded with the assay components, including glucose, and given time to reach equilibrium prior to analyzing in the plate reader at room temperature. The actual glucose concentration was defined to be the

prepared concentration. Triplicate fluorescence scans were collected from each well of the microplate in the parallel and perpendicular directions. The actual FA value for each well was calculated by subtracting the TRIS background from each measurement, accounting for the differences in detector sensitivity to polarized light with the G-factor, and solving for FA with Equation 1. The modeled and experimental glucose responses of each assay configuration are shown in Figure 30.

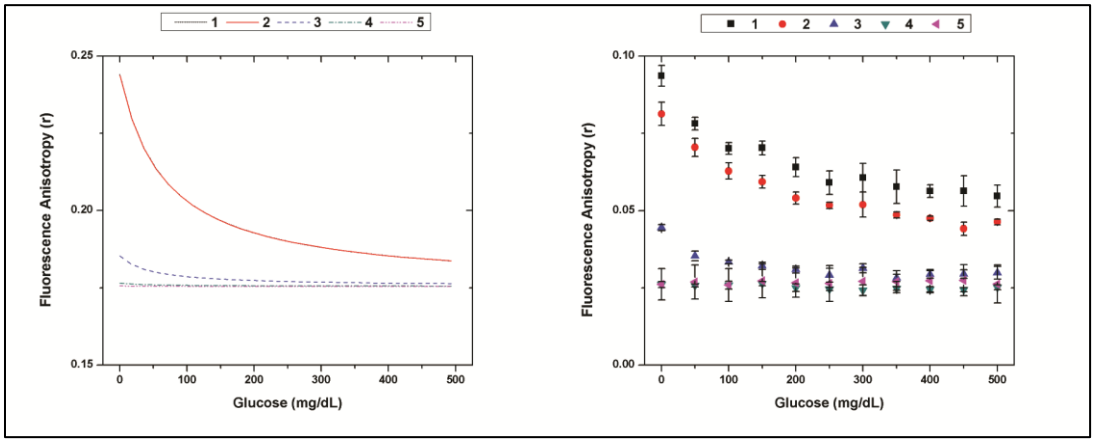

Figure 30: (left) Modeled FA glucose response and (right) experimentally observed FA glucose response for the assay configurations in Table 5. The modeled curves for 1 and 2 lay on top of each other and the error bars depict the standard deviation from the triplicate runs.

The experimental response for each assay configuration displayed the trend that was predicted with the model. For the same concentration of FITC-dextran, the assays using higher concentrations of ConA elicited a higher dynamic range across physiological glucose concentrations. At 1 µM ConA and lower, there was effectively no response from the assay, which was predicted as shown in Figure 26. In addition, a

large range of dextran concentrations (100 nM to 1 µM) for a given ConA concentration (100 µM) showed an effective, dynamic response. The dynamic range of the assay could be increased further by using concentrations of ConA up to 500 µM. However, the solubility of the protein limited the highest concentrations of ConA to be 100 µM. This extended dynamic range could be obtained if the fluorescent CL had a higher affinity to ConA, decreasing the required ConA concentration.

Any assay has theoretical limits for what is possible. To display the relative effectiveness of each assay to achieve its full potential, the percent optimization was determined for the individual mechanisms. The percent optimization of the transduction mechanisms was defined as the expected change in anisotropy for each assay over the maximum possible change in anisotropy (0.4). The percent optimization of the recognition mechanism was defined as the expected change in %CLB for each assay over the maximum possible change in %CLB (~45%). To get the experimental sensitivity in the same units of percent optimized, the observed change in the anisotropy from 0 to 300 mg/dL was compared to the maximum possible expected change in anisotropy for a competitive binding assay to physiological glucose concentrations (0.4 * 45% = 0.18). Figure 31 displays the percent optimization of the transduction and recognition mechanisms as modeled for each assay and the percent optimization of the experimentally observed change in anisotropy. As the optimization of the recognition mechanism is increased, the experimental sensitivity increases as well. This validates the ability to use the model to identify the optimal characteristics of the assay to maximize the individual mechanisms in order to maximize the experimentally observed

sensitivity to glucose. By maximizing the degree to which each mechanism is optimized, we could achieve the ideal competitive binding assay for glucose sensing. Figure 31 suggests that we could see significant improvements in each of the mechanisms.

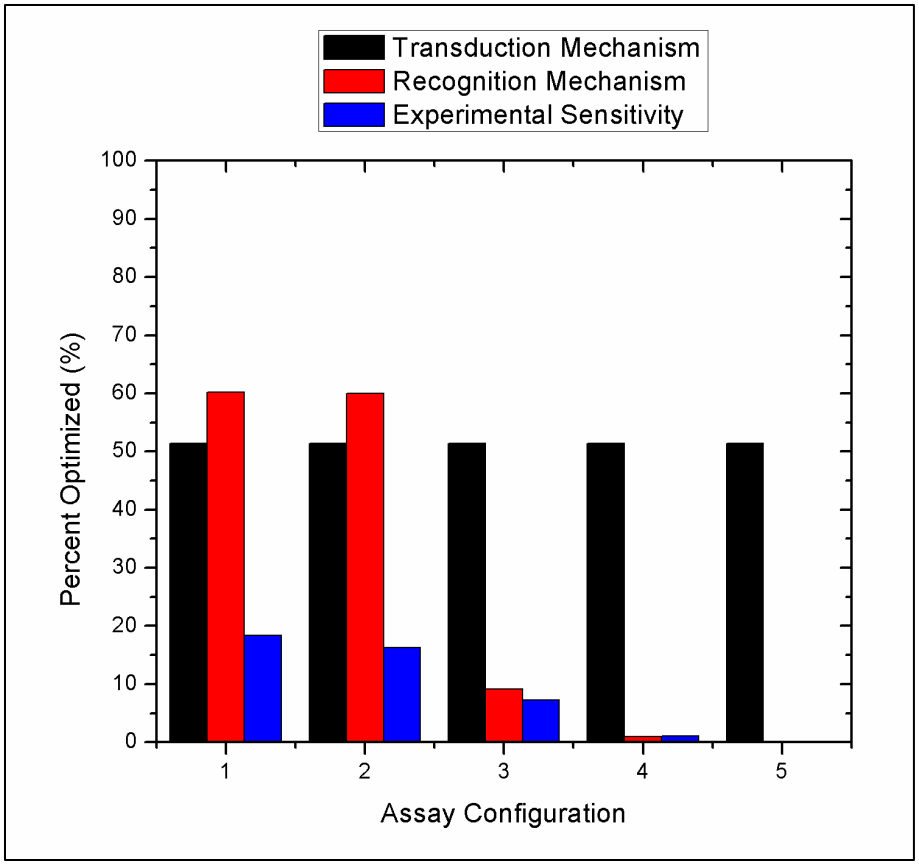

Figure 31: Comparison of the level of optimization of the transduction and recognition mechanisms with the experimentally observed sensitivity.

Calibration of Optimized Sensing Assay

One data set from the 1 μM FITC-dextran and 100 μM ConA assay was used to calibrate a predictive fit to the assay's glucose response using FA. Equation 8, which is commonly used for fitting competitive binding assays, was used to fit the data.[127] Using terminology of Findlay and Dillard, *D* is the FA response at infinite glucose concentration, *A* is the FA response in the absence of glucose, *Glu* is the glucose concentration, *C* is the inflection point on the calibration curve (IC_{50}), and *B* is the slope factor. This equation was solved by parameter optimization using the curve fitting toolbox in MATLAB. The calibration data and the associated optimized fit using Equation 13 are displayed in Figure 32.

$$FA = D + \frac{(A - D)}{1 + \left(\frac{Glu}{C}\right)^{B}} \tag{13}$$

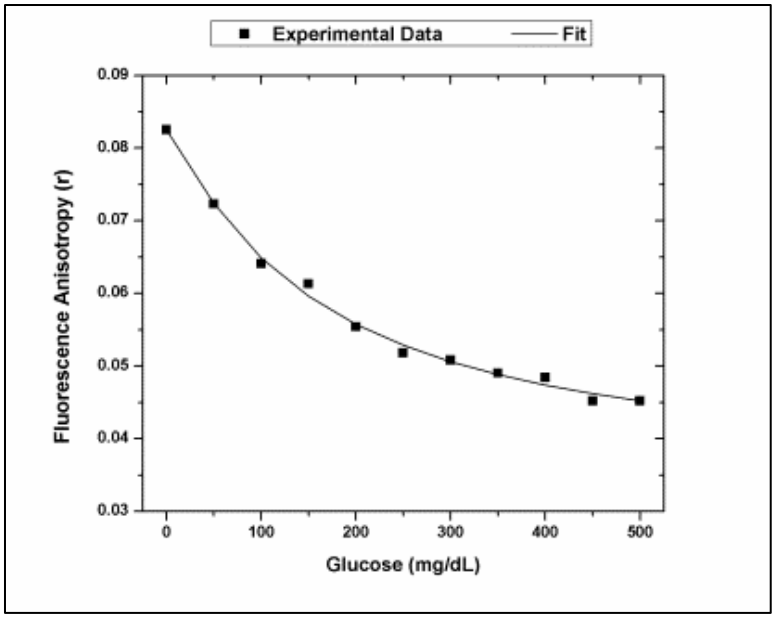

Figure 32: Experimental glucose-response for 100 µM ConA and 1 µM 4 kDa FITC-dextran and the corresponding calibration fit. (A = 0.0825, B =1.126, C = 160.4, D = 0.03485). The R-square value for this fit is 0.9951.

Prediction Capabilities of Assay

All collected data points for the 1 µM FITC-dextran and 100 µM ConA assay from 0 mg/dL and 300 mg/dL glucose concentrations were used to determine the error associated with the prediction. This included 7 calibration data points and 20 prediction data points. The actual versus predicted glucose concentrations for the 1 µM FITC-dextran and 100 µM ConA assay were then plotted in Figure 33 for further analysis. Linear regression was also performed on the predictive data to give a standard error of prediction.

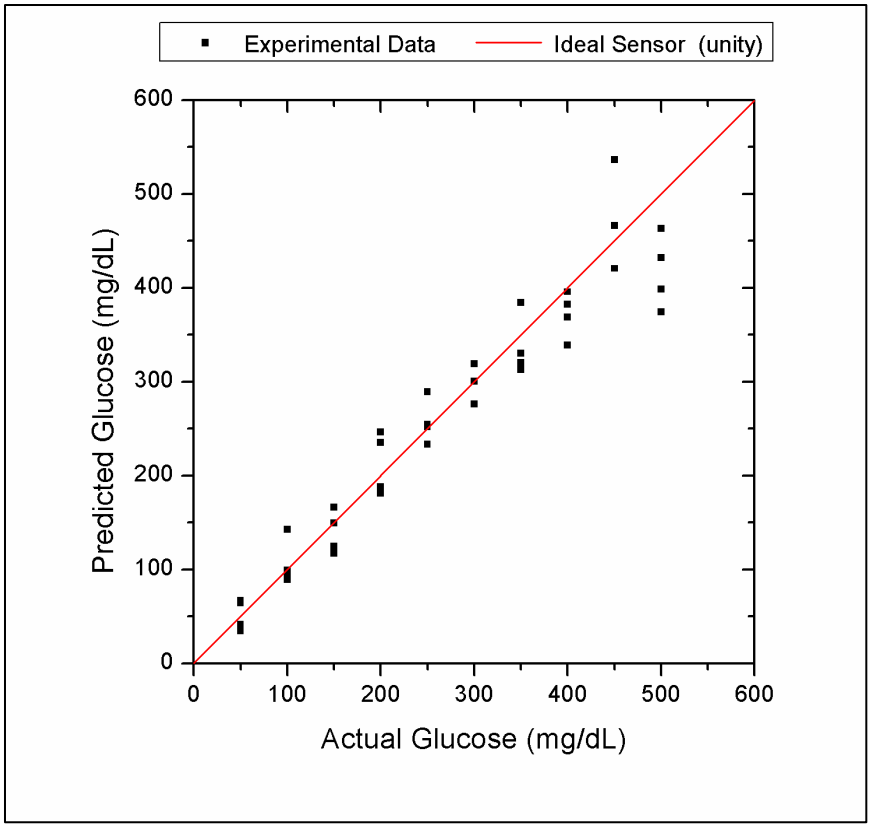

Figure 33: Predicted glucose vs. actual glucose for the FA competitive binding assay using 1 µM 4 kDa FITC-dextran and 100 µM ConA.

The assay displayed a prediction error of 22.4 mg/dL. This is the convolution of the pipetting, recognition, transduction, and detection errors within the system. Therefore, the standard error of prediction demonstrates an upper limit to the recognition error associated with ConA in a glucose-based sensor, and could be shown to be even lower. For example, the detection error could be decreased by using a spectrofluorometer system equipped with polarizers that have a higher extinction ratio (e.g. Glan-Thompson) than the sheet polarizers used in fluorescent microplate readers.

Nevertheless, this level of predictive error shows that the lectin, ConA, can be quite effective at predicting glucose concentrations in a sensor that has independently been optimized with regards to its recognition and transduction mechanisms.

Adjusted Model with the Relative Quantum Yield

While the model is validated to be capable of predicting trends and optimized regions, there do exist a few differences between the experimental data and the model that are important to note. The experimentally determined FA is lower than the modeled FA values which could be explained by local fluorophore motion allowed by the linkage between the fluorophore and the ligand.[128] This shift in FA could also be seen if the dextran structure and the dextran/ConA complex were not perfectly spherical. The ellipsoidal nature of the bound and unbound dextran would result in a shorter rotational correlation lifetime, decreasing the observed FA. Either way, the change in FA is similar to those predicted.

Another difference between the modeled and experimental results is the upwards shift of the FA values relative to the baseline at 500 mg/dL glucose for assays with higher ConA concentrations. This shift could be attributed to an increase in viscosity from the high protein concentrations. As seen in Equation 7, the rotational correlation lifetime of a fluorophore is directly proportional to the viscosity of the solution in which it resides. As slight increases in viscosity would be expected at 100 μM ConA, the FA of the fluorescent molecules within the sample could increase accordingly.

The slight difference between the predicted change and actual change to glucose could potentially be explained via changes in the fluorescence lifetime upon ConA binding to the 4 kDa FITC-dextran. In this original model, the quantum yield and the lifetime of FITC-dextran were assumed to remain constant upon binding. To test this assumption with regards to the predicted anisotropy response, the fluorescence lifetime of the free and bound states of 4 kDa FITC-dextran was experimentally determined.

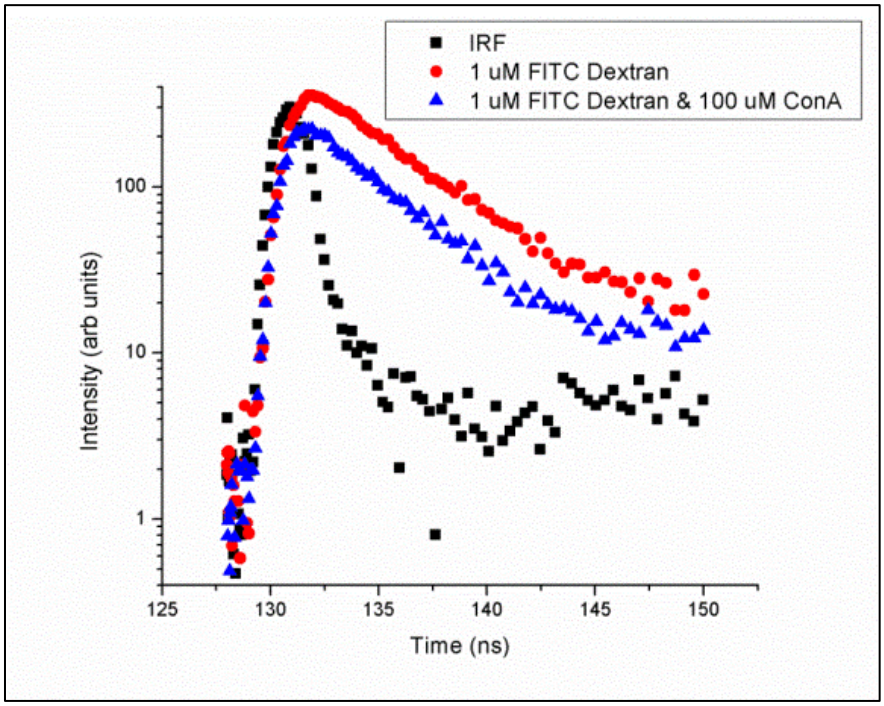

Figure 34: Fluorescence lifetime studies of 1 µM FITC-dextran and 1 µM FITC-dextran with 100 µM ConA. The IRF is from the pulsed LED.

Fluorescence Lifetime Studies

These fluorescence lifetime studies were performed using a stroboscopic technique on a TM-200 PTI spectrofluormeter in the Materials Characterization Facility (MCF) at Texas A&M University. This spectrofluorometer was equipped with a 460 nm LED and a R928 photomultiplier tube collecting emission at 520 nm. Figure 34 shows the fluorescence decays of 1 µM FITC-dextran (alone) and 1µM FITC-dextran paired with 100 µM ConA. The fluorescence decay of the FITC-dextran solution was fit with a single fluorescence lifetime. Then, the solution with FITC-dextran and ConA was fit with two fluorescence lifetimes where one was fixed to be lifetime of the FITC-dextran solution, presumably the lifetime of the free population.

The fits generated a single 3.897 ns lifetime for the 1 µM FITC-dextran with a chi-squared value of 1.297. For the combined assay, it generated a 3.897 ns lifetime and a 1.73 ns lifetime for the free and bound populations with a chi-squared value of 1.097. The fit for the combined assay showed at t=0 showed ~66% with the free lifetime and 34% with the bound lifetime, which agreed with the predicted competitive binding modeling for this assay at 0 mg/dL glucose. The modeled anisotropy response was then adjusted to account for the effect of this change with regards to an adjusted bound anisotropy and an adjusted fractional intensity from the bound population. Table 6 shows the predicted anisotropy of 4 kDa FITC-dextran bound to ConA using the initial model that assumes the lifetime is unchanged upon binding to ConA (~4 ns) and the adjusted model that accounts for the change in lifetime (1.7 ns) using Equation 6.

Table 6: Initial modeled FA and Adjusted modeled FA to account for the change in fluorescence lifetime of the bound population.

Competitive Ligand (CL)	**Initial FA $_{\text{bound to ConA}}$**	**Adjusted FA $_{\text{bound to ConA}}$**
4 kDa FITC-dextran	0.382	0.392

If the quantum yield of the fluorescent ligand changes upon binding to ConA, then the total fluorescence intensity coming from the samples should be glucose dependent. The fractional fluorescence intensity that comes from the bound population is no longer equal to the percent of the fluorescent ligand that is bound. Instead, it is related to the total fractional fluorescence intensity that can be expected due to the glucose binding. Equation 14 was then used to describe the total fluorescence intensity (F_{tot}) of the 1 μM FITC-dextran and 100 μM ConA assay after adjusting for the change to lifetime upon binding (RQY = relative quantum yield). The RQY_{bound} was defined by Equation 15, and the RQY_{free} is defined to be 1. The %CLB(glu) was used from the model like before. To determine whether this change in fluorescence intensity was reasonable, it was compared with experimental data and shown in Figure 35. The total fluorescence signal from each well in the microplate was calculated by summing the parallel and perpendicular intensities.

$$F_{tot}(glu) = RQY_{bound} * \%CLB(glu) + RQY_{free} * (1 - \%CLB(glu)) \quad (14)$$

$$RQY_{bound} = \frac{\tau_{bound}}{\tau_{free}} \quad (15)$$

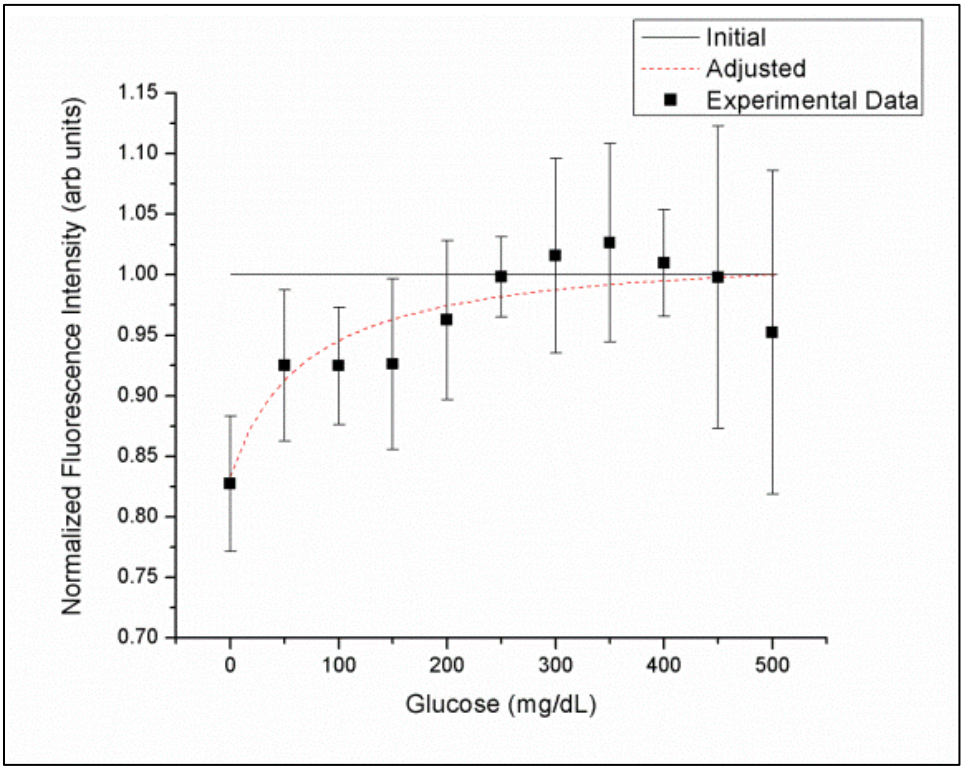

Figure 35: Total fluorescence intensity from the 1 µM FITC-dextran and 100 µM ConA assay as a function of glucose. The initial model assumed no change in lifetime upon binding. The adjusted model accounted for changes in the fluorescence lifetime.

The initial model assumes that the fluorescent intensity is independent of binding (normalized intensity =1). The adjusted model accounts for the relative change in quantum yield to generate the normalized fluorescence intensity (Figure 35). The experimental data more accurately follows the adjusted model when compared to the

initial model. Each data point is a uniquely loaded well, and the large standard deviation can be attributed to pipetting error.

Adjusted Model

After confirming that the fluorescence does seem to be increasing across physiological glucose concentrations, an adjusted model of the anisotropy can then be generated. Equation 16 is the adjusted model for the anisotropy in terms of the adjusted fluorescence contributions from the free and bound populations and the adjusted anisotropy of the bound populations. The F_{tot} was used as described in Equation 14. The comparison of this model with the original model is shown in Figure 36.

$$r_{adjusted}(glu) = \frac{RQY_{bound} * \%CLB(glu)}{F_{tot}} * r_{b-adj} + \frac{RQY_{free} * (1 - \%CLB(glu))}{F_{tot}} * r_f \quad (16)$$

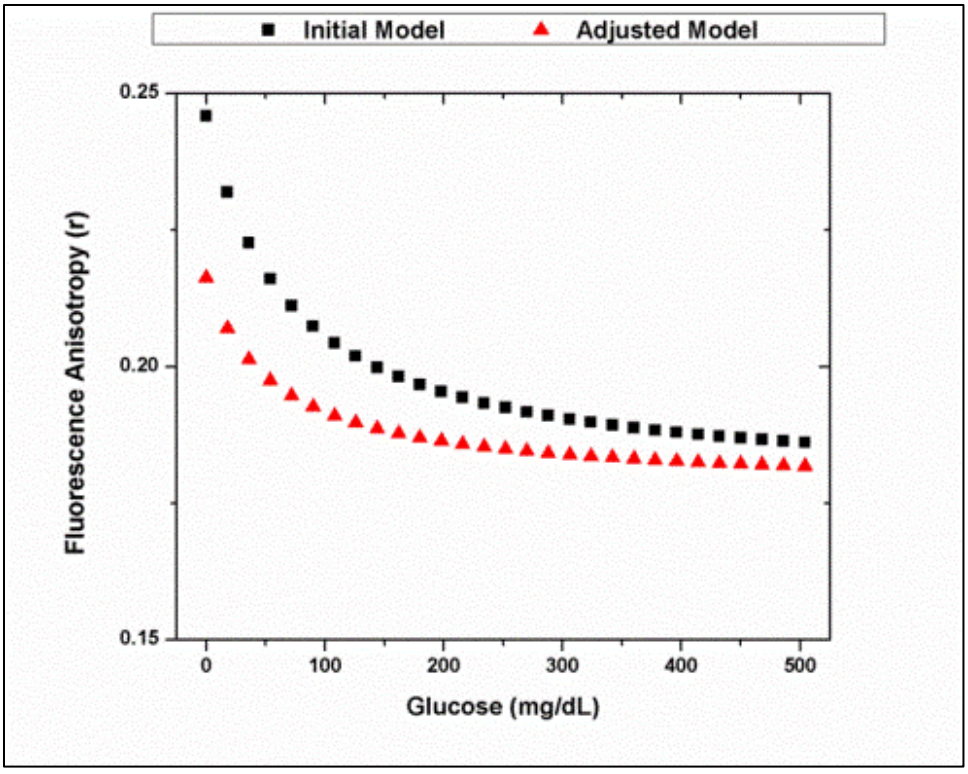

Figure 36: Initial and adjusted models of the glucose response for the 1 µM FITC-dextran and 100 µM ConA assay. The initial model assumed no change in lifetime upon binding. The adjusted model accounted for changes in the fluorescence lifetime.

When compared to the experimental, glucose-dependent changes to the anisotropy (~.035), the adjusted model does more accurately predict the change (.035) than the initial model (.060). However, it is important to note that the trend is similar. This is due to the fact that the decrease in fluorescent lifetime increases the expected anisotropy of the bound population but decreases the percent of the fluorescence that comes from the bound population also (Equation 16). This combination limits the effect that lifetime changes have on the expected anisotropy response, allowing the

aforementioned assumption to remain relatively valid when choosing an appropriate fluorophore for these studies.

This anisotropy response could be further improved by using a fluorophore that undergoes less of a change in lifetime upon binding to ConA. However, without *a priori* knowledge of the fluorescence lifetime upon binding, the initial assumption that the fluorescence lifetime is unchanged upon binding can allow the user to identify an appropriate fluorescent CL. For this work, an assay based on 4 kDa FITC-dextran and ConA can be optimized using the initial model, and experimental data from the optimized assay of 1 μM 4 kDa FITC-dextran and 100 μM ConA elicits an appreciable change in anisotropy.

Model of Previous ConA-Based Assays

Now that the model has been validated, it can be used in an attempt to describe the previous work with ConA. This work will primarily use the model for the recognition mechanism to model two distinct assays. The first uses a fluorescent ligand that displays a typical association constant for monovalent sugars ($K_a = 10^{-3}\ M^{-1}$).[126] The other assay uses typical association constant for multivalent presentation of sugars on a dendrimer ($K_a = 10^{-6}\ M^{-1}$).[61,129] Concentrations of each component in the competitive binding assays are used to maximize the binding while staying below the solubility limit of ConA (100 μM).

One assumption for this model was that the binding is monovalent. Monosaccharides have proven to remain stable with ConA in free solution. However,

multivalent sugars (like the dendrimer modeled here) show aggregation and precipitation over time. To be able to use this model to describe the equilibrium binding as a result of aggregation, it is run at different time points to account for the time-dependent aggregation. To account for the level of aggregation in those runs, the affinity is changed accordingly. It is well known that when a single protein binds to two ligands simultaneously, it's apparent affinity increases significantly due to chelation. Time-dependent aggregation can then be tracked in this model using increasing affinities. Therefore, to account for this in our model for steady-state equilibrium binding, we ran the glucose response for the same assay but with an increasing affinity between the fluorescent ligand and ConA.

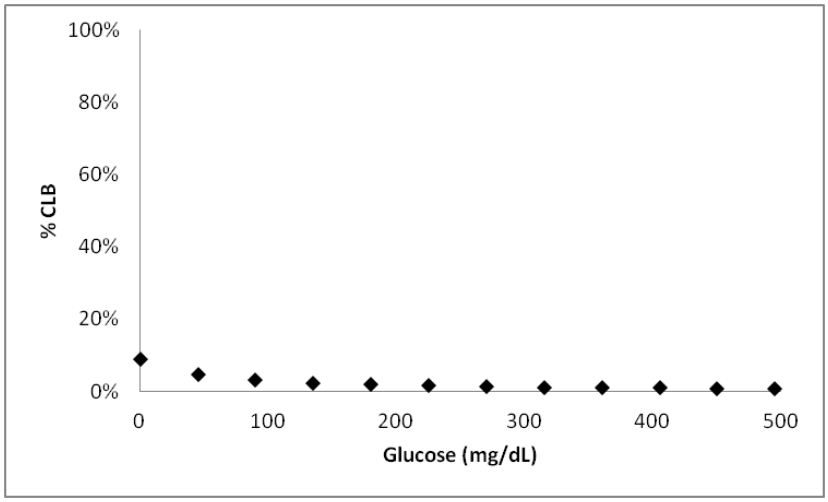

Figure 37: Predicted glucose-dependent binding for assay that uses a competing ligand that presents a single glucose residue.

Figure 37 shows the recognition mechanism of an assay that uses a competing ligand that presents a single monosaccharide that binds to ConA. Because of the low affinity and the solubility limit of ConA, the ConA concentration cannot be high enough to allow for significant binding between ConA and the competing ligand. Therefore, increasing glucose concentrations do not significantly change the %CLB (competing ligand bound). This displays the primary reason that groups use multivalent ligands as competitors: to increase the association constant in order to lower the required ConA concentration so the recognition mechanism can be optimized.

Figure 38 shows the recognition mechanism of an assay that uses a competing ligand that presents multiple monosaccharides on its surface (like a glycosylated dendrimer). The increased association constant allows the assay to be optimized (blue diamonds) and significantly respond to physiological glucose concentrations. However, as the affinity increases due to aggregation and chelation, the competitive binding shifts keeping ConA bound to the competing ligand over the same glucose range (red square, green triangle, gray x's). Eventually, the assay does not respond to physiological glucose concentrations. It could be reversed, but it would require significantly higher glucose concentrations than what is seen in the body.

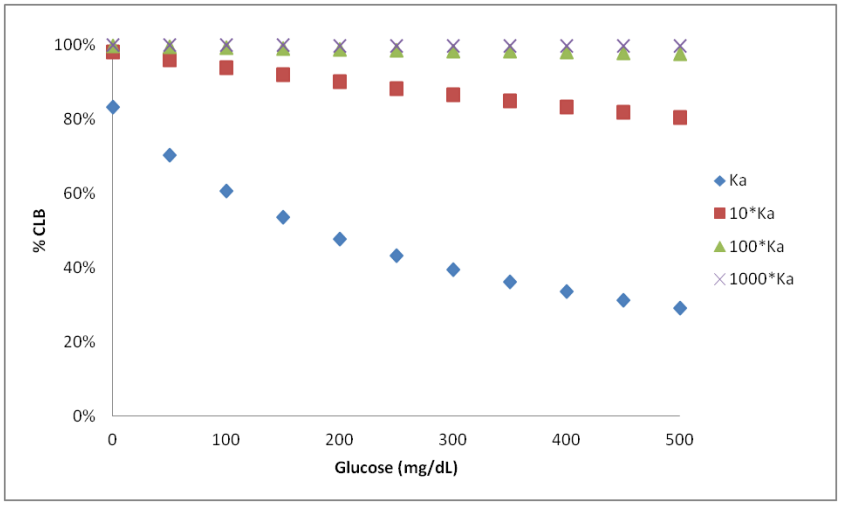

Figure 38: Predicted glucose-dependent binding for assay that implements a multivalent competing ligand. The time-dependent aggregation increases the affinity and changes the glucose response.

These results for the recognition mechanism using the monovalent and multivalent competing ligand were combined with an ideal fluorescence transduction mechanism to show what one would measure for the different assays. With a modeled fluorescence anisotropy that changes from 0.05 to 0.35 upon binding to ConA, Figure 39 shows the responses for the monovalent ligand (black) and the multivalent ligand (gray).

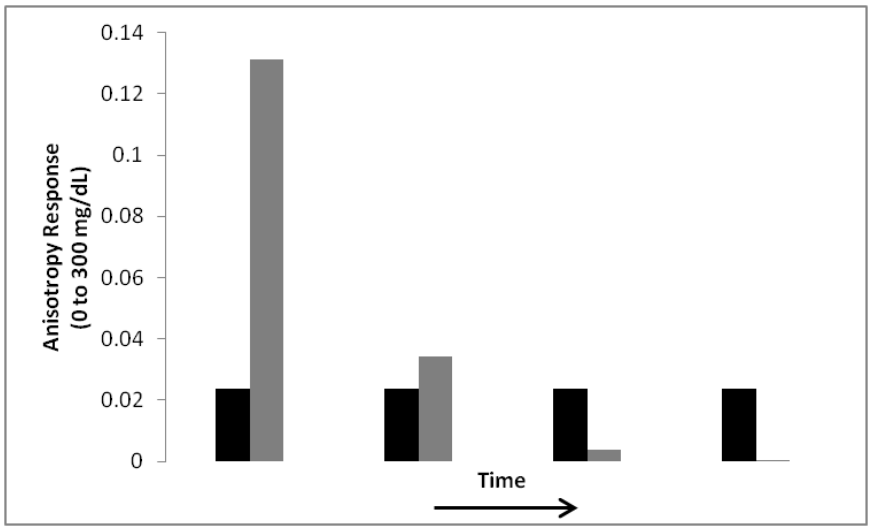

Figure 39: Predicted glucose responses over time for assays that use either monovalent (black) or multivalent (gray) competing ligands.

Because the monovalent ligand does not allow for extended aggregation between multiple components, the affinity stays constant over time and the resulting anisotropy response does as well. However, because the affinity is weak, the sensitivity of the response is low because the recognition mechanism is not capable of being properly tuned. On the other hand, the increased affinity of the multivalent originally allows the recognition mechanism to be properly tuned, as seen by the very sensitive anisotropy response (gray). However, as time-dependent aggregation occurs, the increasing affinity changes the assay to require higher glucose concentrations to induce competitive binding. This effectively decreases the assay's sensitivity to physiological glucose concentrations over time and causes it to lose repeatability/reversibility.

This describes the apparent tradeoff between sensitivity and repeatability that is typical of the ConA-based competitive binding assays found in the literature. Using

traditional approaches, the fluorescence assay cannot achieve a stable, optimized recognition mechanism in free solution. Monovalent competing ligands show a non-optimized recognition mechanism, but the glucose response is constant over time. On the other hand, multivalent competing ligands allow for high initial sensitivities due to optimized recognition mechanisms, but aggregation-induced increases in affinity display changes in the fluorescent response over time. To avoid this trade-off in free solution and display the full potential of such an assay, higher affinities must be generated while preventing this aggregation over time. If such an assay were able to be made, it is expected generate a response like the red columns in Figure 40.

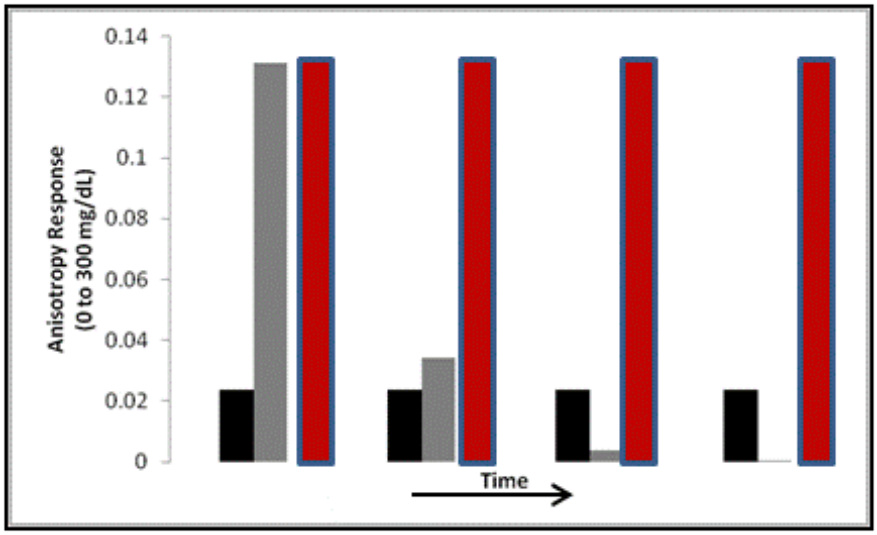

Figure 40: Assays that achieve higher affinities without allowing for aggregation with ConA are expected to display repeatability (red).

Defining Ideal Assay Characteristics

These models for the recognition and transduction mechanisms can be used to identify a ligand that can best optimize the ConA-based competitive binding assay. Because of the linear nature of the fluorescence anisotropy, it is essential for both mechanisms to be optimized. Figure 41 shows four hypothetical cases for different levels of optimization for the recognition and transduction (fluorescence) mechanism. Only when both are optimized is the measured sensitivity high.

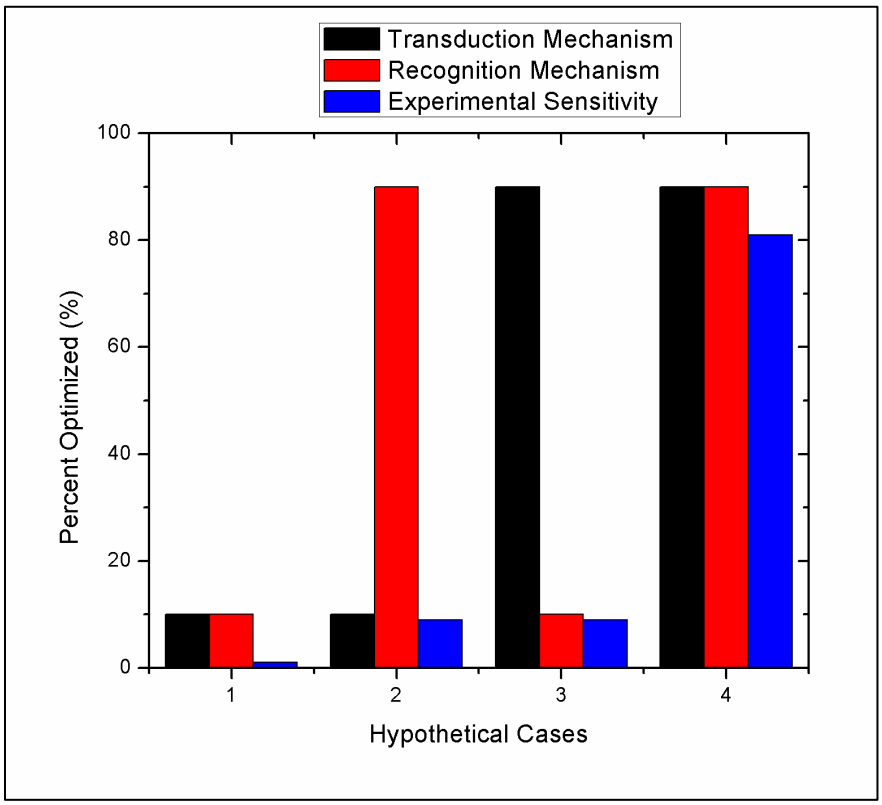

Figure 41: Hypothetical cases that show the relationship between the level of optimization of the fluorescence and recognition mechanisms and the expected experimental sensitivity of the assay.

Recognition Mechanism

The 2D-sensitivity plots can be useful in identifying regions of interest. Figure 42 shows the recognition sensitivity of an assay with 500 nM, fluorescent ligand with a zone circled with a dotted line. Obviously, the goal is to be in the dynamic portion of this graph (the dark red). Because ConA is insoluble above 100 µM, the assay requires a competing ligand to be chosen that has an affinity between 10^5 M^{-1} and 10^7 M^{-1}. It is important to note that the ConA could eventually be labeled with a fluorophore for FRET studies. Therefore, high ConA concentrations could result in significant absorption from the acceptor fluorophore. The higher affinities (in the tolerable zone) allow lower ConA concentrations to be used.

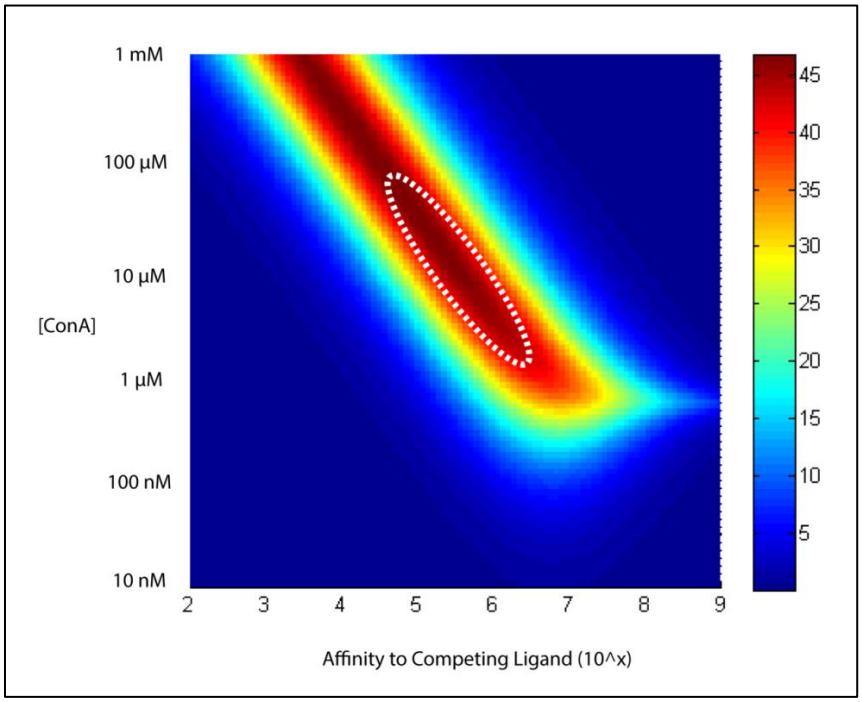

Figure 42: Recognition sensitivity of 500 nM fluorescent ligand. Within the dotted line is the ideal region for the assay to stay below the solubility limit of ConA.

Transduction Mechanism

The 2D map for the transduction sensitivity of an anisotropy based assay is shown in Figure 43 with a desired region circled in a dotted white line. While there are regions on this graph that display slightly higher sensitivities than those in the dotted line, these are relatively impractical. For this ligand to compete with glucose for the binding site on ConA, it must at least have a glucose or mannose residue, and for it to be fluorescent it must have a fluorophore. So, a ligand will most likely have a MW of at least ~600 Da, and probably closer to 1 kDa. For this range of MWs, a fluorophore with a lifetime of 2-15 ns is expected to display an ideal sensitivity with regards to the fluorescence anisotropy transduction mechanism.

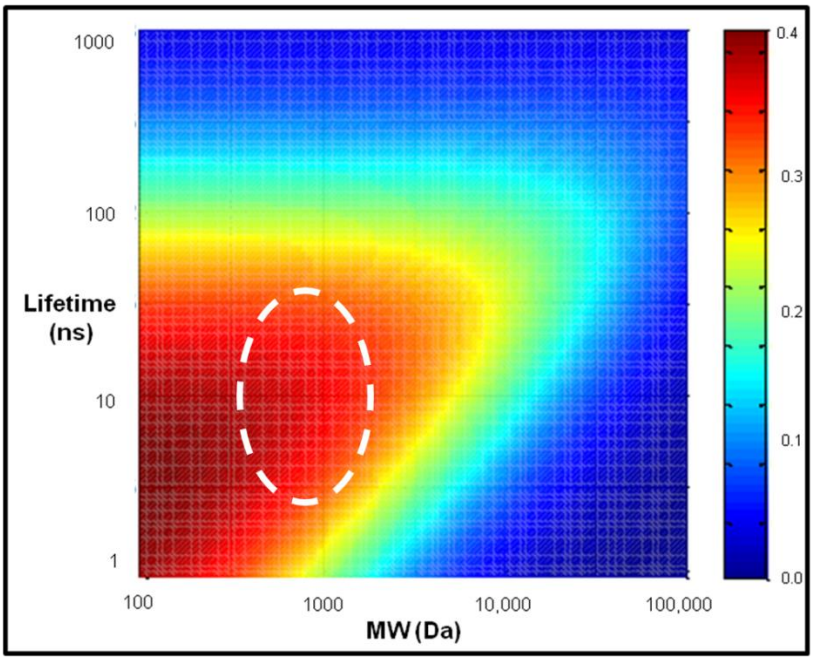

Figure 43: Transduction sensitivity using fluorescence anisotropy with the optimized zone circled in the white dotted line. This would display a MW of ~1 kDa and a fluorescence lifetime of 2-15 ns.

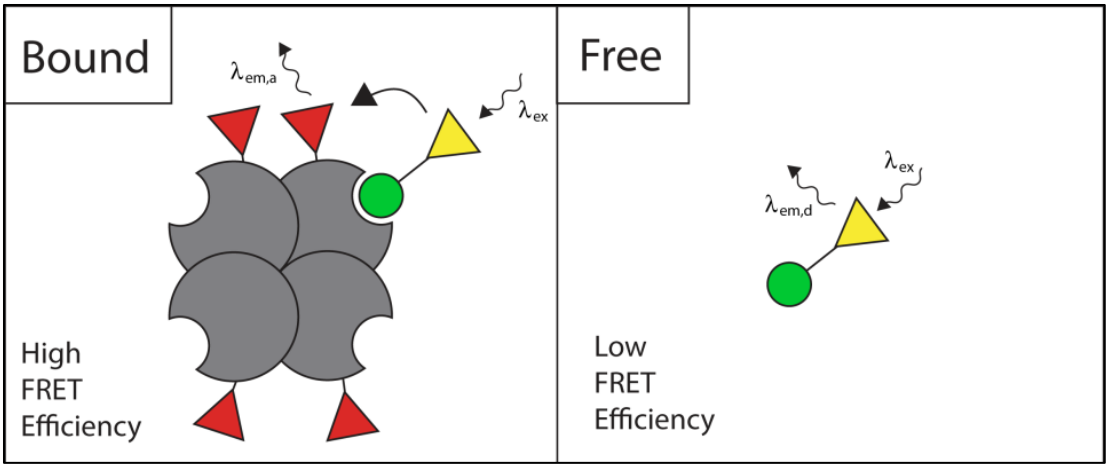

Figure 44: Schematic representation of the transduction mechanism for a FRET assay based on competitive binding with ConA.

Ultimately, this assay would be well-suited to employ FRET as the transduction mechanism to track the binding (Figure 44). This would allow the assay to be implanted and interrogated through a highly scattering environment like tissue. The goal of such an assay would be to maximize the difference in the FRET efficiency between the bound and the free populations. Assuming that the assay is configured in a way to avoid diffusion effects on the FRET efficiency, the efficiency of the unbound population can safely be assumed to be low. Therefore, to create a 2D sensitivity map of the transduction mechanism for FRET, the FRET efficiency of the bound population can be modeled. This efficiency is described with Equation 17, showing that it is a function of the distance between the donor and the acceptor (r) and the Förster radius of the FRET pair that's chosen (R_0). This Förster radius is a value that is defined by the FRET pair

that is chosen and is associated with the spectral overlap of the donor and acceptor fluorophores.

$$E = \frac{1}{1 + \left({}^{r}/_{R_0}\right)^6} \tag{17}$$

This equation can be solved for a given Förster radius and a given distance between the donor and nearest acceptor fluorophore. Figure 45 displays the collective solutions to all possible combinations for Förster radius and distances from 1-10 nm. The blue zone indicates an area that is expected to show low FRET efficiency. The red zone indicates an area that is expected to show high FRET efficiency. It is effectively when the distance between the donor and acceptor is shorter than the Förster radius of the FRET pair.

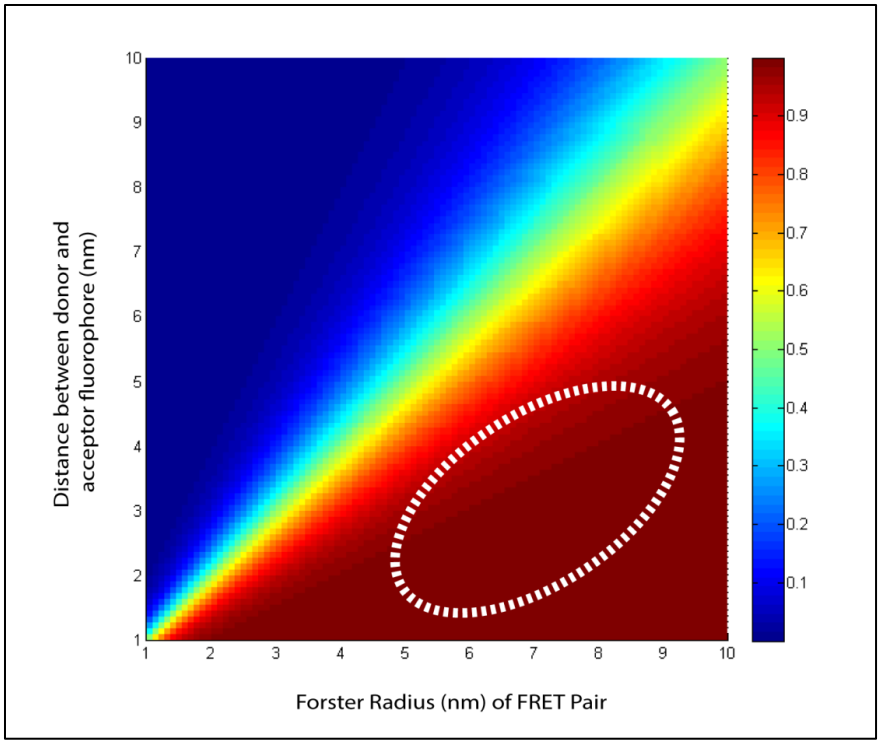

Figure 45: Efficiency of the FRET transduction mechanism upon binding with the target zone circled in the white dotted line.

The dotted line indicates desirable characteristics for the ConA-based competitive binding assay to maximize the sensitivity when using FRET as the transduction mechanism. These types of Förster radii can be achieved by the choice of the donor and acceptor that are used in the assay. It is the average distances between the donor and acceptor fluorophores upon binding that has been the problem to date. Many of the competing ligands that have been paired with ConA are so large that, even upon binding to one of the moieties, the fluorophores are too far apart to undergo energy transfer. The traditionally used multivalent ligands are expected to have this problem (70 kDa dextran is ~10 nm in diameter) and could show an average distance as indicated

by the black dot. The goal for the transduction mechanism is to identify a ligand that can allow the distance between the donor and acceptor to be within the Förster radius upon every binding event.

This modeling of each individual mechanism shows that a fluorescence anisotropy ConA-based assay would be optimized with a fluorescent ligand that has a MW of ~1 kDa, a fluorescence lifetime of ~5 ns, and an affinity to ConA of ~10^6 M^{-1}. A FRET assay does not depend on the MW of the ligand, but would require the average distance between the donor and acceptor to be significantly shorter than the Förster radius of the FRET pair. A fluorescent ligand that meets these requirements, does not allow for aggregation to occur and is either neutral or negatively charged is given the term 'smartly-designed fluorescent ligand' for a ConA-based glucose sensing assay.

Conclusions

This chapter displayed models of the recognition and transduction mechanisms of the ConA-based competitive binding assay, and generated 2D sensitivity maps for the variables in the assay. These models were validated with experimental results with 4 kDa FITC-dextran as the fluorescent ligand. An assay based on this ligand was optimized and developed into a fluorescence anisotropy sensor for glucose concentrations.

Unlike enzymatic assays that are directly dependent on the rates of diffusion, affinity-based assays are much less sensitive to changes in diffusion rates. Therefore, these affinity-based assays have the potential to be optimized in free solution before

encapsulating the assay into a deliverable form (e.g. microcapsules). As a result, this work displays the capability for models to play an important role in the development of implantable sensors based on affinity binding. Accordingly, the validated model was then used to describe previous attempts at the ConA-based sensor. We identified that the primary barriers to ConA sensors are (1) the apparent obstacle of needing to use multivalent ligands for affinity enhancement even though they aggregate with ConA in free solution causing irreversibility and (2) the inability for the average distance between the donor and acceptor fluorophores of the bound population to be within the Förster radius of the chosen FRET pair.

CHAPTER IV

SMARTLY-DESIGNED FLUORESCENT LIGAND FOR CONA-BASED ASSAYS

Introduction

In the last chapter, we introduced the requirements for a dynamic competitive binding assay in which the fluorescence of the competing ligand is tracked with anisotropy. Briefly, this required the competing ligand to have an affinity that is higher than what is typically seen for monosaccharides. To date, this has been achieved by implementing fluorescent ligands that presented multiple monosaccharides on a single ligand (e.g. dextrans & dendrimers). This multivalent presentation is known to increase the apparent affinity to a receptor through proximity effects.[129,130] However, groups have continued to report visual aggregation due to extensive crosslinking, resulting in the lack of reversibility of the assay in free solution. This aggregation problem of ConA-based sensors has been identified as their primary barrier, and we have proposed that the irreversibility is due to the aggregation arising from multivalent ligands being paired with multivalent receptors. Ever since the original assay was introduced in 1982, there has been a tradeoff between long-term repeatability/reversibility and initial sensitivity in free solution.

In this chapter, we introduce a smartly-designed fluorescent ligand that is engineered to display the ideal properties for the recognition and transduction mechanisms of a ConA-based assay. This ligand displays the unique capability to achieve the required affinity without allowing for aggregation, and it can be effectively

inhibited with glucose and mannose. This smartly-designed fluorescent ligand is synthesized, characterized, and implemented into both an anisotropy based assay and a FRET-based assay for glucose sensing.

Types of Affinity Enhancement

While the binding of monosccharides to lectins is generally a weak interaction with a dissociation constant of ~mM, nature employs different strategies to increase the affinity of these events.[130] One method is to increase the number of monosaccharides that are presented on a molecule. While ConA only binds to a single monosaccharide on the structure, the high local concentration of monosaccharides makes the dwell time longer and causes the affinity to appear higher. As previously mentioned, groups have attempted to achieve the higher affinities that are required for ConA-based glucose sensing by using molecules that use this approach. However, as shown in Chapter 4, this can lead to aggregation over time which results in a lack of reversibility.

Another approach that nature uses to achieve increased affinities to a given lectin is by using subsite binding.[129] This approach has an extended binding site near the primary binding site on the lectin for specific sugar moieties. Because additional interactions are made between the sugar and the full binding site, the affinity is increased. The difference between proximity effects and subsite binding are shown in Figure 46.

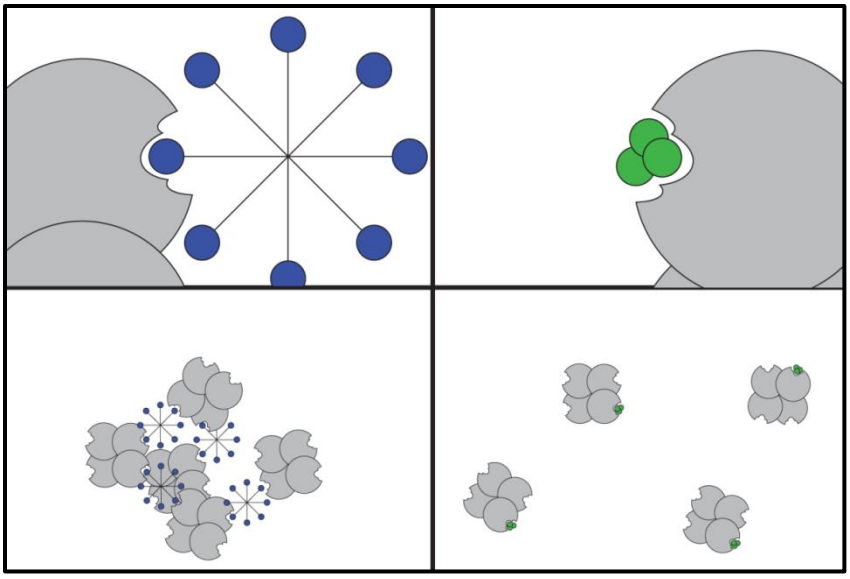

Figure 46: Types of affinity enhancement with ConA. (left) Competing ligands that employ proximity effects lead to aggregation with ConA. (right) Chelation through subsite binding can potentially avoid aggregation if a single ligand is presented.

ConA's Full Binding Site

Adjacent to ConA's primary binding site is an extended pocket that has been shown to form additional hydrogen bonds to the core trimannose of N-linked glycans (trimannose).[131,132] Groups have performed X-ray crystallography studies with ConA and various ligands. The crystallography data was obtained for ConA's interaction with methyl-alpha-mannose and the core trimannose (1CVN and 5 CAN), and the relative orientations of the ConA's binding to each ligand was determined using the Ligand-Interaction tool in the Maestro software (v. 9.5).[131,133] Figure 47 shows the amino acids (black dots) in the crystallography structure that are within a distance that is capable of forming hydrogen bonds. These amino acids display the extended binding site to which

the core trimannose binds. This shows that ConA forms hydrogen bonds with each mannose group of the trimannose, which should increase the affinity without leaving moieties for additional ConA to bind. It also shows that the trimannose could compete with the monosaccharide for binding to a ConA subunit because they both bind to the primary binding site.

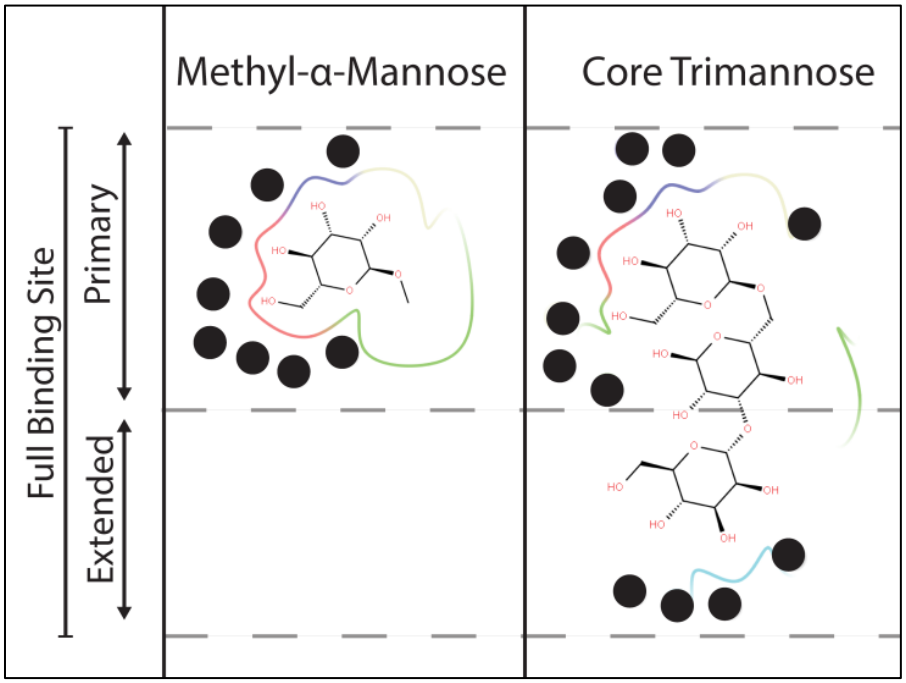

Figure 47: Comparison between carbohydrate binding to the primary binding site of ConA and the full binding site of ConA, using the crystal structures from ref. 131 & 133. Black dots: amino acids capable of forming of hydrogen bonds with the sugar (3.5 Å).

Aggregation Studies

To explore whether the interaction of ConA with the core trimannose leads to aggregation in free solution, dynamic light scattering (DLS) measurements were

performed. This interaction was compared to the interactions between ConA and other high-affinity ligands that are commonly used in ConA-based assays. Dextran, dendrimer and trimannose were added to separate cuvettes of ConA solutions in TRIS buffer, and allowed to interact for 12 hours at 22 deg C. The TRIS buffer was 10 mM TRIS, 1 M NaCl, 1 mM CaCl2, 1 mM MnCl2, at pH 7.4. The dextran was 2 MDa and used as received from Sigma. The dendrimer was a generation three glycosylated dendrimer (24 terminal amines, 24 terminal glucose residues) were used as provided by Dr. Eric Simanek (Texas Christian University).

Dynamic light scattering was then used to examine the average size of particles formed in comparable solutions. As controls, solutions of the individual components were also scanned to determine the particle size in the absence of aggregation. The final concentration was 3 μM for the competing ligand and 3 μM for ConA. Negative controls were run for each competing ligand (3 μM) without ConA present. ConA was also independently added to a separate control cuvette (3 μM). All solutions were in TRIS buffer and were filtered prior to combining the solutions. After 12 hours, the solutions were mixed to allow for the re-suspension of any settled material and dynamic light scattering studies were performed. The reported data is the average particle size as determined by percent-volume.

Figure 48 shows that the average size of the particles is much larger after 12 hours for solutions of ConA paired with dendrimer and dextran, indicating that ConA and the high-affinity ligands have already formed extensive aggregates. In comparison, the average size of particles in the solution that contains trimannose and ConA has not

increased in size, indicating that, if binding occurred, a single presentation of trimannose significantly decreases the extent of aggregation and potentially prevents it completely.

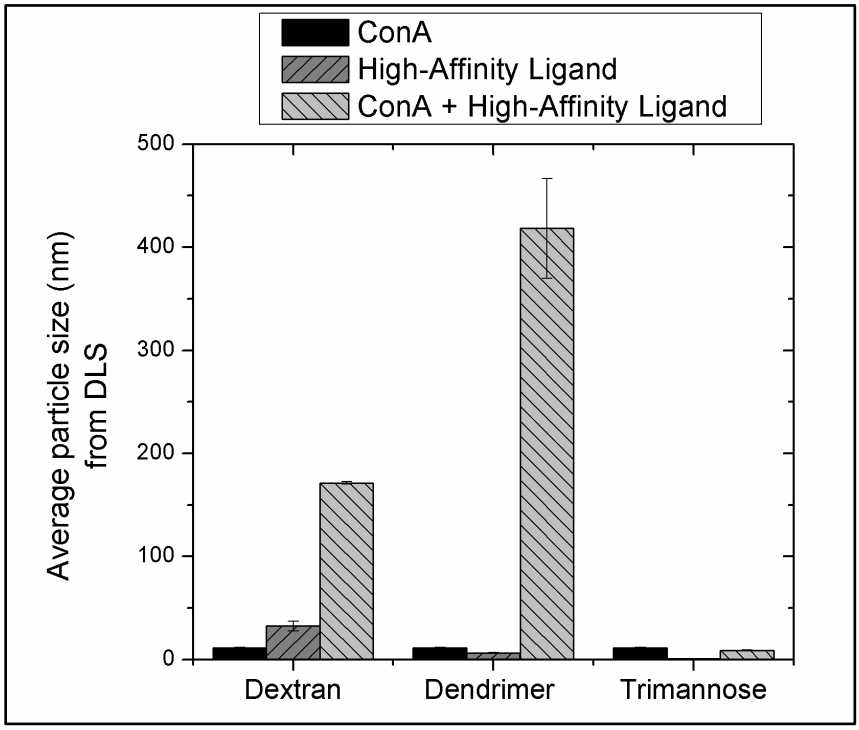

Figure 48: Average particle size of solutions with ConA and various high-affinity ligands. The error bars indicate the standard deviation of 3 different samples.

Smartly-Designed Fluorescent Ligand Concept

Figure 49 shows a modular representation of a fluorescent ligand that is composed of (A) a sugar moiety portion that can bind to ConA and (B) a fluorophore. The working hypothesis is that the full potential of ConA assays (in terms of the recognition mechanism) can be shown if the fluorescent ligand can display the higher affinity without aggregating with ConA. We just showed that the core trimannose does

not aggregate with ConA, and the crystallography information that suggests the affinity should be increased due to the subsite binding. Therefore, we attempt to generate a smartly-designed fluorescent ligand where the (A) portion of the fluorescent ligand is based on a single presentation of the core trimannose.

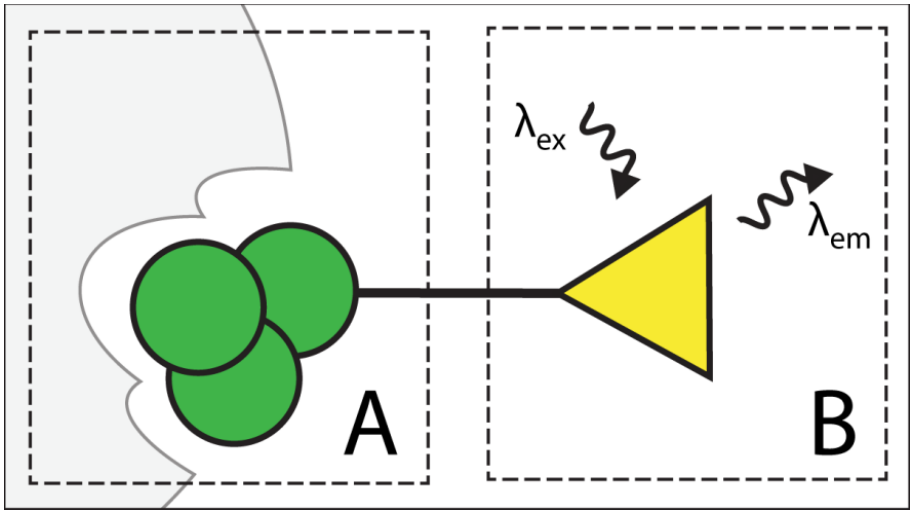

Figure 49: Recognition (A) and transduction (B) components of a fluorescent competing ligand. A smartly-designed fluorescent ligand would be engineered to maximize both mechanisms.

Preparation of Smartly-Designed Fluorescent Ligand

Synthesis of APTS-Mannotetraose

The goal, therefore, is to generate a fluorescent ligand that displays the core trimannose. Ideally, this would result in a molecule that had a fully-preserved trimannose group and a single fluorophore. Therefore, the commonly used periodate oxidation method to generate carbonyl groups on a polysaccharide for fluorophore

attachment was not appropriate.[134] This would destroy the ring mannose moieties required for binding to ConA's full binding site and could introduce several fluorophores to a single glycan.

Reductive amination is a more controlled method that has been used to label glycans for subsequent chromatographic or electrophoretic separation and identification of the glycans.[135-138] By using an amine-bearing fluorophore, this method introduces a single label at the reducing termini of the glycan. This causes the reducing sugar of the glycan to be acyclic but leaves the remaining sugars of the glycan in their cyclic, unaltered form to be recognized by receptors.[139] Thus, we used the trimannose bearing mannotetraose to maintain the trimannose structure after conjugation.

8-Aminopyrene-1,3,6-trisulfonic acid (APTS) was chosen as the amine-bearing fluorophore to attach to the mannotetraose. APTS is a water-soluble fluorophore whose fluorescence is independent of pH over a wide range. It has been used to label an unknown population of glycans enzymatically cleaved from glycoproteins via reductive amination to facilitate their separation via capillary electrophoresis due to its three negative charges per fluorophore at neutral pH.[136] Because ConA's isoelectric point is around 5, these negative charges also minimize non-specific electrostatic interactions between the fluorescent ligand and ConA at physiological pH.

Mannotetraose was purchased from Dextra Laboratories and 8-Aminopyrene-1,3,6-trisulfonic acid (APTS) was provided by Dr. Gyula Vigh. Mannotetraose (0.9 mg, 1.35×10^{-6} mol) was mixed with 13.5 μL of 1 M APTS (1.35×10^{-5} mol) prepared in 15% acetic acid aqueous solution. Then, 54μL of 15% acetic acid aqueous solution was also

added into the mixture. The acidic environment promotes the ring-opening of the reducing terminus of mannotetraose. The reaction mixture was stirred for 5 minutes at room temperature. Then, 13.5μL of 1M sodium cyanoborohydride ($NaBH_3CN$, $1.35x10^{-5}$ mol) in THF was added into the reaction and had it stirred for 14 hours at room temperature. The schematic is shown in Figure 50. Sodium cyanoborohydride is a reducing agent that converts the Schiff base into the stable APTS-mannotetraose (APTS-MT) conjugate. APTS-glucose and APTS-maltotriose were also synthesized using this method.

Note that this reaction step should be performed in a properly ventilated fume-hood as hydrogen cyanide gas (toxic) can be liberated from the solution. Other groups have shown that 2-picoline borane is another effective reducing agent for the reductive amination of glycans with fluorophores.[140]

This type of reaction can be performed to conjugate the glycan to other fluorophores as well. Most often, these fluorophores have an aromatic amine to maximize the efficiency of the reaction over a shorter time.[135,138] These aromatic amines can be deprotonated even under the acidic conditions for the reductive amination. Groups have also used fluorophores that present hydrazides and thiosemicarbazides in non-reducing conditions.[139,141] This allows the reducing sugar to return to the cyclic form and still be attached via the hydrazide. This is more stable than the Schiff base, but it is not as stable as the conjugate that has been reduced.

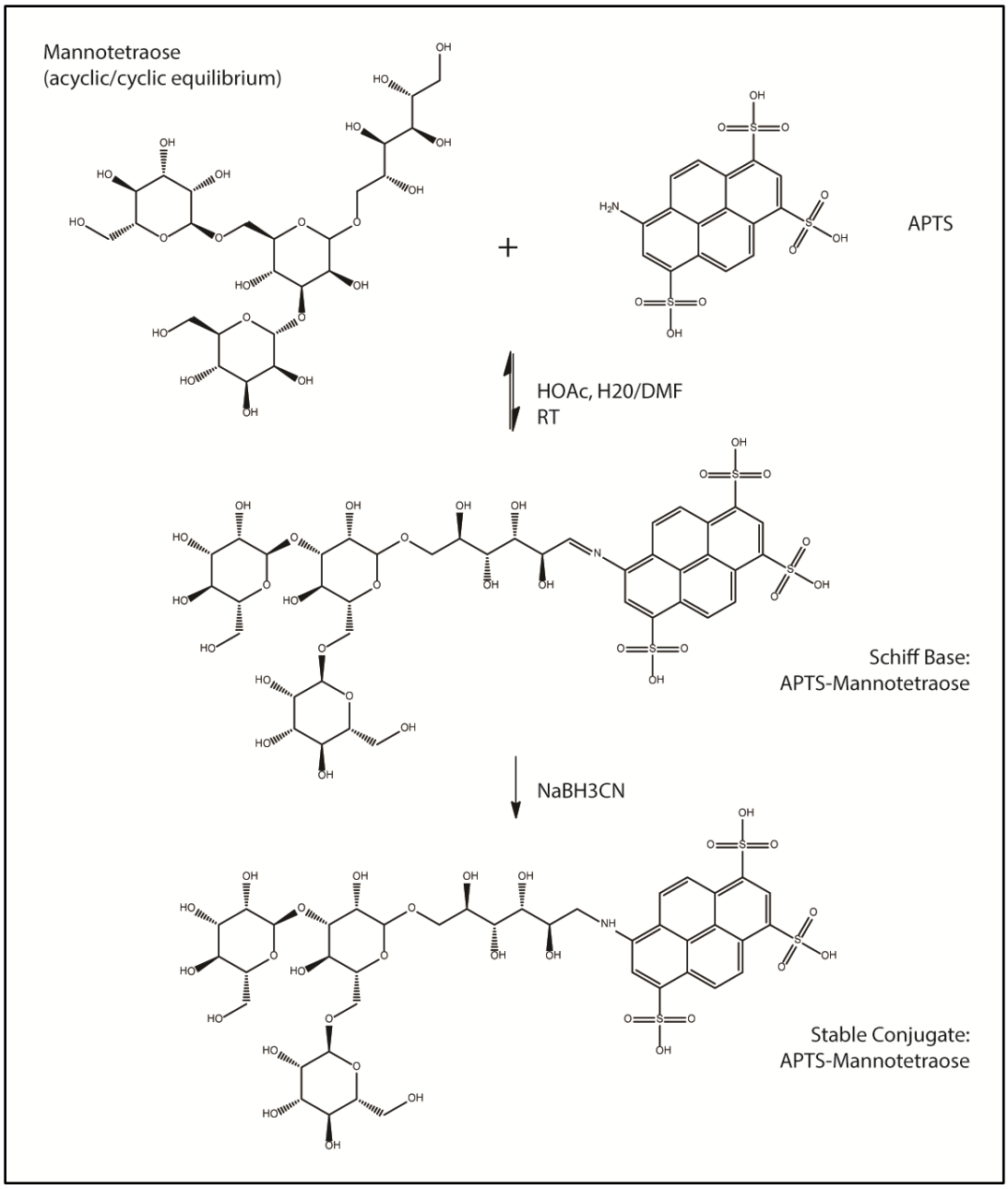

Figure 50: Synthesis of APTS-MT via reductive amination to form a ligand with a single fluorophore and a single trimannose moiety.

Separation with HILIC Chromatography

Following the reductive amination synthesis, the crude product was purified by hydrophilic interaction liquid chromatography (HILIC) and identified via its change in absorbance. An HPLC system containing a solvent delivery module Model 126, an auto injector Model 508 and a photodiode array detector Model 168 operating under 32 Karat software control (Beckman-Coulter, Fullerton, CA) was used for reaction monitoring. HILIC separations were obtained on a 4.6 mm I.D., 150 mm long analytical column packed with a 3 µm HILIC stationary phase (Phenomenex, Torrance, CA). Solvents used were A: 100% water; B: 5% water, 95% acetonitrile both containing 10 mM ammonium formate, 5mM formic acid, pH 9. Isocratic: 80 %B, 10 min. The chromatogram is shown in Figure 51.

Confirmation with Mass Spectrometry

Mass spectra of this sample were acquired in negative ion mode using an MDS SCIEX (Concord, Ontario, Canada) API QStar Pulsar. Sample was dissolved in (methanol) and electrosprayed using ionspray (needle) at- 4.5 kV. Sheath gas and curtain gas flow rates were set to 40 and 20 psi, respectively. The sample flow rate was 7 µl/min. Multiply charged ions were detected.

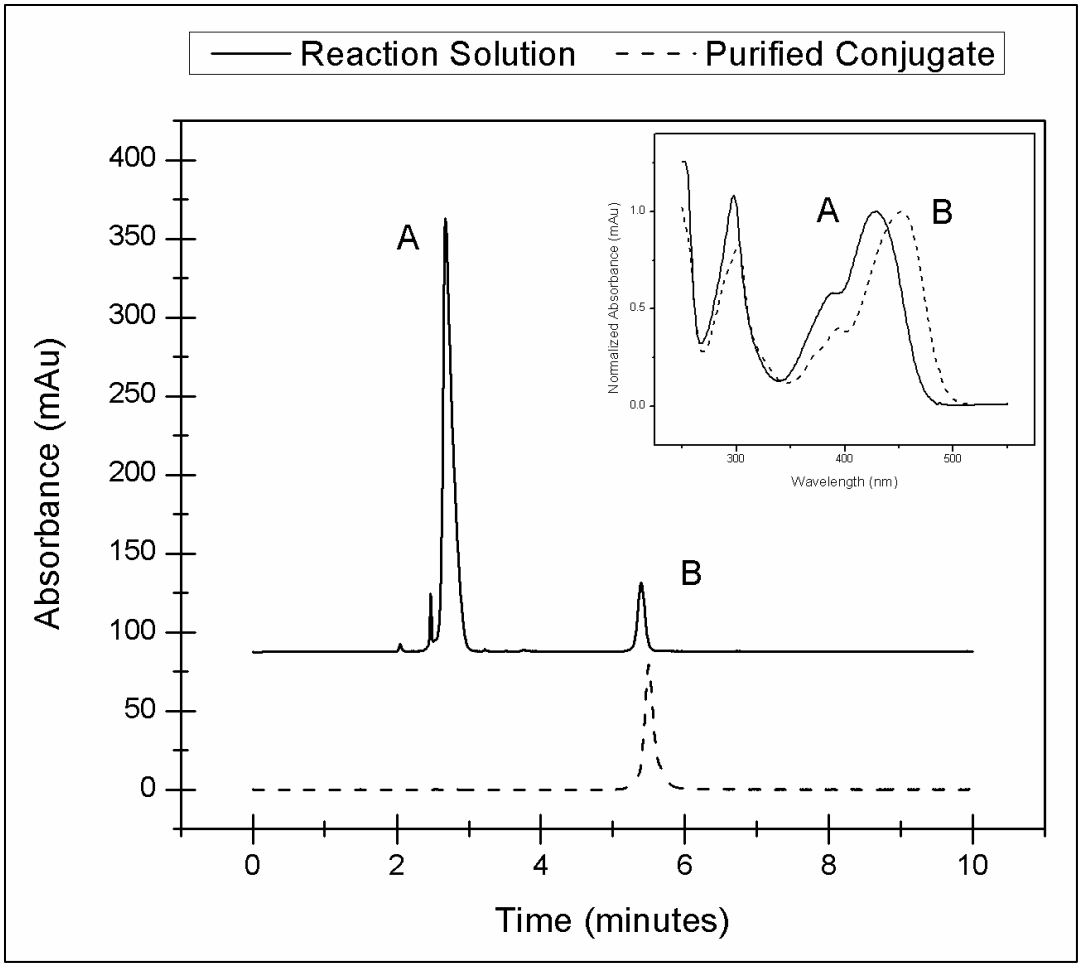

Figure 51: Separation of (A) APTS free dye from (B) APTS-MT product using HILIC chromatography. Inset: Comparison of the absorption spectra.

Fluorescence Characterization of APTS-MT

Excitation/Emission/Intrinsic Anisotropy

The final concentrations of the APTS-MT and APTS-glucose were determined using absorbance spectroscopy with the extinction coefficients found in the literature for APTS.[142] This was performed on a Cary-instrument using the appropriate corrections. Steady state fluorescence and intrinsic anisotropy measurements were performed on a

Fluorolog-3 from Horiba Jobin Jvon. For steady-state fluorescence measurements, solutions of 100 nM APTS and APTS-MT were made to avoid inner filter effects in TRIS buffer. Excitation and emission scans were performed to determine the fluorescence spectra of APTS-MT.

Intrinsic anisotropy measurements were performed by adding the fluorescent molecule of interest in a 50% glycerol solution at a concentration of 100 nM and setting the temperature to 5 deg C. This effectively slowed the rotation of our fluorescent molecules to negligible amounts (while in the excited state) which can allow the steady-state anisotropy value to be equivalent to the intrinsic anisotropy. Quartz cuvettes were used to avoid birefringence effects on the measured anisotropy. The anisotropy was recorded by collecting the emitted fluorescence at 520 nm with 5 nm bandpass. The G-factor was calculated for each sample. Ten measurements were taken for each sample, and the recorded anisotropy was the average of those measurements. Figure 52 shows the results of this steady-state fluorescence characterization for APTS and APTS-MT.

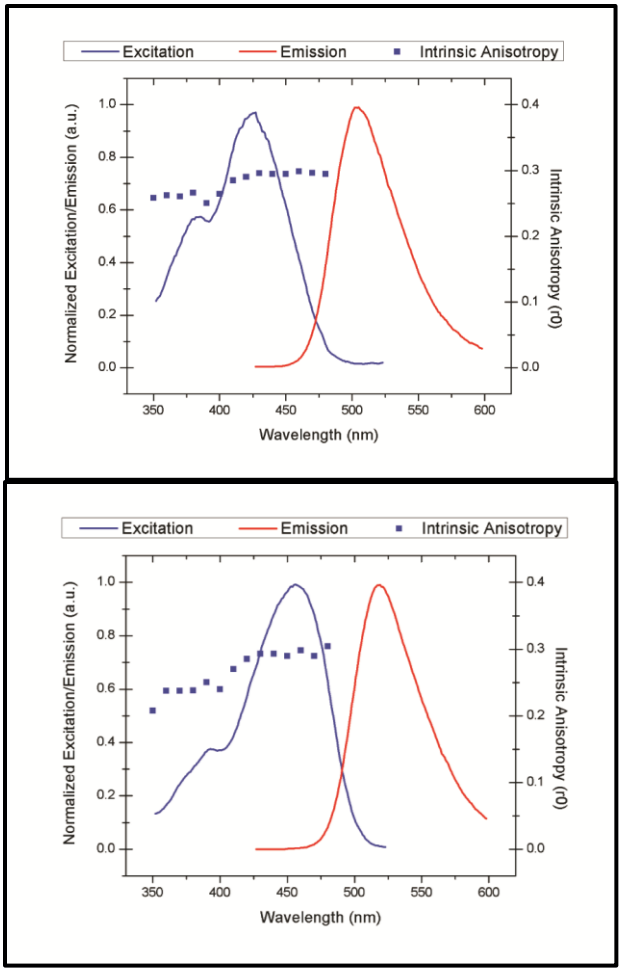

Figure 52: Fluorescent properties of APTS (top) and APTS-MT (bottom). Note that the excitation and emission shifts approximately 20 nm.

The fluorescence of unconjugated APTS shows an excitation maximum at ~425 nm and an emission maximum at ~505 nm. After conjugation, the APTS-MT smartly-designed fluorescent ligand shows an excitation maximum at ~460 nm and an emission maximum at~520 nm. APTS-glucose shows similar spectra to APTS-MT. All spectra are corrected for the instrument response. This shift in the fluorescence spectra upon conjugation is due to the reorientation of the electron density of the pyrene backbone,

and the shift in absorbance has commonly been used to identify via unique populations during chromatography. The fluorophore shows a relatively high stokes shift of approximately 70 nm, which allows for a large band of fluorescence wavelengths to be collected to improve without problems arising from scattered light.

Regarding the steady-state anisotropy, the fluorophores are effectively immobilized for the given fluorescence lifetime under these conditions. The intrinsic anisotropy is relatively stable for both conjugates near the excitation maximum, with a value of ~0.3. If a longer-lifetime fluorophore was used, higher viscosities and lower temperatures would need to be used.

Fluorescence Lifetime and Dynamic Anisotropy

The fluorescence lifetime and dynamic anisotropy data were collected using a DeltaFlex time correlated single photon counting system from Horiba that was equipped with a 482 nm DeltaDiode pulsed source. The emission was set to 520 nm with the slit-width allowing 8 nm bandpass. A 500 nm high-pass filter was used to avoid any scattered excitation light. The effect that ConA binding has on the rotational correlation lifetime of APTS-MT was studied using a solution of 200 nM APTS-MT with and without 1 μM ConA present. Quartz cuvettes were used to avoid birefringence effects on the anisotropy measurements. Neutral density filters were used to adjust the fluorescence intensity to allowable levels. For fluorescence lifetime measurements, the excitation polarizer was in the vertical orientation and the emission polarizer was set to the magic angle (~54.7°). Data was taken until the maximum counts were 10,000.

Silica particles in DI were used as the sample to scatter light to determine the pulse-shape of the 482 nm source. For dynamic fluorescence anisotropy measurements, the fluorescence emission was collected in parallel and perpendicular configurations until the difference of the first point was 15000 counts. The fluorescence intensity decays were analyzed with the Decay Analysis Software (v. 6.6) from Horiba, and fits were used according to the expected distribution in the solution. The dynamic anisotropy decays were analyzed by using a reconvolution algorithm to determine the best-fit rotational correlation lifetimes. The fluorescence lifetime decay is shown in Figure 53, which displays a single exponential decay of ~5.3 ns. The dynamic anisotropy curves with the modeled rotational correlation lifetimes are shown in Figure 54.

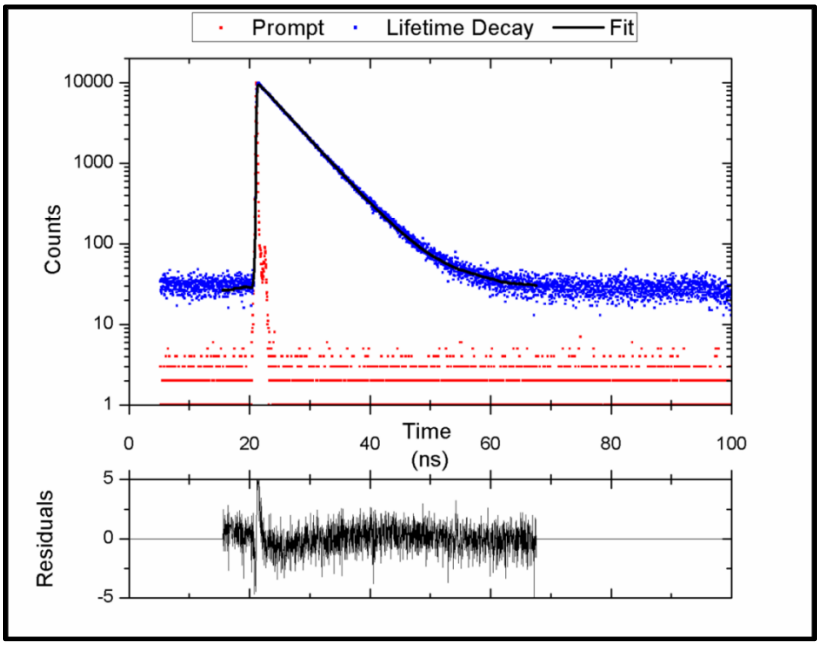

Figure 53: Fluorescence decay curve of APTS-MT, showing a lifetime of ~5.3 ns.

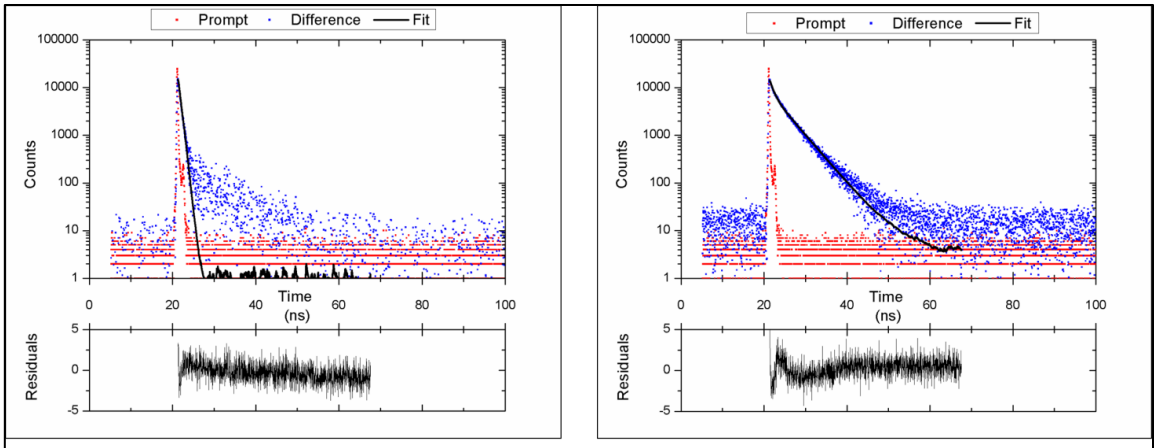

Sample	r_{tot}	r_1	θ_1	r_2	θ_2
200 nM APTS-TM	0.3109	0.3109	0.6061	-	-
200 nM APTS-TM w/ 1 uM ConA	0.3006	0.1673	1.010	0.1333	20.47

Figure 54: Dynamic anisotropy and rotational correlation lifetimes of APTS-MT with and w/o ConA

The reconvolution algorithm for the dynamic anisotropy displays rotational correlation lifetimes for the free and bound APTS-MT at ~1 ns and ~20 ns. The relative ratio between r1 and r2 is the relative fluorescence intensities between the two populations when the sample is initially pulsed. Therefore, if you assume that the quantum yield does not change upon binding and the solution is at steady-state binding, this is a measure of the relative concentrations of the APTS-MT in solution. These values suggest that at 1 µM, approximately 50% of the APTS-MT is bound to ConA, which is approximately what is expected with regard to the affinity.

These rotational correlation lifetimes are a measure of how fast the fluorescent particle is rotating in free solution. It would be ideal, therefore, for the fluorescence

lifetime to be between the rotational correlation lifetime of the bound fluorescent ligand and the free fluorescent ligand (Figure 55) to maximize the change of in the steady-state anisotropy.

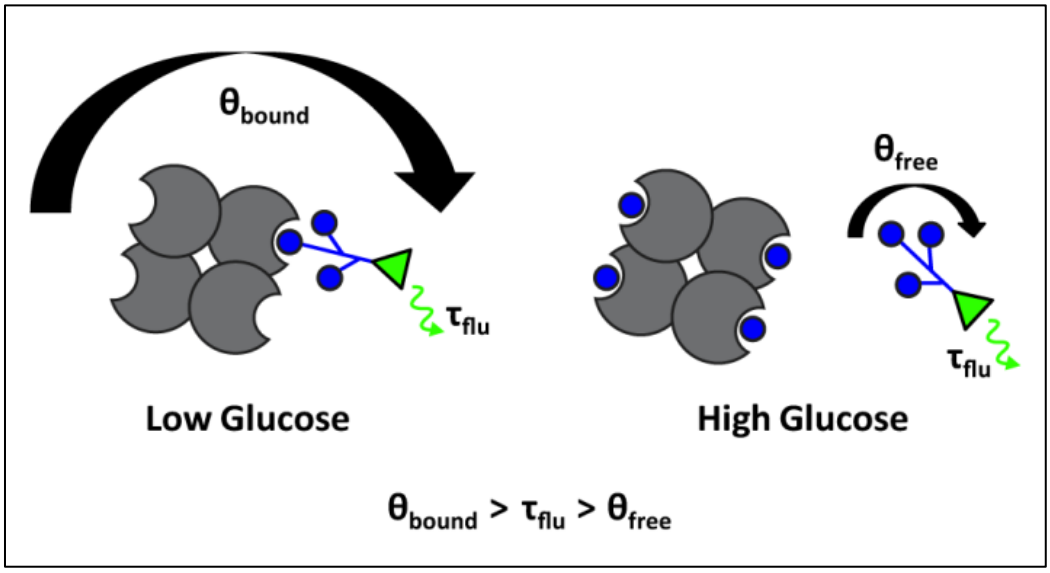

Figure 55: Schematic of the relationship between rotational correlation lifetimes and fluorescence lifetime. The optimal fluorescent lifetime is between the rotational correlation lifetimes of the bound and free fluorescent ligand.

Binding Characterization

A filter-based fluorescence microplate reader that was equipped with polarizers and the appropriate fluorescence filters for APTS was used to perform binding studies. The equilibrium-binding between ConA and APTS-MT was performed by loading a microplate with serial dilutions of ConA and the same concentration of APTS-MT (500 nM). The plate was allowed to reach equilibrium at room temperature (22 deg C), and

scans were performed in the perpendicular and parallel directions. Background was subtracted from each value. The G-factor was calculated from the fluorescence anisotropy for free APTS-trimannose at a value of 0.03, and this G-factor was used for the remaining experiments. Assuming the change in fluorescence lifetime upon binding to ConA to be negligible, the ConA-dependent anisotropy was calculated and shown in Figure 56. These results were fit with a Boltzmann curve to determine the association constant to be $5.61*10^6\ M^{-1}$.

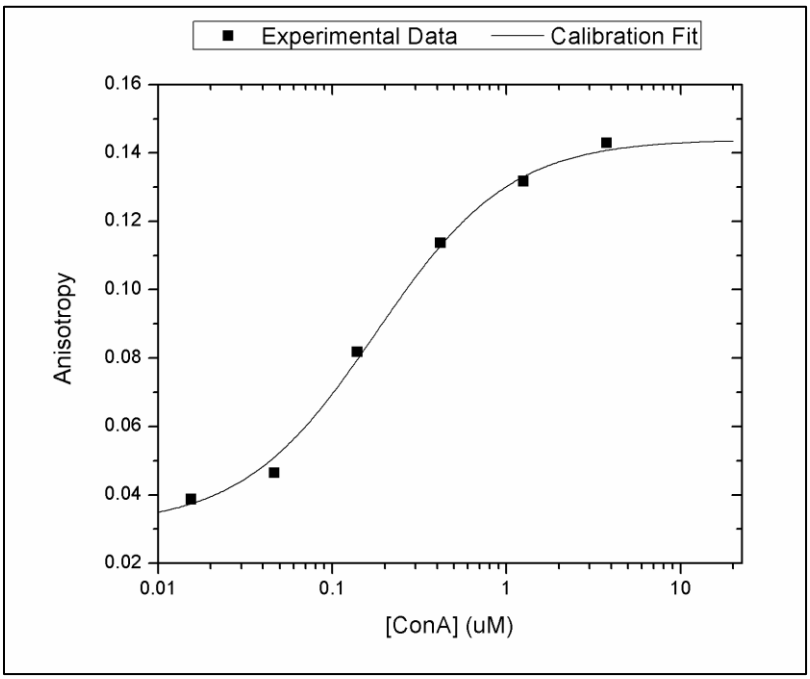

Figure 56: Fluorescence anisotropy response of 200 nM APTS-MT to increasing [ConA]. The K_a was determined to be $5.61*10^6\ M^{-1}$.

Implementation of Smartly-Designed Fluorescent Ligand

Comparison to Ideal Characteristics

The experimentally determined characteristics of the APTS-MT can then be plotted on the 2D sensitivity maps to have an idea of its expected ability to optimize these mechanisms. It is shown as the black X on the recognition map of Figure 57 and on the transduction map of Figure 58. The white x is the 4 kDa FITC-dextran from the previous chapter. This shows that it is expected to show significantly improved results when compared to the results from the 4 kDa FITC-dextran.

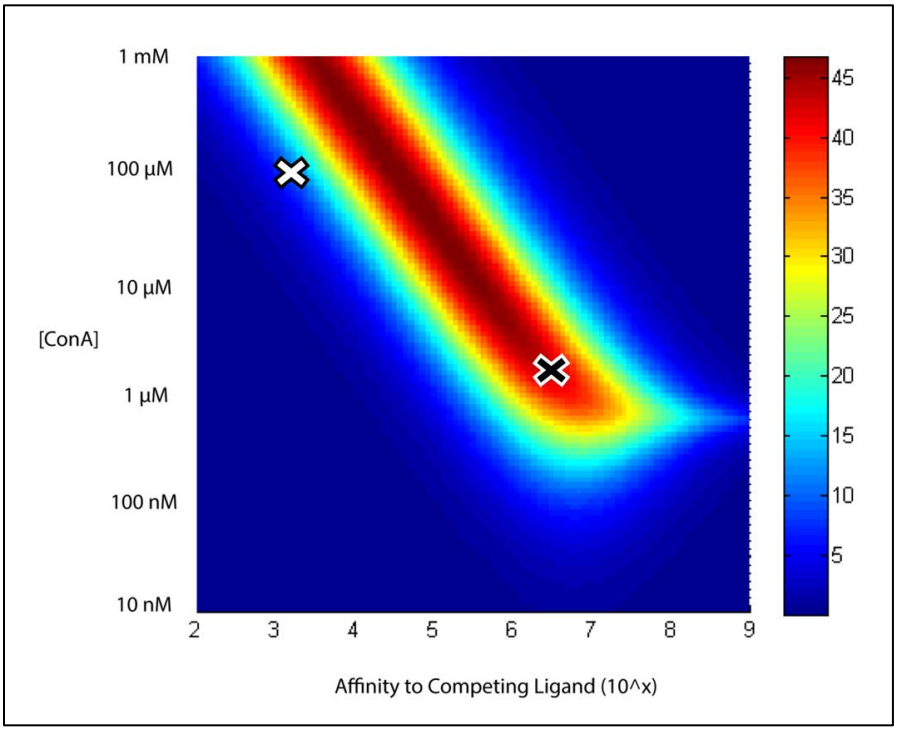

Figure 57: Modeled recognition sensitivity of ConA-based sensor with a fluorescent competing ligand at 500 nM. The white X represents 4 kDa FITC-dextran. The black X represents APTS-MT.

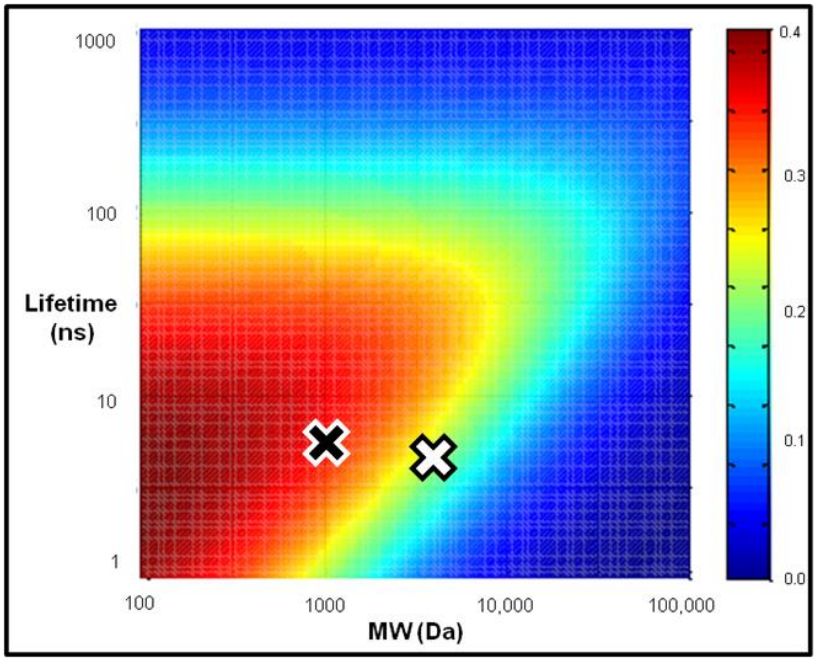

Figure 58: Modeled transduction sensitivity (anisotropy). The white X represents 4 kDa FITC-dextran. The black X represents APTS-MT

The suitability of the fluorescence lifetime to transduce the binding event can also be shown by directly comparing it with a curve from the measured rotational correlation lifetimes. The steady-state anisotropy for each rotational correlation lifetime was predicted for the full range of possible fluorescence lifetimes. Figure 59 shows the difference between these two curves in the red. The ideal fluorophore for a specific change in rotational correlation lifetimes would display a fluorescence lifetime that generates the largest change in the steady-state anisotropies. The APTS-MT fluorescence lifetime of 5.3 ns matches the peak of that curve, making it ideal to optimize the transduction mechanism of the fluorescence assay.

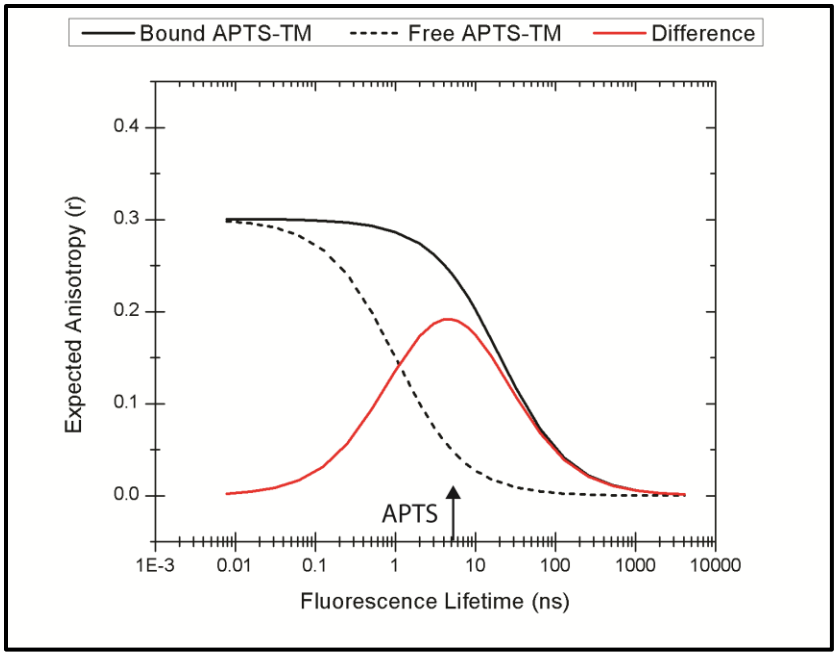

Figure 59: This shows the expected steady-state anisotropy of the bound (solid) and free (dotted) APTS-MT for a range of fluorescence lifetimes. The difference of the bound and free is indicated in red, and the APTS-lifetime is shown with the arrow.

Fluorescence Anisotropy Based Assay

Various Sugars

Using the results from the modeled assay, the concentrations of the binding assay were chosen to be 200 nM APTS-MT and 1 µM unlabeled ConA. Following a similar strategy as the affinity-binding studies between APTS-MT and ConA, microplate wells were loaded with this assay with varying concentrations of methyl mannose, glucose, and galactose from ~0.2 mg/dL to ~10,000 mg/dL. The assay was given an appropriate time to reach equilibrium at room temperature (22 deg C) and the steady state anisotropy

was scanned using the filter-based fluorescence microplate reader. The results are displayed in a semi-log plot in Figure 60

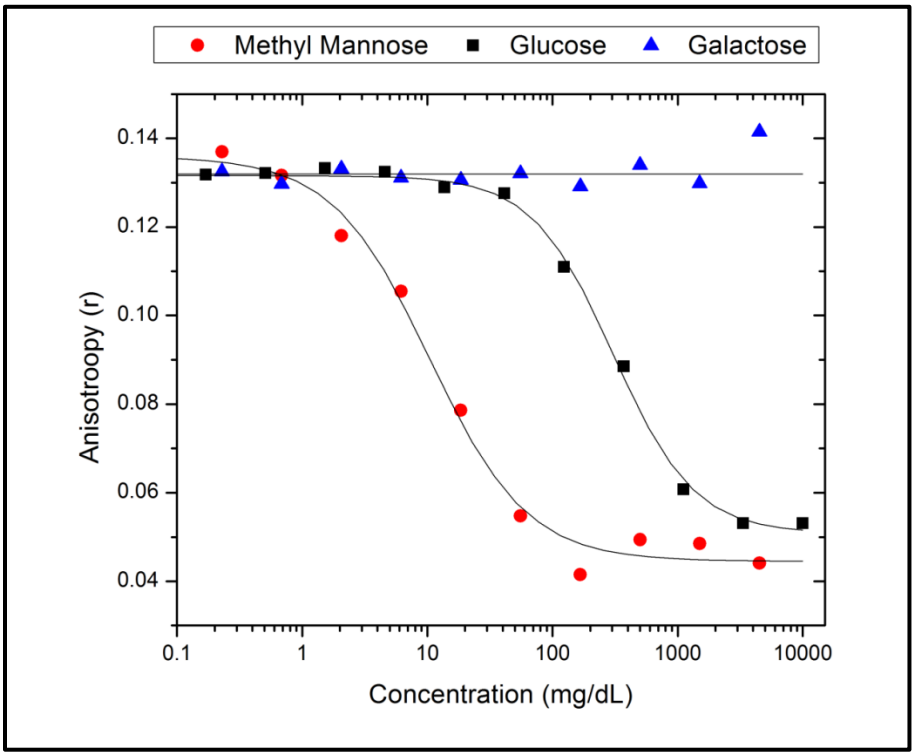

Figure 60: Fluorescence anisotropy response of the 200 nM APTS-MT, 1 µM ConA assay to methyl mannose, glucose, and galactose

The responses in Figure 60 shows that the binding of the APTS-MT to ConA is effectively inhibited by monosaccharides that are known to only bind to the primary binding of ConA (mannose and glucose). In addition, methyl mannose is known to have a binding affinity that is ~20-40 times higher than glucose.[123] The concentration that causes a 50% reversal of the binding is on that order of increase for glucose. This is

what is expected from the Chung-Prusoff equation for competitive binding.[143] Lastly, galactose has no response on the assay, which is also to be expected. Galactose shows no affinity to ConA, therefore it is not expected to displace the APTS-MT. This set of results is highly encouraging and suggests that the APTS-MT is truly undergoing true competitive binding.

Calibration and Prediction of Glucose

Additional anisotropy experiments were performed with the assay to have more measurements in the physiologically relevant glucose concentrations. The actual glucose concentrations were determined on a YSI biochemistry analyzer. These anisotropy values, shown in Figure 61 were used to generate a calibration fit via the typical competitive binding equation, and this equation was used to predict the glucose concentrations. The prediction glucose vs. actual glucose (using the same data set) curve is shown in Figure 62. This shows a standard error of calibration of 8.5 mg/dL and a mean absolute relative difference (MARD) of 6.5% across physiologically relevant glucose concentrations. In comparison to the prediction vs. actual plot of the assay based on the 4 kDa FITC-dextran, the points using the APTS-MT are much closer to the central line. The slight fluctuations are expected to either be pipetting error rather than error with the assay.

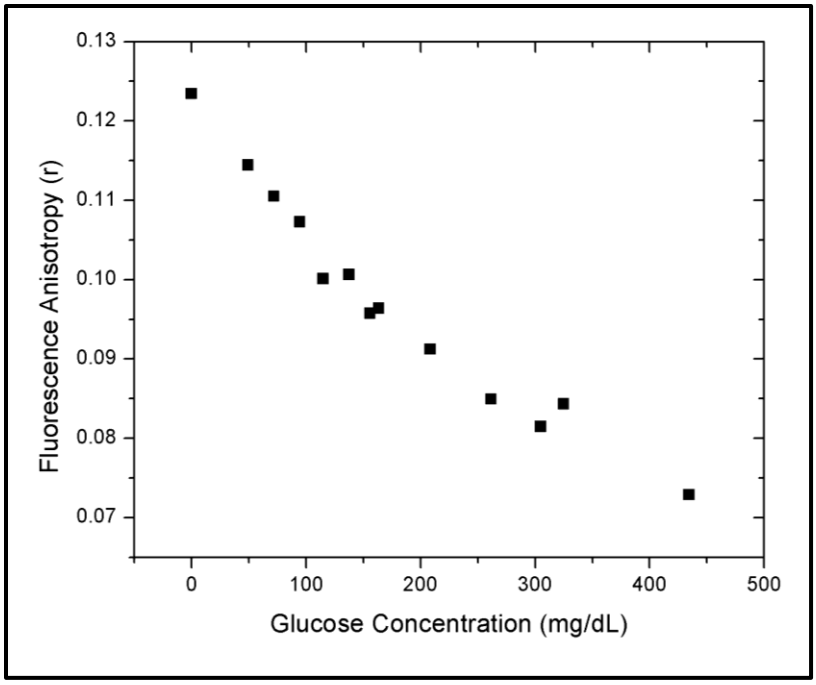

Figure 61: Fluorescence anisotropy response to physiological glucose concentrations using a 200 nM APTS-MT, 1 µM ConA solution in TRIS buffer at 22 deg C.

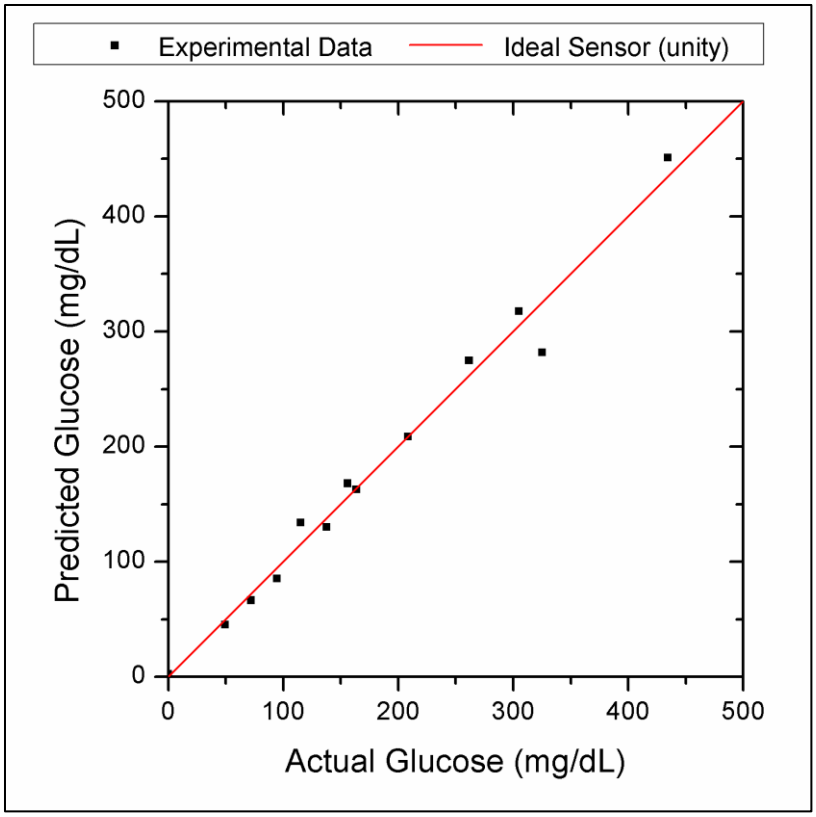

Figure 62: Predicted glucose vs. actual glucose for the FA competitive binding assay using 200 nM APTS-MT and 1 µM ConA.

FRET-Based Glucose Assay

Even though this optimized anisotropy-based assay transduces the glucose concentrations effectively, an assay based on FRET has the potential to increase the sensitivity further. The anisotropy-assay is only as good as the polarizers that are being used. In this case, we are using polarizers with an extinction of 6000:1. Even with improved polarizers, there will be considerable more error in an optimized anisotropy assay than an optimized FRET assay. As a result, a FRET assay was then generated to use the smartly-designed fluorescent ligand as the donor.

The APTS-MT is expected to be extremely well-suited to translate to a FRET-based assay because it is the first fluorescent ligand for ConA-based assays that displays a fluorophore directly next to the only moiety to which ConA can bind. Traditional ligands paired with ConA (such as 70 kDa dextran) have been 10 nm in diameter and have displayed multiple places for ConA to bind. Upon binding of an acceptor-labeled ConA to the multivalent fluorescent ligand, the fluorophore on the fluorescent ligand could be various distances to the acceptor fluorophores on ConA. Because of the possible distances between donor and acceptor fluorophores, this can result in a binding event that appears to still be in free solution.

This APTS-MT avoids that fate by bringing the fluorophore to within ~1 nm of ConA's binding site every time that ConA binds the APTS-MT. Therefore, with the appropriate acceptor fluorophore on ConA and with high enough degree of labeling, the expected FRET efficiency upon binding can be very high. For these experiments, TRITC was used as the acceptor fluorophore and was labeled to ConA. The degree of labeling was approximately 4 fluorophores per ConA. Fluorescence measurements were performed on an ISS PC1 spectrofluoremeter. The concentrations used to obtain the excitation/emission spectra for APTS-MT and TRITC-ConA was 100 nM and 1 μM, respectively. This is expected to have a Förster radius similar to FITC/TRITC (~5 nm). The excitation and emission properties are shown in Figure 63.

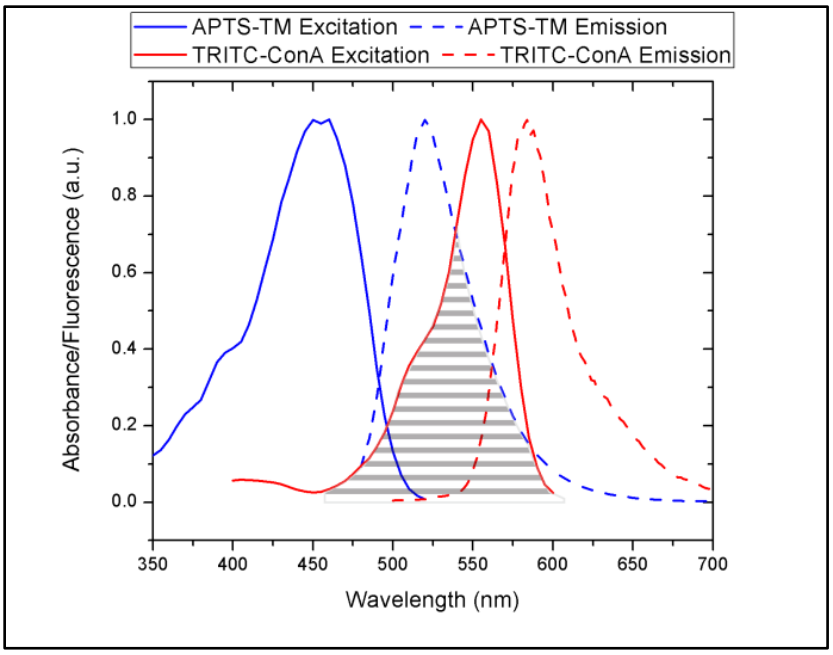

Figure 63: The excitation and emission properties of the APTS-MT and the TRITC-ConA used in the FRET assay. The shaded area indicates the spectral overlap.

A 100 nM APTS-MT solution was then made in TRIS buffer for titration experiments. Increasing TRITC-ConA concentrations were added to the cuvette, and fluorescence measurements were taken. The resulting spectra are shown in Figure 64, which display a decrease in the donor fluorescence (APTS-MT) and an increase in the acceptor fluorescence (TRITC-ConA).

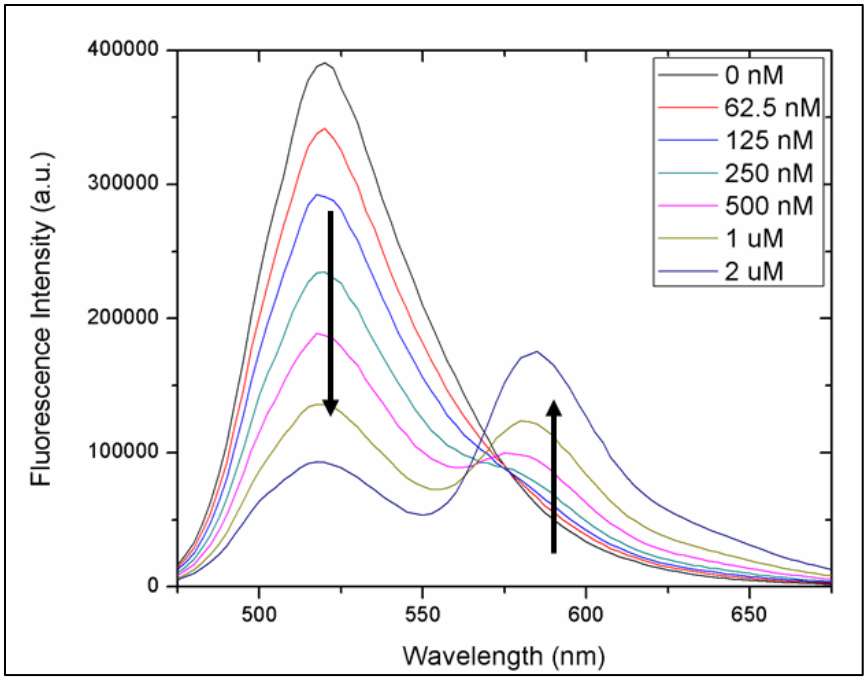

Figure 64: Fluorescence emission from a sample with 100 nM APTS-MT and increasing [TRITC-ConA].

The fluorescence intensity at 520 nm (from the APTS-MT) for each TRITC-ConA concentration was normalized to the fluorescence intensity at 520 nm in the absence of TRITC-ConA. These values were then plotted as a function of the APTS-ConA concentration and are shown in Figure 65. This data was fitted with Equation 18 to account for both of the components that decrease the fluorescence intensity. This includes: (1) the energy transfer associated with binding to the TRITC-ConA and (2) the effects that adding the acceptor fluorophore to the bulk solution. This fitting shows that the affinity of the APTS-MT and TRITC-ConA binding is 3,522,367 M^{-1}, which is slightly lower than the affinity obtained from anisotropy measurements with unlabeled

ConA. The fitting also showed that b was equal to 0.1968, which indicates the intensity that is expected to be seen if 100% of the APTS-MT was bound. This value can be used as a measure of the average FRET efficiency of the bound population, and suggests that the efficiency for this competitive binding pair is ~80.3%. This confirms that the smartly-designed fluorescent ligand can effectively bring the fluorophore to within the Förster radius of the FRET pair upon binding.

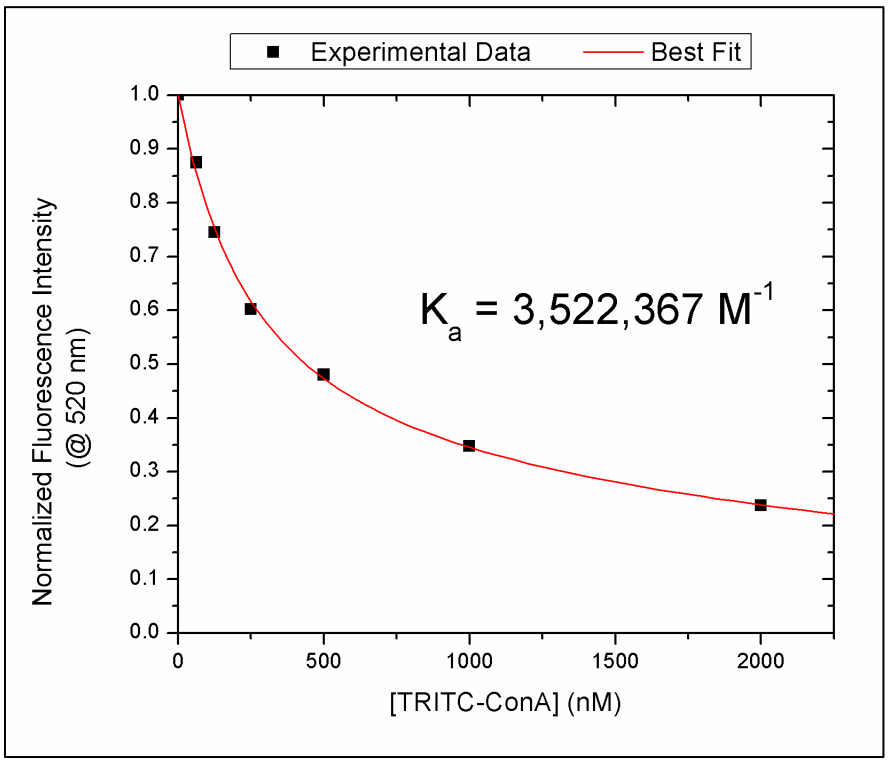

Figure 65: Decrease in fluorescence intensity from APTS-MT as a function of [TRITC-ConA] and the best fit using Eq. 18. The K_a of the specific binding is shown.

$$y = \left((a-b)/\left(1+(x/c)\right)+b\right)+d*x \qquad (18)$$

The acceptor-peak fluorescence intensity should show a similar affinity; however, the tail of the emission from the APTS-MT overlaps with the emission of the TRITC-ConA. Therefore, spectral un-mixing was performed to study the acceptor fluorescence. These unmixed spectra of TRITC-ConA emission are shown in Figure 66. The peak of this emission at 585 nm of each of these curves was plotted as a function of the TRITC-ConA concentration and shown in Figure 67. Again, this is fit with Equation 18 to account for both of the components that increase (in this case) the fluorescence intensity. This fit shows that the affinity of the APTS-MT and TRITC-ConA binding is 3,258,390 M^{-1}, which agrees well with the information obtained from the donor peak.

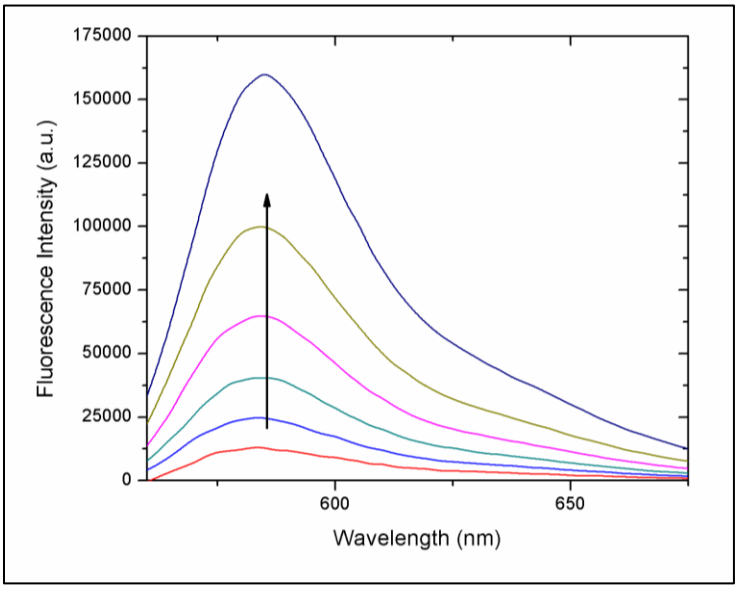

Figure 66: Fluorescence intensity of the TRITC-ConA as a function of increasing [TRITC-ConA] after spectral unmixing to remove the APTS-MT emission.

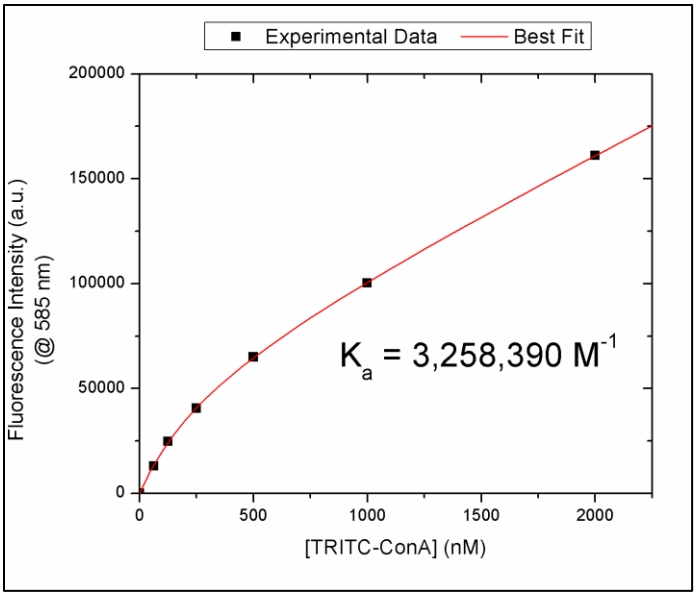

Figure 67: Increase in the fluorescence intensity from TRITC-ConA as a function of [TRITC-ConA], and the best fit using Eq. 18. The K_a of the specific binding is shown.

A FRET-based competitive assay was then generated that was comprised of 100 nM APTS-MT and 1 µM TRITC-ConA in TRIS buffer. This was used to track the competitive binding to various sugars with the fluorescence. Upon titration of highly concentrated aliquots of methyl-alpha-mannose and glucose, sufficient was time was given to allow for equilibrium to be reached before fluorescence measurements were made. Excitation was performed at 450 nm with a 15 nm bandpass and emission was collected from 475 nm to 675 nm to collect both APTS and TRITC's emission. The responses are shown in Figure 68. The blue and red lines show indicate the wavelengths (520 nm and 600 nm) that are used to generate the fluorescence ratio (520:600).

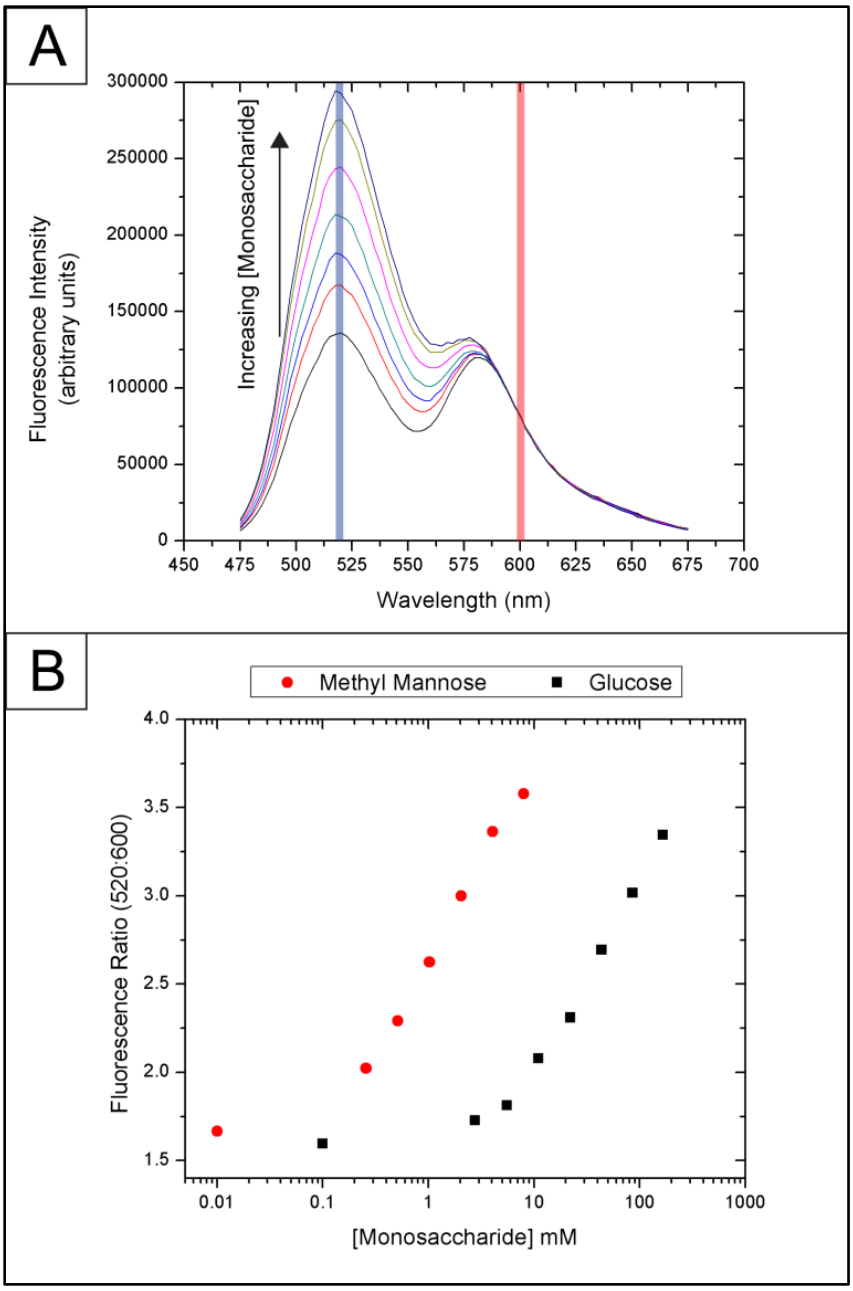

Figure 68: Fluorescence response to increasing concentrations of methyl mannose and glucose in the FRET assay (100 nM APTS-MT and 1 µM TRITC-ConA), showing the (A) spectra and (B) ratio on a semilog plot.

The resulting spectra show that increasing concentrations of the monosaccharides increase the relative fluorescence of the donor-fluorophore, which is characteristic of competitive binding. The acceptor emission appears to increase slightly with increasing concentrations of monosaccharides, but this is due to the spectral overlap of the tail of the emission of APTS-MT at longer wavelengths. By taking a ratio of the main peak of the donor fluorescence (at 520 nm, blue line) and the tail of the acceptor fluorescence (at 600 nm, red line), a ratiometric signal was generated. These ratiometric responses show a similar effect to what is seen for the anisotropy-based assay as seen in the semilog plot in Figure 68B. The assay responds to lower concentrations of methyl-mannose than glucose, which is to be expected because of ConA's higher affinity to methyl-mannose.

Figure 69 shows the glucose dependent fluorescence ratio on a linear plot with the best fit data using the aforementioned curve for competitive binding data. The r^2 of this fit is 0.9986. This specific assay shows a linear response across the physiological glucose concentrations. The prediction glucose vs. actual glucose (using the same data set) curve is shown in Figure 70. Again, the error associated with this fit is most likely due to pipetting error. This assay could be tweaked to maximize the response, as the effective IC_{50} for the fit is 792 mg/dL. The response could also be increased by labeling ConA with additional acceptor fluorophores to increase the FRET efficiency upon binding to the APTS-MT.

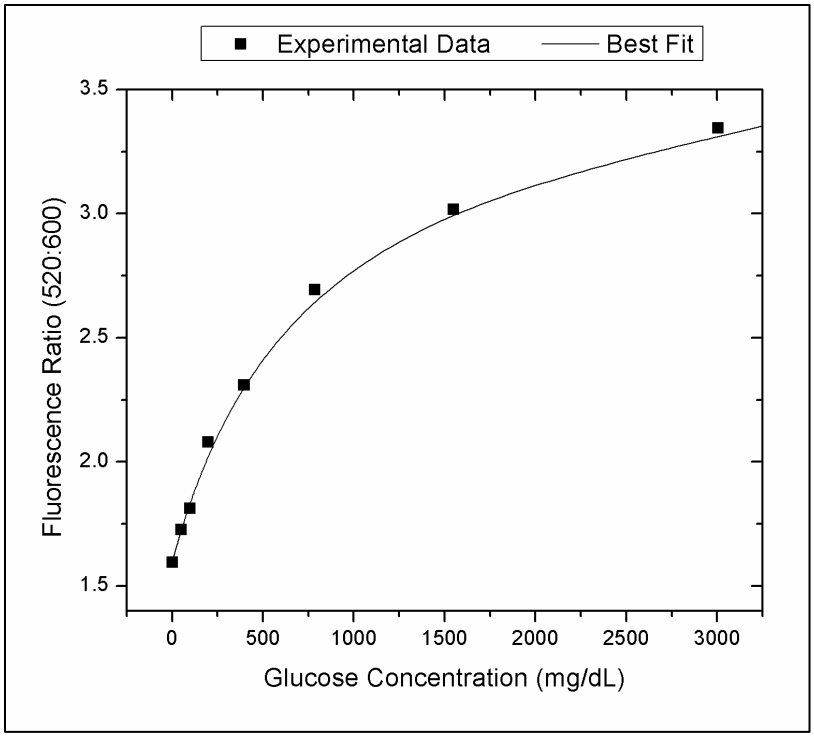

Figure 69: Glucose-dependent fluorescence ratio using the FRET-based sensing assay with the smartly-designed fluorescent ligand.

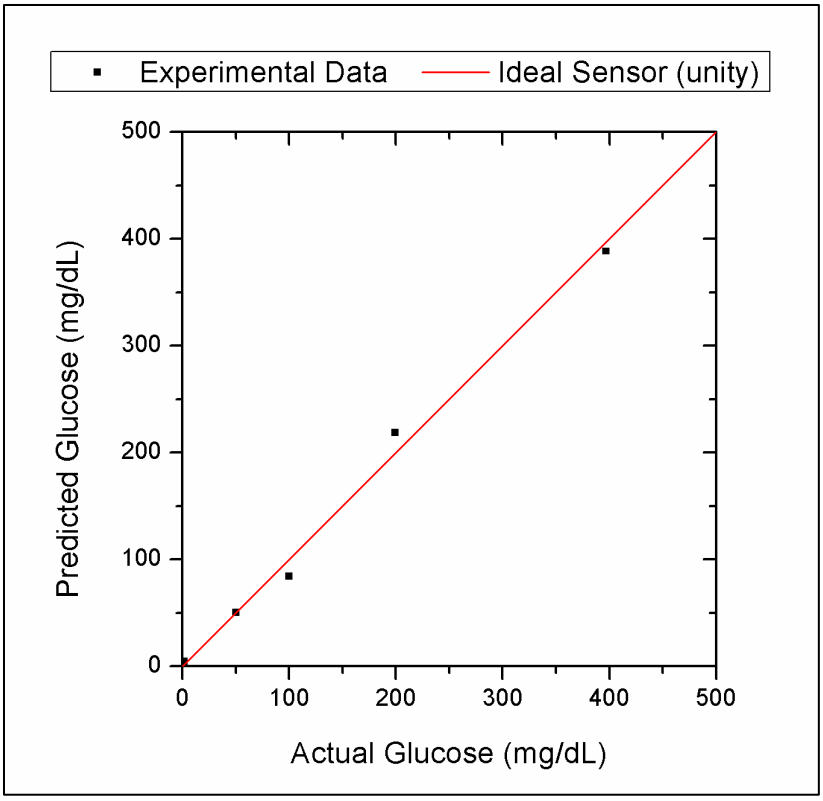

Figure 70: Predicted glucose vs. actual glucose for the FRET competitive binding assay using 100 nM APTS-MT and 1 µM TRITC-ConA.

Conclusions

This chapter introduces a modular approach to the design of a smartly-designed fluorescent ligand to achieve the desired qualities as outlined in the previous chapter. The core trimannose was identified as a potential high-affinity ligand for ConA due to binding of it to the extended binding site of ConA (also known as subsite). This core trimannose showed no aggregation when paired with ConA, and a fluorescent ligand was synthesized to present a single trimannose moiety. This smartly-designed fluorescent ligand was characterized and shown to be in the optimized regions of the sensitivity

maps as previously defined. According to those maps, the assay was implemented into anisotropy and FRET-based assays for glucose. These assays showed a dynamic response across physiological glucose concentrations – where the error was most likely due to pipetting error rather than instrument error.

The comparison of this first generation smartly-designed fluorescent ligand to previously-used high-affinity fluorescent ligands is shown in Table 7. This ligand is expected to remain stable when paired with ConA as it shows a single sugar motif, to avoid crosslinking between multivalent components and it is negatively charged to avoid electrostatic effects. Finally, the fluorophore is near the motif to allow for the FRET-efficiency upon binding to be maximized.

Table 7: Comparison of various ligands with regard to desirable characteristics for a ConA-based sensor, including the 1st generation smartly-designed fluorescent ligand (APTS-MT)

	Dendrimer	Dextran	1st Gen SFL
Single Sugar Motif	✗	✗	✓
Neutral or Neg Charged	✗	✓	✓
Fluorophore Near Motif	✗	✗	✓

CHAPTER V

A 2ND GENERATION SMARTLY-DESIGNED FLUORESCENT LIGAND BASED ON GLYCATED OVALBUMIN*

Introduction

Requirements for Final Assay

The previous chapter introduced the smartly-designed fluorescent ligand concept to overcome the irreversibility/aggregation problems that have plagued ConA-based glucose sensing assays in free solution. This smartly-designed fluorescent ligand: (1) displays a single moiety that can bind to ConA's full binding site, (2) is negatively charged, and (3) is fluorescently labeled. An obstacle remains for this strategy to be used in a continuous glucose sensor: the size of this smartly-designed fluorescent ligand must be increased to prevent leaching from the semi-permeable membrane that allows for glucose diffusion. Figure 71 is a cartoon schematic that shows the relationship of various ligands to the pore size of the semi-permeable membrane.

---

* Part of this chapter is reprinted from B. M. Cummins, J. Simpson, Z. Gryczynski *et al*. "ConA-based glucose sensing using the long-lifetime Azadioxatriangulenium fluorophore" (2014) with kind permission of SPIE, Copyright 2014.

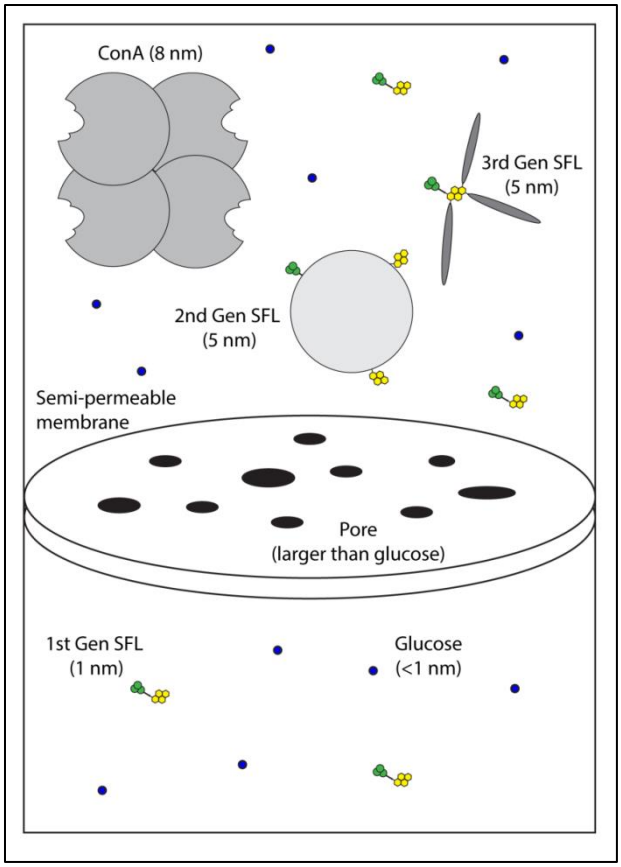

Figure 71: Schematic representation of the semi-permeable membrane and the molecular sizes that will be required for the smartly-designed fluorescent ligand to prevent leaching.

Ovalbumin Characteristics

This chapter introduces ovalbumin (the primary protein in egg-white) as the high-affinity fluorescent ligand in a ConA-based glucose sensing assay. We have identified ovalbumin as a possible template for a 2nd generation smartly-designed fluorescent ligand as: (1) it has a single glycosylation site that can present a high-mannose glycan (contains the core trimannose), (2) it is negatively charged at

physiological pH (with an isoelectric point of 4.5), (3) it has a molecular weight of 45 kD, and (4) it has numerous lysine residues that can be labeled with an amine-reactive fluorophore.[144] Table 8 shows the comparison of the expected fluorescent glycated ovalbumin in comparison to the fluorescent dextran, fluorescent dendrimer and the 1st generation smartly-designed fluorescent ligand. While this strategy does not display the fluoroophore near the sugar motif, this strategy was can possibly be used as a cost-effective method to generate the bulked-up, 2nd-generation, smartly-designed fluorescent ligand without a significant number of synthetic steps.

Table 8: Comparison of various ligands with regard to desirable characteristics for a ConA-based sensor, including the proposed 2nd generation smartly-designed fluorescent ligand based on ovalbumin.

	Dendrimer	Dextran	1st Gen SFL	2nd Gen SFL - Ovalbumin
Single Sugar Motif	✗	✗	✓	✓
Neutral or Neg Charged	✗	✓	✓	✓
High MW	✓	✓	✗	✓
Fluorophore Near Motif	✗	✗	✓	✗

Aadioxatriangulenium (ADOTA) Fluorophore

This preliminary study uses the Azadioxatriangulenium ($ADOTA^+$) fluorophore as $ADOTA^+$ has fluorescence properties ideal for tracking the binding between ovalbumin and ConA.[145-147] $ADOTA^+$ displays excitation and emission maxima at 540 nm/560 nm with a fluorescence lifetime of ~23 ns. It has moderate brightness with a molar extinction coefficient of 9,800 $cm^{-1}M^{-1}$ and a quantum yield of 0.49 (determined in acetonitrile), with an intrinsic anisotropy has been shown to be 0.38.[148,149] The structure of ADOTA-NHS is shown in Figure 72. With these fluorescence properties, $ADOTA^+$ can allow binding studies between relatively large molecules to be tracked with anisotropy,[150] and it can be used to avoid the shorter fluorescence lifetimes that are common for endogenous fluorophores.[151]

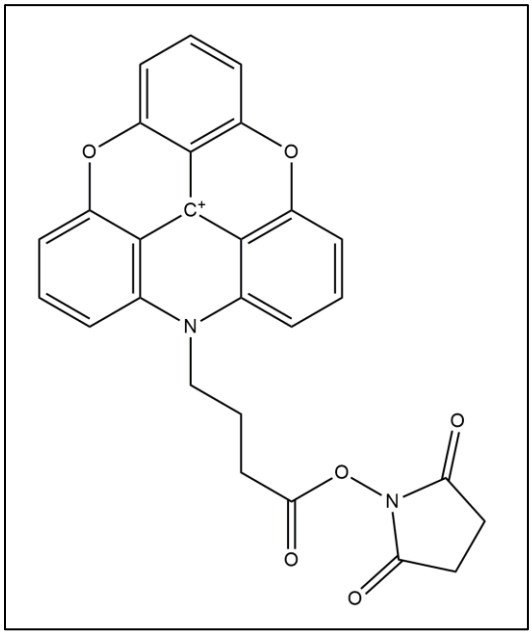

Figure 72: Structure of ADOTA-NHS

Preparation of ADOTA-Labeled Glycated Ovalbumin

The ConA-based assay, as we present it, tracks the fluorescence intensity from the fluorescently-labeled ovalbumin. As a result, it is essential that all of the ovalbumin can bind to ConA. If a portion of the fluorescently labeled ovalbumin cannot bind to ConA, it will serve as a background signal that is not sensitive to glucose concentration and will increase the error of the sensor. The glycans on proteins can display a significant amount of variation, and a large fraction of proteins that can be glycated do not actually display glycans. A schematic of the preparation of the ADOTA-labeled glycated ovalbumin (ADOTA-OVA) and how it will be implemented in the assay is shown in Figure 73.

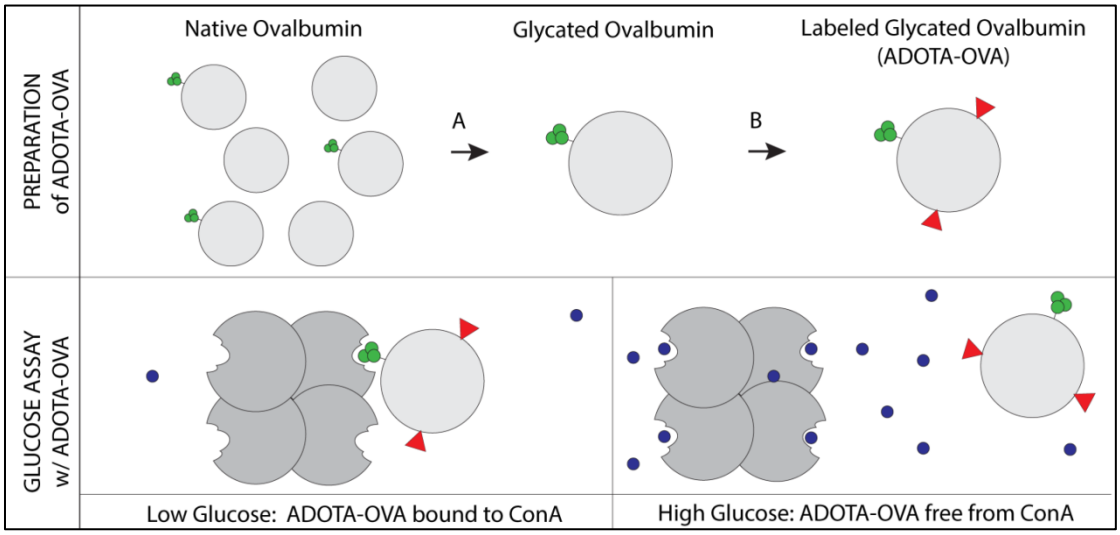

Figure 73: Top: Schematic of the preparation of ADOTA-OVA from native ovalbuminm, including (A) affinity chromatography and (B) fluorescent labeling. Bottom: Schematic glucose response of the ConA-based assay with the ADOTA-OVA

Affinity Chromatography

We separated the glycated fraction from the non-glycated fraction of our ovalbumin sample by performing affinity-chromatography with ConA-functionalized resin. The protein elution from the column was tracked by monitoring the absorbance at 280 nm. After the non-glycated fraction eluted from the column, high concentrations of mannose were used to elute the glycated fraction. This glycated fraction was collected and dialyzed in sodium bicarbonate buffer to prepare it for labeling. The elution profile of the affinity chromatography is shown in Figure 74.

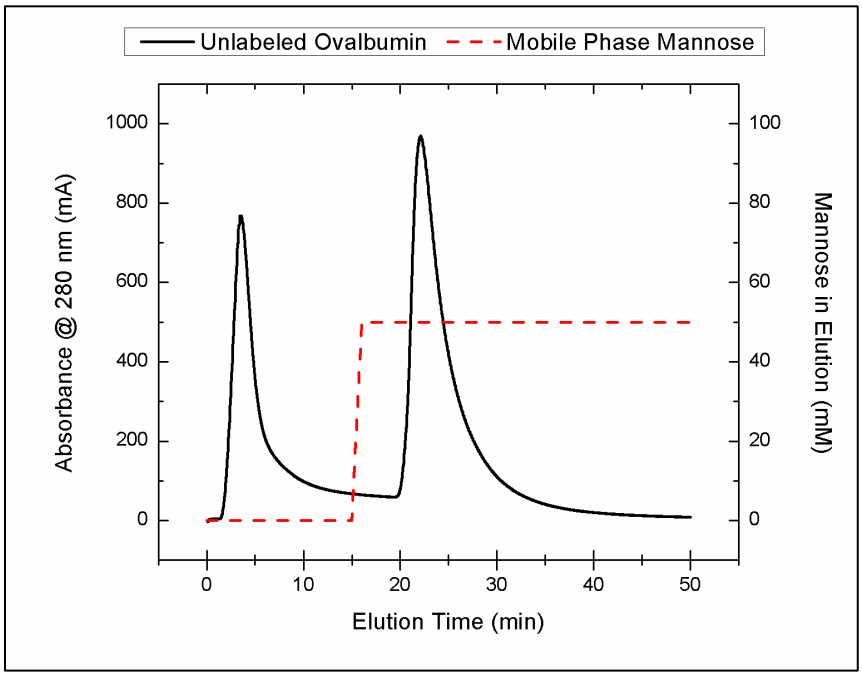

Figure 74: Affinity chromatography of the native ovalbumin sample to separate the non-glycated fraction (1st peak) from the glycated fraction (2nd peak).

Fluorescent Labeling of Ovalbumin

This glycated fraction of the ovalbumin was labeled with the ADOTA-NHS according to traditional amine-reactive protocol. Briefly, ADOTA-NHS was dissolved in DMSO, added dropwise to the solution of glycated ovalbumin in sodium bicarbonate buffer (pH 9 to deprotonate the primary amines), mixed well, and allowed to react for 1 hour in the dark at room temperature. Afterwards, the free dye was removed via dialysis against TRIS buffer, and the solution was filtered with syringe filters. In other samples, the free dye was removed via size exclusion chromatography (SEC) with the HPLC pump system. For both the SEC and syringe filter step, it was clear that a significant amount of fluorescent material was getting stuck in the matrices. Because this solution should not be capable of labeling the Sephadex media or the cellulose membranes, this could indicate that the ADOTA-OVA aggregated with itself. Unfortunately, if ADOTA-OVA aggregates with itself, this would present multiple glycans on the surface of a single complex and decrease the effectiveness of the ovalbumin to serve as a smartly-designed fluorescent ligand. Nevertheless, this ADOTA-OVA was tested experimentally to determine its ability to be used in a glucose sensor. If it truly is aggregating, there are potential methods to decrease these non-specific interactions.

To determine the concentrations and degree of fluorescent labeling, UV/VIS absorbance measurements were performed in TRIS buffer. Using the molar extinction coefficients, the concentration and degree of labeling of the ADOTA-OVA was determined. Similar UV/VIS studies were performed with the AF647-ConA that was purchased from Invitrogen. The degree of labeling of the ADOTA-OVA was

determined to be approximately 1.5 ADOTA fluorophores per glycated ovalbumin. The degree of labeling of the AF647-ConA was determined to be approximately 3 AF 647 fluorophores per ConA.

An expected 3D representation of the ADOTA-glycated ovalbumin was developed by using the x-ray crystallography structure of ovalbumin found published (PDB: 3VVJ) and altering it in the Maestro software. To the asparagine residue (Asp-292), a high mannose glycan was attached. Two ADOTA fluorophores were attached to two of the primary amines coming from the lysine groups. This representation is shown in Figure 75.

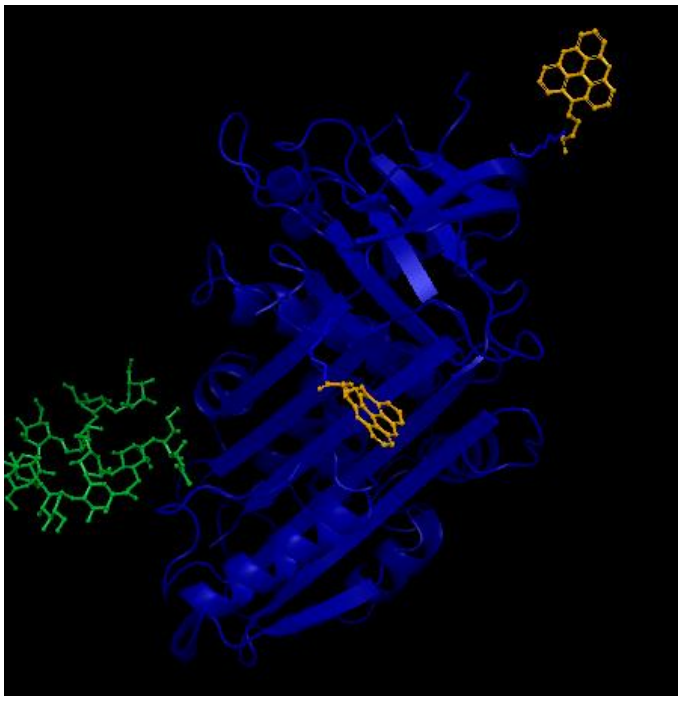

Figure 75: Expected structure of the ADOTA-glycated ovalbumin as modified from the crystallography structure for ovalbumin (blue) (3VVJ) with the glycan (green) and ADOTA (yellow).

Fluorescence Anisotropy with ADOTA-OVA

Figure 76 shows the 2D sensitivity map for the anisotropy transduction mechanism as previously defined. Fluorescence anisotropy is typically limited to tracking small fluorescent ligands to large receptors. Since ovalbumin is relatively large in size (~45 kDa), most organic fluorophores would not show a change in anisotropy upon binding as they typically display a fluorescence lifetime of a few ns. ADOTA can allow the equilibrium binding of ovalbumin and ConA to be tracked with fluorescence anisotropy because of its longer fluorescence lifetime (~20 ns). The white dot displays the expected location of ADOTA-OVA on this map of the transduction sensitivity.

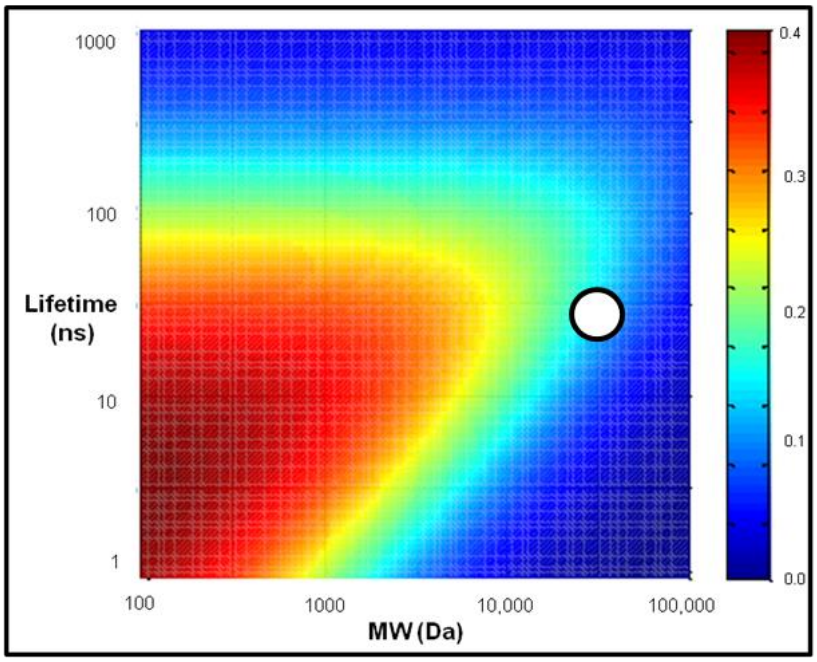

Figure 76: The fluorescence anisotropy sensitivity as a function of MW and lifetime. The white dot represents ADOTA-OVA.

Being able to track the ovalbumin-ConA interactions with anisotropy, allows the association constant to be determined in a realistic environment. This association constant can then be confidently used in the competitive binding model to generate an optimized assay for the desired glucose concentration range. The fluorescence anisotropy of a 500 nM solution of ADOTA-glycated ovalbumin was tracked as a function of ConA concentration using a Fluorolog 3 spectrofluorometer and is shown in Figure 77. This data was fit with a Boltzmann curve, and the affinity was determined to be 587,000 M^{-1}. This anisotropy could be used as a glucose-sensor like in the previous chapter; however, the limited change in anisotropy for this competitive binding pair is expected to have problems with glucose prediction.

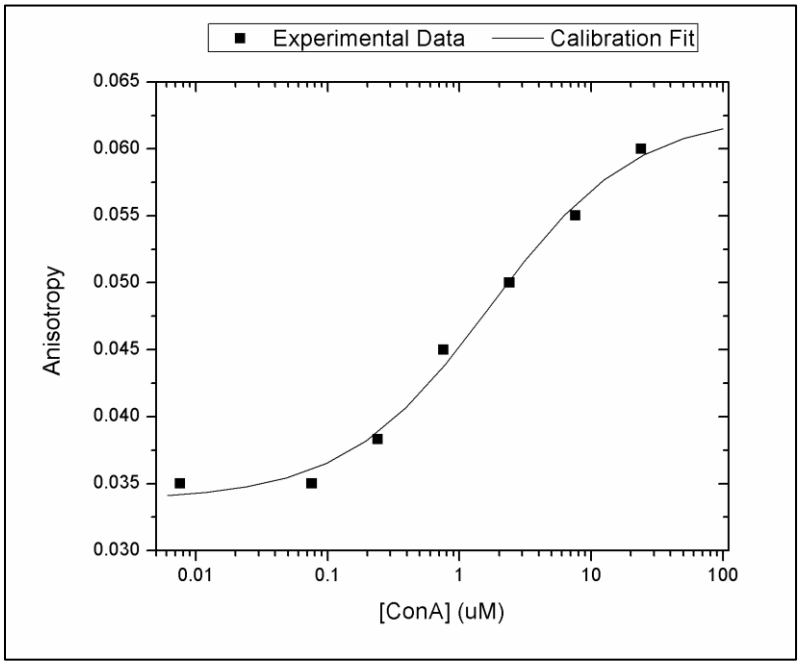

Figure 77: Fluorescence anisotropy response of 500 nM ADOTA-OVA to increasing [ConA]. The K_a was determined to be 587,000 M^{-1}.

FRET-Based Studies with ADOTA-OVA

The eventual goal for the ADOTA-OVA is to be paired with ConA behind a semi-permeable membrane to create a fluorescent sensor that can track glucose concentrations *in vivo*. As a result, it is essential for this assay to function as a FRET-based assay. To track the competitive binding with energy transfer, an acceptor fluorophore was added to ConA. For this work, AF647 was chosen as a suitable dye to allow for spectral overlap while minimizing the direct excitation of the acceptor fluorophore. Figure 78 shows a schematic of the energy transfer from the ADOTA-OVA to the AF647- ConA.

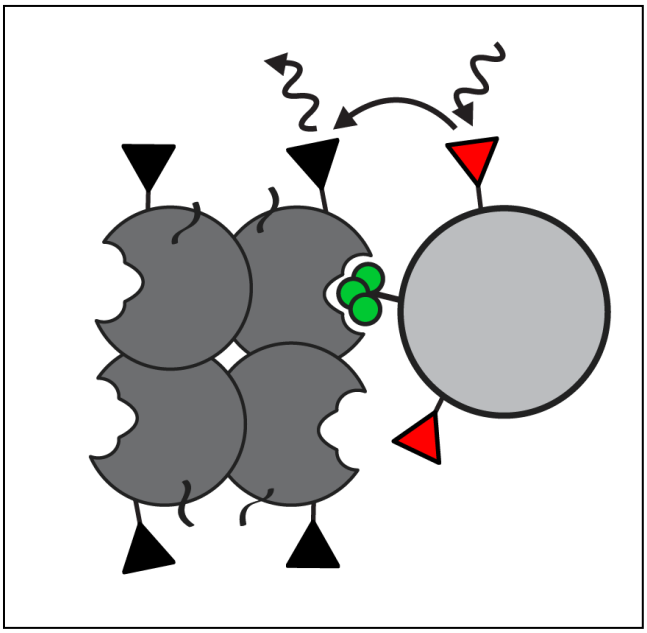

Figure 78: Schematic of the energy transfer upon binding of the ADOTA-OVA (light gray) to the AF647-ConA (dark gray tetramer) via the single N-linked glycan (green)

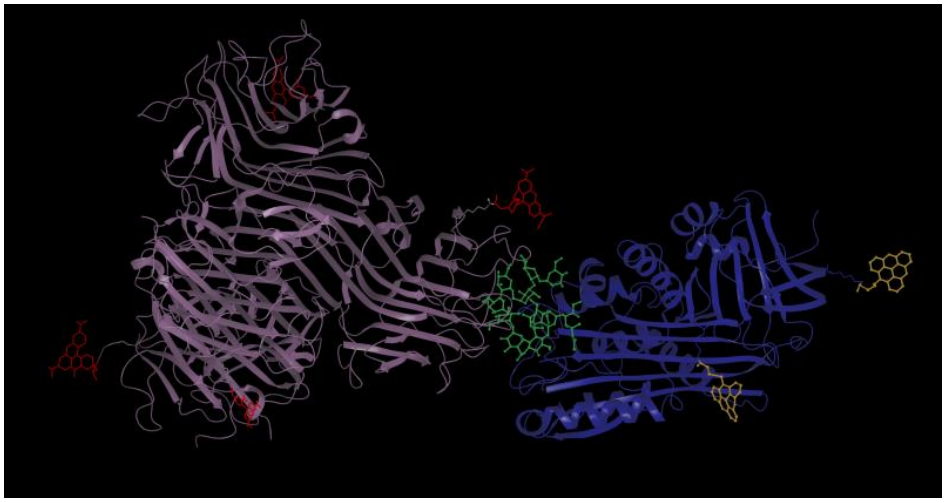

Figure 79: Molecular representation of the expected binding of ADOTA-OVA to the AF647-ConA.

The 3D representation of the interaction between the ADOTA-glycated ovalbumin and AF647-ConA was done in a similar way with the Maestro software. This representation is shown in Figure 79. This can help one see the types of distances that are between the donor and acceptor fluorophores upon binding of a portion of the high-mannose glycan to the full binding site of ConA. The steady-state excitation and emission spectra for ADOTA and AF647 are shown in Figure 80.

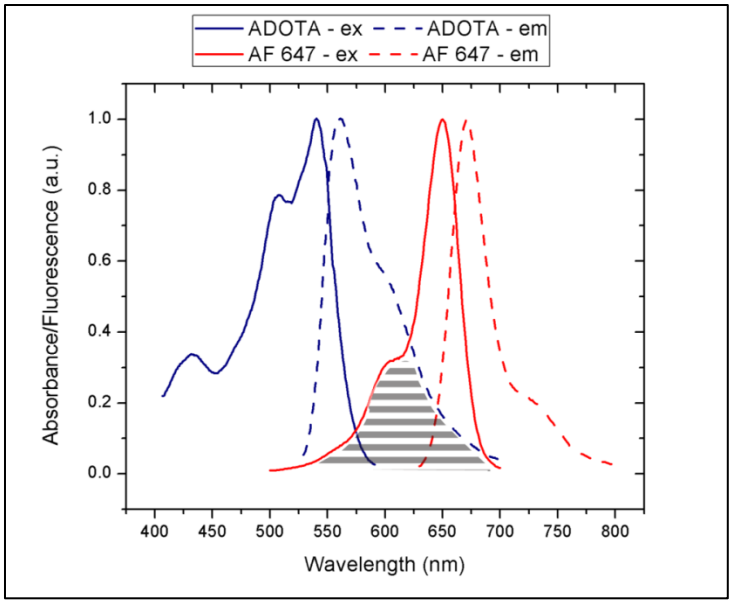

Figure 80: Excitation/Emission spectra of ADOTA^{+} and AF 647 in TRIS. The dashed horizontal line -indicates the spectral overlap which is required for energy transfer.

Stopped Flow Measurements

The stopped-flow technique is one that mixes two solutions together very quickly to allow for the kinetics of a solution to be monitored over time. This can be useful to study receptor-ligand interactions of a fluorescence-based assay that is engineered to change its fluorescence properties upon binding. For such an assay, the receptor is loaded into one syringe and the ligand is loaded into the other syringe. The solutions are driven to the mixing chamber which occurs in a cuvette. If this cuvette is placed in a typical spectrofluorometer, the fluorescence intensity can be tracked as a function of time. It is also possible to monitor anisotropy as a function of time, but this measurement requires the spectrofluorometer to be in a T-format configuration with two

emission pathways where one collects perpendicular fluorescence and the other collects parallel.

Using our FRET-based assay with ADOTA-OVA and AF647-ConA, the intensity of the ADOTA-OVA is expected to decrease upon binding to AF647-ConA. It is important to note, that the concentration of interest is the final concentration. These studies used identical syringes for the receptor and ligand. So, the concentrations in the cuvette were half of what was loaded into the syringes. Originally, the ADOTA-OVA was loaded at concentration of 1 µM. Three different ConA concentrations were loaded into the receptor chamber (0.33 µM ConA, 0.66 µM ConA, and 2 µM ConA). The trigger from the stopped-flow accessory was an input to the software to begin fluorescence collection. The excitation was set to 500 nm, and the emission was set to 550 nm to measure the emission peak from the ADOTA-OVA. The fluorescence intensity was measured every 0.1 second for 100 seconds.

These time-dependent fluorescence decays can then be normalized to the initial fluorescence intensity. The initial intensity decreases due to two primary reasons – neither of which is due to binding events. Because the AF647 can be directly excited by the excitation light, the increasing concentrations of the AF647 cause a decrease in the excitation light that actually gets to the ADOTA fluorophore. In addition, because of the spectral overlap of the ADOTA emission and AF 647 excitation, there exists the possibility of the ADOTA-emission being reabsorbed by AF647. While it's also possible that diffusion-dependent energy transfer could occur, the concentrations are not high enough to make this occur on the time-scale that ADOTA is in the excited state.

After normalizing the fluorescence decays to the initial fluorescence, they can be fit with a single exponential decay. This is shown in Figure 81.

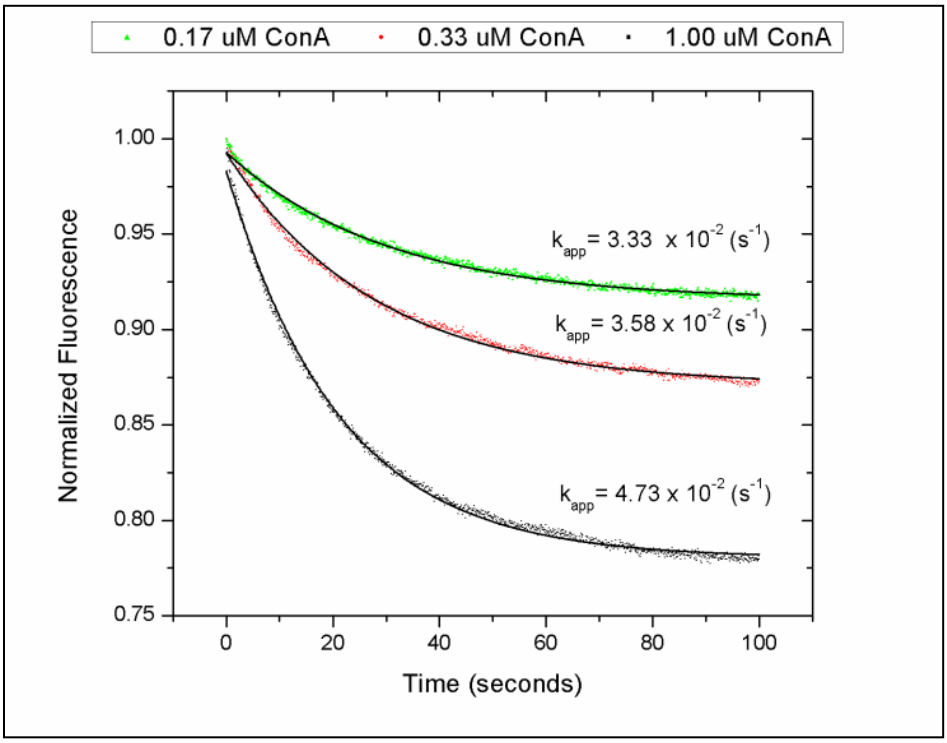

Figure 81: Stopped flow measurements of 500 nM ADOTA-OVA as a function of [AF647-ConA] in TRIS buffer at 22 deg C and the exponential decay constants.

The traditional practice for stopped flow measurements is to plot these apparent rate constants as a function of the receptor concentration like in Figure 82.[152] The best fit line to this data generates the expected k_{on} and k_{off} rates. The k_{on} rate is the slope of that line and the k_{off} rate is the y-intercept at low ovalbumin concentrations. These results show that the association constant (equivalent to k_{on}/k_{off}) is approximately 554,000 M^{-1} which is very similar to the previous results that were determined with

anisotropy. By knowing the kinetic rate constants, the time-dependent competitive binding can be determined using numerical methods.

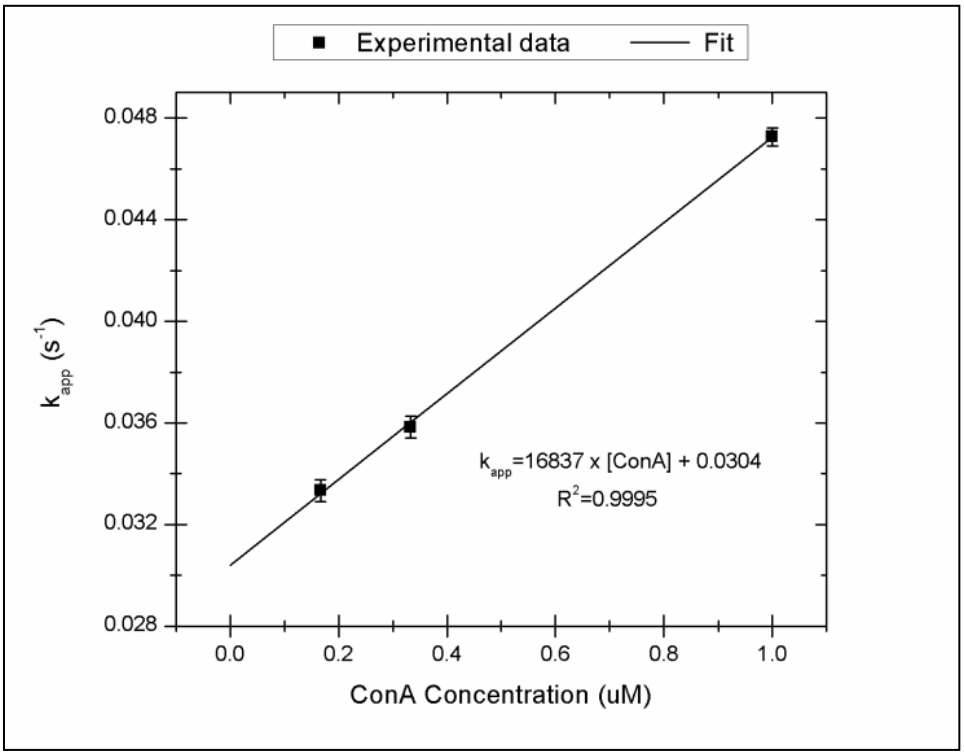

Figure 82: The exponential decay constants vs. [AF647-ConA] which can be used to get the kinetic rate constants of ADOTA-OVA to ConA from the slope and y-intercept.

Steady-State FRET Based Glucose Assay

To test the steady-state glucose response, the assay was chosen to have 500 nM ADOTA-OVA and 1 µM AF647-ConA. This assay was loaded into a cuvette of TRIS buffer, and highly concentrated glucose aliquots were added to minimize dilution effects. Upon each addition, the solutions were mixed well and given time to equilibrate. At

each glucose concentration (0 mg/dL-500 mg/dL)), the steady-state fluorescence was measured on a Fluorolog 3. Excitation was at 500 nm with a 10 nm bandwidth. Emission was collected from 530 nm to 750 nm with a 5 nm bandwidth.

The assay displayed glucose-dependent fluorescence spectra that are characteristic of competitive binding (Figure 83). The fluorescence of the ADOTA-OVA increased with increasing concentration, indicating that the concentration of ADOTA-OVA undergoing FRET (bound population) was decreasing. The emission of each fluorophore is sufficiently separated to minimize the effect that the changing fluorescence intensity of ADOTA has on the AF 647 fluorescence. The ratio of the donor to acceptor maxima (560 nm to 670 nm) as a function of glucose concentration is also shown. This shows that the fluorescence of this ADOTA-OVA and AF 647 ConA assay primarily changes from 0-300 mg/dL, and then begins to flatten out.

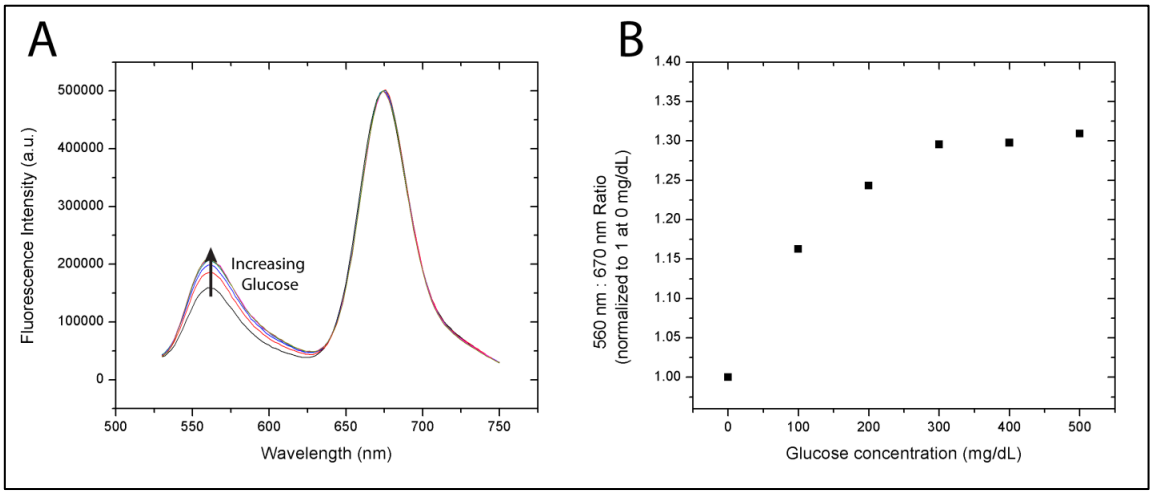

Figure 83: Glucose response of the fluorescence assay comprised of 500 nM ADOTA-OVA and 1 µM AF647-ConA.

By using the ovalbumin as the fluorescent ligand, it reverts back to one of the problems that the traditional ligands (i.e. dextran) displayed. The molecule itself is large enough to allow a large percentage of the bound population to display a low FRET efficiency with the acceptors on the ConA. That said, this assay still shows a significant increase across physiological glucose concentrations (~30% fluorescence increase), and it could potentially be increased further by increasing the AF647-ConA concentrations further. This could also be increased by site-specific labeling of the N-terminus of the ovalbumin. In the crystal structure, the N-terminus appears to be fairly close to where the high-mannose glycan resides and could allow for improved FRET efficiency. Figure 84 shows the 2D sensitivity map, and plots where an assay based on 1 μM ConA would be expected to reside (white arrow). By increasing the concentration of the AF647-ConA, this fluorescence response is expected to increase further.

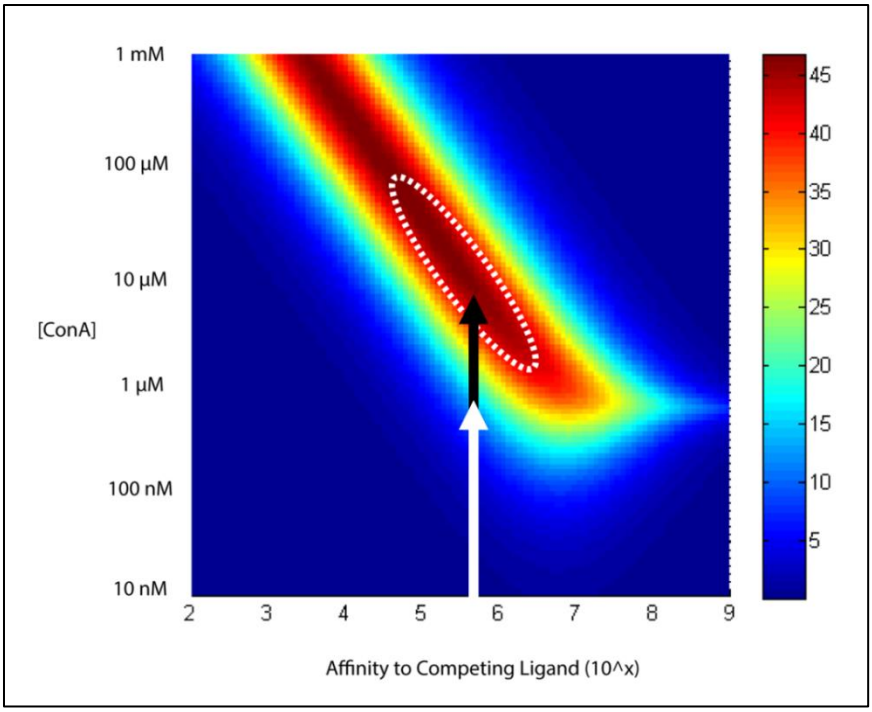

Figure 84: 2D plot of sensitivity of recognition scheme with the assay from Figure 83 (white line) and where it could be to increase the sensitivity (black line)

FRET-based Glucose Assay with Fluorescence Lifetimes

An assay was generated using 500 nM ADOTA-OVA and 4 µM AF647-ConA for FRET-based studies where the fluorescence lifetime decays were analyzed instead of the steady-state intensity. The fluorescence lifetime was collected using a DeltaFlex time correlated single photon counting system from Horiba that was equipped with a 482 nm DeltaDiode pulsed source. The emission was set to 540 nm with the slit-width allowing 8 nm bandpass. A high-pass filter of 500 nm was used to block scattered excitation light. The excitation polarizer was in the vertical orientation and the emission polarizer was set to the magic angle. Data was taken until the maximum counts were

1,000. Silica particles in DI were used as the sample to scatter light to determine the pulse-shape of the 482 nm source. The fluorescence decays of the 500 nM ADOTA-OVA and the assay of the 500 nM ADOTA-OVA with 4 µM AF647-ConA are shown in Figure 85.

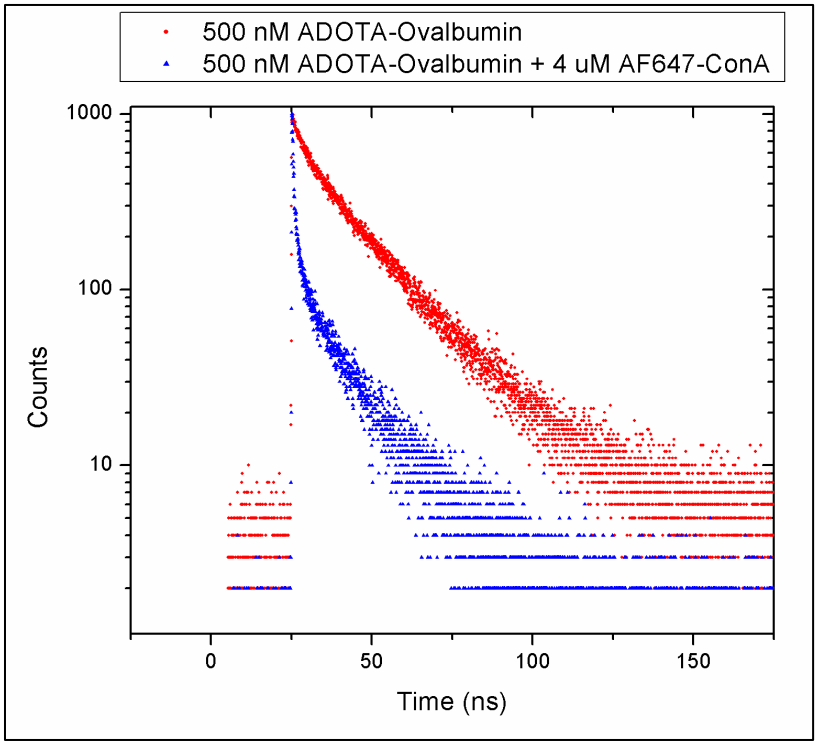

Figure 85: Time-dependent fluorescence decay of (a) 500 nM ADOTA-OVA and (b) 500 nM ADOTA-OVA with 4 µM AF 647 ConA in TRIS buffer at 22 deg C.

The time-dependent fluorescence decays were fit with three exponentials. Two of these lifetimes were fixed: one for the shorter lifetime at 2.07 ns and the other for the longer lifetime at 18.19 ns. A third lifetime (on the order of picoseconds) was also implemented in the fit to account for the scatter that was seen in the experiments. The

full decay of each solution was fit using with this equation by minimizing the residuals. The weighted intensities at time zero of the short and long lifetime decays (B1 and B2) were then recorded as a function of glucose concentration. These values are expected to be a function of the equilibrium binding between ADOTA-OVA and AF647-ConA. The population that is capable of undergoing FRET is expected to primarily display the shorter lifetime. The population that does not undergo FRET is expected to primarily display the longer lifetime. Therefore B2/(B1+B2) should correlate to how much of the ADOTA-OVA is free. The glucose-dependent response to this value is shown in Figure 86. The competitive binding equation was again used to fit this data, and a best fit was generated with am IC_{50} of 386.9 mg/dL. The prediction glucose vs. actual glucose (using the same data set) curve is shown in Figure 87. The standard error of calibration was 8.25 mg/dL, and the calibration MARD was 4.19%.

Improvements could potentially be made on the assay by increasing the degree of labeling on ConA or performing site-specific labeling on the ovalbumin with the $ADOTA^{+}$ fluorophore. Both of these strategies could improve the average FRET efficiency of the bound ovalbumin population.

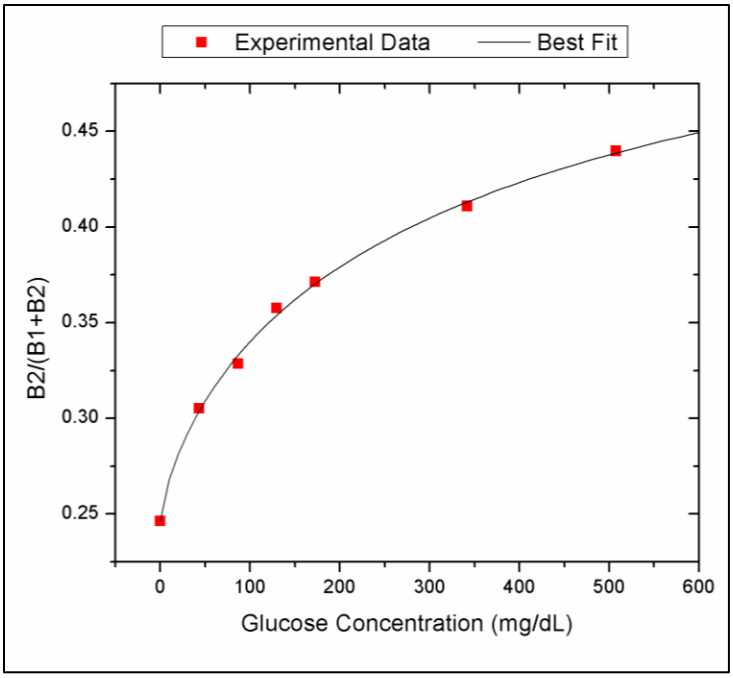

Figure 86: Glucose-dependent ratio of the long-lifetime component of an assay comprised of 500 nM ADOTA-OVA and 4 µM AF 647 ConA.

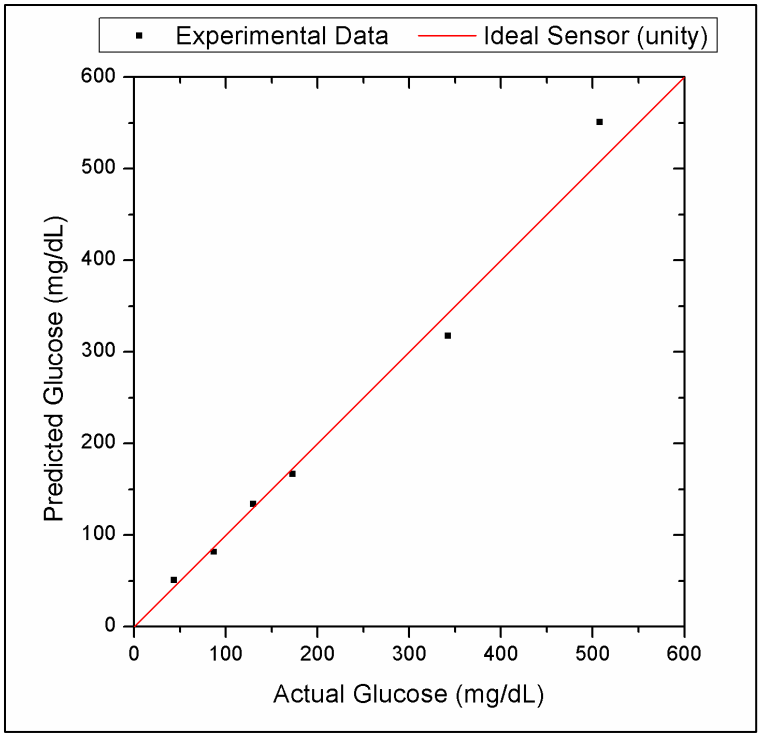

Figure 87: Predicted glucose vs. actual glucose for the FRET competitive binding assay using 500 nM ADOTA-OVA and 4 µM AF647-ConA tracking fluorescence lifetimes.

Conclusions

This work introduces the naturally-occurring ovalbumin as the core-component of a 2nd generation smartly-designed fluorescent ligand to be paired with ConA in a fluorescence glucose sensor. The glycated fraction of ovalbumin was separated with affinity chromatography and labeled with the long-fluorescence-lifetime ADOTA^{+} dye to allow the binding to be tracked via fluorescence. A FRET assay was generated by pairing ADOTA-OVA with AF647-ConA that showed a fluorescence response across physiologically relevant glucose concentrations. This could be tracked by looking at the changes in fluorescence lifetime of the ADOTA fluorophore and the steady-state

fluorescence intensity. This preliminary work indicates that the ADOTA-OVA fluorescent ligand could potentially allow the translation of the smartly-designed fluorescent ligand concept into a continuous glucose monitoring device

CHAPTER VI

SUMMARY AND FUTURE WORK

In summary, the goal of this research was to engineer a homogeneous ConA-based competitive binding assay that could remain stable in free solution and predict the glucose concentration of that solution from the fluorescence signal of the assay.

The initial work used glycosylated dendrimers as the competing ligand. Different versions of the glycosylated dendrimer were tested in an attempt to identify a specific version that enabled the assay to most-effectively track physiological glucose concentrations. These versions varied in size, number of sugar residues, type of surface chemistry, number of charges on the surface, and the fluorophore that was used. Assays were generated with a range of dendrimer and ConA concentrations and examined for the change in fluorescence properties across physiological glucose range. One version of this assay was encapsulated via the microporated microsphere approach and the response of these sensors was tested with physiological glucose concentrations. These sensors displayed some reversibility over time; however, the extent of their fluorescent response changed. The assays that used this type of glycosylated dendrimer continued to display problems with stability and reversibility in free solution and it showed several inconsistencies that were later attributed to electrostatic interactions and aggregation. The problems with this approach resulted in the desire to explore alternative assay configurations.

Mathematical modeling was then performed to identify the characteristics of an assay that could allow for dynamic fluorescence changes to physiological glucose concentrations. This work separated the recognition and transduction mechanisms of a fluorescent competitive binding sensor, and each mechanism was modeled independently. The transduction mechanism was chosen to be fluorescence anisotropy to make the system simpler and allow it to be linear. The sensitivity of the measured anisotropy is then the convolution of the sensitivities of each mechanism, making it necessary for both to respond accordingly. For the transduction mechanism, the steady-state anisotropy was modeled for fluorescent competing ligands of different molecular weight and fluorescent lifetimes. The expected steady-state anisotropy was modeled for the free-state and the bound-state (to tetrameric ConA) for each ligand, assuming each version was a perfect sphere at the molecular weight of the complex. For the recognition mechanism, an exact solution to the competitive binding equation was used for a set of affinities and concentrations. From these models, 2D sensitivity plots were generated for each mechanism to identify optimal assay configurations, and a combined model was made to predict the change in anisotropy for various assays.

The combined model was then validated by testing the glucose response of assays that paired 4 kDa FITC-dextran with different concentrations of ConA. After predicting the correct trends, this model was used to explain the previous problems associated with ConA-based glucose sensing assays in free solution. From this explanation, we postulate the hypothesis that the full potential of ConA-based assays can be shown if a fluorescent competing ligand is employed that achieves the high-affinity

required without allowing for aggregation to occur with ConA. In addition, we identified ideal characteristics to maximize both the recognition and transduction mechanism.

We overcome the apparent dilemma between sensitivity and aggregation by identifying an alternative method to achieve the increased affinities. Instead of using proximity effects that requires a multivalent presentation of monosacccharides, we employed the use of ConA's extended binding site. The core trimannose is shown to form additional hydrogen bonds to the extended binding site while binding to the same primary binding site. A smartly-designed fluorescent ligand was designed and synthesized to achieve the desirable characteristics as previously identified without allowing for aggregation to occur. A single presentation of the core trimannose showed no aggregation when paired with ConA, unlike dextrans and dendrimers.

A fluorophore (APTS) was attached to the reducing terminus of mannotetraose via reductive amination to generate fluorescent ligand that presented a single core trimannose. This first generation smartly-designed fluorescent ligand was fully tested to determine its fluorescent properties (intensity, intrinsic anisotropy, lifetime) as well as its binding affinity to ConA. Then, this smartly-designed fluorescent ligand was paired with ConA in a fluorescence anisotropy based glucose sensor. Afterwards it was paired with fluorescently labeled ConA in a FRET assay. The responses to several sugars are shown, displaying that glucose and mannose concentrations can directly compete for binding sites on ConA with the smartly-designed fluorescent ligand. This smartly-designed fluorescent ligand (1) presented a single core trimannose moiety, (2) was

negatively charged, and (3) held the fluorophore close to the trimannose moiety. This approach can allow the assay to remain stable over time, suggesting that this strategy could truly show the full potential of ConA-based assays. However, for this smartly-designed ligand concept to be translated into a prototype device, the molecular weight must be increased to prevent leaching from the semi-permeable membrane.

In an attempt to generate a low-cost bulked-up ligand that can allow the smartly-designed fluorescent ligand concept to be translated into a prototype device, various glycoproteins were explored. Ovalbumin – the primary protein found in egg-white - was been identified as a possible template for a 2nd generation smartly-designed fluorescent ligand as: (1) it has a single glycosylation site that can present a high-mannose glycan (contains the core trimannose), (2) it is negatively charged at physiological pH (with an isoelectric point of 4.5), (3) it has a molecular weight of 45 kDa, and (4) it has numerous lysine residues that can be labeled with an amine-reactive fluorophore. Affinity chromatography was used to collect only the glycated fraction, and this fraction was labeled with a red-emitting, long-lifetime fluorophore (ADOTA) to track the binding. Anisotropy studies were performed with unlabeled ConA and energy transfer studies paired the ADOTA-glycated ovalbumin with AF647- ConA. Many of these studies showed very promising glucose-sensing results. However, the ovalbumin seems to be aggregating with itself in a buffer that mimics the interstitial fluid in the absence of ConA. If this is true, a single complex would present multiple trimannose groups. Such a complex would be similar to the multivalent ligands that cause problems with stability and repeatability.

Future work involves creating stable, bulked up versions of the smartly-designed fluorescent ligand. This could either be done by stabilizing the ovalbumin approach through a process like PEGylation or by generating a purely synthetic ligand. In addition, fluorophores could be chosen that excite/emit further into the red, to minimize the background from endogenous auto-fluorescence. Such an assay could be encapsulated within the desired matrix and has the potential to remain stable for long periods of time if it were paired with stabilized versions of ConA that are currently being pursued in the Optical Biosensing Lab,.

REFERENCES

(1) In *Biochemistry*, Stryer, Ed.; Freeman & Company: New York, 1995.

(2) Ahmed, N.; Thornalley, P. J. *Diabetes, Obesity and Metabolism* **2007**, *9*, 233-245.

(3) Philippe, J. *Endocrine Reviews* **1991**, *12*, 252-271.

(4) *Diabetes Care* **2013**, *36*, S11-S66.

(5) Moore, P. A.; Zgibor, J. C.; Dasanayake, A. P. *Journal of the American Dental Association (1939)* **2003**, *134 Spec No*, 11S-15S.

(6) Taylor, R.; Agius, L. *Biochemical Journal* **1988**, *250*, 625-640.

(7) Nathan, D. M.; Cleary, P. A.; Backlund, J. Y. C.; Genuth, S. M.; Lachin, J. M.; Orchard, T. J.; Raskin, P.; Zinman, B. *New England Journal of Medicine* **2005**, *353*, 2643-2653.

(8) Rajashree, R.; Ravishankar, M. V.; Kholkute, S. D.; Goudar, S. S. *International Journal of Diabetes and Metabolism* **2012**, *20*, 37-42.

(9) Undlien, D. E.; Lie, B. A.; Thorsby, E. *Trends in Genetics* **2001**, *17*, 93-100.

(10) *Diabetes* **1995**, *44*, 1249-1258.

(11) Ratner, R. E. *Diabetic Medicine* **1998**, *15*, S4-S7.

(12) Federation, I. D. *IDF Diabetes Atlas*, 6th ed.: Brussels, Belgium, 2013.

(13) CDC. *National diabetes fact sheet: national estimates and general information on diabetes and prediabetes in the United States*; Centers for Disease Control and Prevention: Atlanta, GA, 2011.

(14) Danaei, G.; Finucane, M. M.; Lu, Y.; Singh, G. M.; Cowan, M. J.; Paciorek, C. J.; Lin, J. K.; Farzadfar, F.; Khang, Y. H.; Stevens, G. A.; Rao, M.; Ali, M. K.; Riley, L. M.; Robinson, C. A.; Ezzati, M. *The Lancet* **2011**, *378*, 31-40.

(15) Mathers, C. D.; Loncar, D. *PLoS Medicine* **2006**, *3*, 2011-2030.

(16) Group, U. H., Group, U. H., Ed.: Minnetonka, MN, 2010.

(17) *New England Journal of Medicine* **1993**, *329*, 977-986.

(18) Al-Tabakha, M.; Arida, A. *Indian Journal of Pharmaceutical Sciences* **2008**, *70*, 278-286.

(19) Bennett, W. L.; Maruthur, N. M.; Singh, S.; Segal, J. B.; Wilson, L. M.; Chatterjee, R.; Marinopoulos, S. S.; Puhan, M. A.; Ranasinghe, P.; Block, L.; Nicholson, W. K.; Hutfless, S.; Bass, E. B.; Bolen, S. *Annals of Internal Medicine* **2011**, *154*, 602-618.

(20) Pickup, J. *Textbook of Diabetes, Third Ed* **2003**, 34+31-34+17.

(21) Ginsberg, B. H. *Journal of Diabetes Science and Technology* **2009**, *3*, 903-913.

(22) Delamater, A. M. *Clinical Diabetes* **2006**, *24*, 71-77.

(23) Klonoff, D. C. *Diabetes Care* **2005**, *28*, 1231-1239.

(24) *New England Journal of Medicine* **2008**, *359*, 1464-1476.

(25) Hermanides, J.; Phillip, M.; DeVries, J. H. *Diabetes Care* **2011**, *34*, S197-S201.

(26) Wang, J. *Chemical Reviews* **2008**, *108*, 814-825.

(27) Wang, J. *Electroanalysis* **2001**, *13*, 983-988.

(28) Vaddiraju, S.; Burgess, D. J.; Tomazos, I.; Jain, F. C.; Papadimitrakopoulos, F. *Journal of Diabetes Science and Technology* **2010**, *4*, 1540-1562.

(29) Wisniewski, N.; Moussy, F.; Reichert, W. M. *Fresenius' Journal of Analytical Chemistry* **2000**, *366*, 611-621.

(30) Koschwanez, H. E.; Reichert, W. M. *Biomaterials* **2007**, *28*, 3687-3703.

(31) Novak, M. T.; Yuan, F.; Reichert, W. M. *Analytical and Bioanalytical Chemistry* **2010**, *398*, 1695-1705.

(32) Koh, A.; Lu, Y.; Schoenfisch, M. H. *Analytical Chemistry* **2013**, *85*, 10488-10494.

(33) Helton, K. L.; Ratner, B. D.; Wisniewski, N. A. *Journal of Diabetes Science and Technology* **2011**, *5*, 632-646.

(34) Gant, R. M.; Abraham, A. A.; Hou, Y.; Cummins, B. M.; Grunlan, M. A.; Coté, G. L. *Acta Biomaterialia* **2010**, *6*, 2903-2910.

(35) Gough, D. A.; Kumosa, L. S.; Routh, T. L.; Lin, J. T.; Lucisano, J. Y. *Science Translational Medicine* **2010**, *2*, 42ra53.

(36) Oliver, N. S.; Toumazou, C.; Cass, A. E. G.; Johnston, D. G. *Diabetic Medicine* **2009**, *26*, 197-210.

(37) Pickup, J. C.; Hussain, F.; Evans, N. D.; Rolinski, O. J.; Birch, D. J. S. *Biosensors and Bioelectronics* **2005**, *20*, 2555-2565.

(38) Ballerstadt, R.; Evans, C.; Gowda, A.; McNichols, R. *Journal of Diabetes Science and Technology* **2007**, *1*, 384-393.

(39) Judge, K.; Morrow, L.; Lastovich, A. G.; Kurisko, D.; Keith, S. C.; Hartsell, J.; Roberts, B.; McVey, E.; Weidemaier, K.; Win, K.; Hompesch, M. *Diabetes Technology and Therapeutics* **2011**, *13*, 309-317.

(40) Nielsen, J. K.; Christiansen, J. S.; Kristensen, J. S.; Toft, H. O.; Hansen, L. L.; Aasmul, S.; Gregorius, K. *Journal of Diabetes Science and Technology* **2009**, *3*, 98-109.

(41) Cobelli, C.; Renard, E.; Kovatchev, B. *Diabetes* **2011**, *60*, 2672-2682.

(42) Haidar, A.; Legault, L.; Dallaire, M.; Alkhateeb, A.; Coriati, A.; Messier, V.; Cheng, P.; Millette, M.; Boulet, B.; Rabasa-Lhoret, R. *CMAJ* **2013**, *185*, 297-305.

(43) Huet, C.; Lonchampt, M.; Huet, M.; Bernadac, A. *Biochimica et Biophysica Acta* **1974**, *365*, 28-39.

(44) Bittiger, H.; Schnebli, H. P. *Concanavalin A as a Tool* **1976**.

(45) Hussain, F.; Birch, D. J. S.; Pickup, J. C. *Analytical Biochemistry* **2005**, *339*, 137-143.

(46) Tolosa, L.; Gryczynski, I.; Eichhorn, L. R.; Dattelbaum, J. D.; Castellano, F. N.; Rao, G.; Lakowicz, J. R. *Analytical Biochemistry* **1999**, *267*, 114-120.

(47) Russell, R. J.; Pishko, M. V.; Gefrides, C. C.; McShane, M. J.; Cote, G. L. *Analytical Chemistry* **1999**, *71*, 3126-3132.

(48) Schultz, J. S.; Mansouri, S.; Goldstein, I. J. *Diabetes Care* **1982**, *5*, 245-253.

(49) Ballerstadt, R.; Schultz, J. S. *Analytical Chemistry* **2000**, *72*, 4185-4192.

(50) Mansouri, S.; Schultz, J. *IEEE* **1984**, 112-115.

(51) Goldstein, I. J.; Hollerman, C. E.; Merrick, J. M. *BBA - General Subjects* **1965**, *97*, 68-76.

(52) Goldstein, I. J.; Hollerman, C. E.; Smith, E. E. *Biochemistry* **1965**, *4*, 876-883.

(53) So, L. L.; Goldstein, I. J. *Journal of Biological Chemistry* **1967**, *242*, 1617-1622.

(54) So, L. L.; Goldstein, I. J. *Journal of Immunology* **1967**, *99*, 158-163.

(55) Smithx, E. E.; Goldstein, I. J. *Archives of Biochemistry and Biophysics* **1967**, *121*, 88-95.

(56) Poretz, R. D.; Goldstein, I. J. *Carbohydrate Research* **1967**, *4*, 471-477.

(57) Poretz, R. D.; Goldstein, I. J. *Immunology* **1968**, *14*, 165-174.

(58) Mangold, S. L.; Cloninger, M. J. *Organic and Biomolecular Chemistry* **2006**, *4*, 2458-2465.

(59) Dam, T. K.; Roy, R.; Das, S. K.; Oscarson, S.; Brewer, C. F. *Journal of Biological Chemistry* **2000**, *275*, 14223-14230.

(60) Cheetham, N. W. H.; Fiala-Beer, E.; Walker, G. J. *Carbohydrate Polymers* **1990**, *14*, 149-158.

(61) Benzeval, I.; Bowyer, A.; Hubble, J. *European Journal of Pharmaceutics and Biopharmaceutics* **2012**, *80*, 143-148.

(62) Ballerstadt, R.; Evans, C.; McNichols, R.; Gowda, A. *Biosensors and Bioelectronics* **2006**, *22*, 275-284.

(63) Liao, K. C.; Hogen-Esch, T.; Richmond, F. J.; Marcu, L.; Clifton, W.; Loeb, G. E. *Biosensors and Bioelectronics* **2008**, *23*, 1458-1465.

(64) Barone, P. W.; Strano, M. S. *Journal of diabetes science and technology* **2009**, *3*, 242-252.

(65) Tang, B.; Cao, L.; Xu, K.; Zhuo, L.; Ge, J.; Li, Q.; Yu, L. *Chemistry - A European Journal* **2008**, *14*, 3637-3644.

(66) Cummins, B. M.; Lim, J.; Simanek, E. E.; Pishko, M. V.; Coté, G. L. *Biomedical Optics Express* **2011**, *2*, 1243-1257.

(67) Ibey, B. L.; Beier, H. T.; Rounds, R. M.; Coté, G. L.; Yadavalli, V. K.; Pishko, M. V. *Analytical Chemistry* **2005**, *77*, 7039-7046.

(68) Tolosa, L.; Szmacinski, H.; Rao, G.; Lakowicz, J. R. *Analytical Biochemistry* **1997**, *250*, 102-108.

(69) Cummins, B. M.; Garza, J. T.; Coté, G. L. *Analytical Chemistry* **2013**, *85*, 5397-5404.

(70) Tolosa, L.; Malak, H.; Raob, G.; Lakowicz, J. R. *Sensors and Actuators, B: Chemical* **1997**, *45*, 93-99.

(71) McCartney, L. J.; Pickup, J. C.; Rolinski, O. J.; Birch, D. J. S. *Analytical Biochemistry* **2001**, *292*, 216-221.

(72) Ibey, B. L.; Beier, H. T.; Rounds, R. M.; Coté, G. L.; Yadavalli, V. K.; Pishko, M. V. *Analytical Chemistry* **2005**, *77*, 7039-7046.

(73) Kojima, C.; Kono, K.; Maruyama, K.; Takagishi, T. *Bioconjugate Chemistry* **2000**, *11*, 910-917.

(74) Tomalia, D. A.; Reyna, L. A.; Svenson, S. *Biochemical Society Transactions* **2007**, *35*, 61-67.

(75) Liu, M.; Kono, K.; Fréchet, J. M. J. *Journal of Controlled Release* **2000**, *65*, 121-131.

(76) Morgan, M. T.; Carnahan, M. A.; Immoos, C. E.; Ribeiro, A. A.; Finkelstein, S.; Lee, S. J.; Grinstaff, M. W. *Journal of the American Chemical Society* **2003**, *125*, 15485-15489.

(77) Chen, H. T.; Neerman, M. F.; Parrish, A. R.; Simanek, E. E. *Journal of the American Chemical Society* **2004**, *126*, 10044-10048.

(78) Neerman, M. F.; Zhang, W.; Parrish, A. R.; Simanek, E. E. *International Journal of Pharmaceutics* **2004**, *281*, 129-132.

(79) Gillies, E. R.; Fréchet, J. M. J. *Drug Discovery Today* **2005**, *10*, 35-43.

(80) Velazquez, A. J.; Carnahan, M. A.; Kristinsson, J.; Stinnett, S.; Grinstaff, M. W.; Kim, T. *Archives of Ophthalmology* **2004**, *122*, 867-870.

(81) Grinstaff, M. W. *Chemistry - A European Journal* **2002**, *8*, 2838-2846.

(82) Turnbull, W. B.; Stoddart, J. F. *Reviews in Molecular Biotechnology* **2002**, *90*, 231-255.

(83) Lee, C. C.; MacKay, J. A.; Fréchet, J. M. J.; Szoka, F. C. *Nature Biotechnology* **2005**, *23*, 1517-1526.

(84) Gupta, U.; Agashe, H. B.; Asthana, A.; Jain, N. K. *Biomacromolecules* **2006**, *7*, 649-658.

(85) Ibey, B.; Beier, H.; Rounds, R.; Pishko, M.; Coté, G. *Progress In Biomedical Optics and Imaging - Proceedings of SPIE* **2006**.

(86) Meadows, D. L.; Schultz, J. S. *Analytica Chimica Acta* **1993**, *280*, 21-30.

(87) Ballerstadt, R.; Gowda, A.; McNichols, R. *Diabetes Technology and Therapeutics* **2004**, *6*, 191-200.

(88) Ibey, B. L.; Yadavalli, V. K.; Thomas, H. R.; Rounds, R. M.; Pishko, M. V.; Cote, G. L., 2005, pp 1-6.

(89) Beier, H. T.; Ibey, B. L.; Pishko, M. V.; Coté, G. L., 2007, pp 644504-644504-644506.

(90) *Amine-Reactive Probes* **2010**.

(91) Cohen, S.; Yoshioka, T.; Lucarelli, M.; Hwang, L. H.; Langer, R. *Pharmaceutical Research* **1991**, *8*, 713-720.

(92) Gombotz, W. R.; Wee, S. F. *Advanced Drug Delivery Reviews* **1998**, *31*, 267-285.

(93) Freiberg, S.; Zhu, X. X. *International Journal of Pharmaceutics* **2004**, *282*, 1-18.

(94) Antipov, A. A.; Sukhorukov, G. B. *Advances in Colloid and Interface Science* **2004**, *111*, 49-61.

(95) Peyratout, C. S.; Dähne, L. *Angewandte Chemie - International Edition* **2004**, *43*, 3762-3783.

(96) Zhu, Y.; Shi, J.; Shen, W.; Dong, X.; Feng, J.; Ruan, M.; Li, Y. *Angewandte Chemie - International Edition* **2005**, *44*, 5083-5087.

(97) McShane, M.; Lvov, Y. *Dekker Encyclopedia of Nanoscience and Nanotechnology* **2009**, 1823-1840.

(98) Kreft, O.; Javier, A. M.; Sukhorukov, G. B.; Parak, W. J. *Journal of Materials Chemistry* **2007**, *17*, 4471-4476.

(99) Gao, C.; Moya, S.; Donath, E.; Möhwald, H. *Macromolecular Chemistry and Physics* **2002**, *203*, 953-960.

(100) Volodkin, D. V.; Larionova, N. I.; Sukhorukov, G. B. *Biomacromolecules* **2004**, *5*, 1962-1972.

(101) Stein, E. W.; Volodkin, D. V.; McShane, M. J.; Sukhorukov, G. B. *Biomacromolecules* **2006**, *7*, 710-719.

(102) Harris, J.; Zalipsky, S. *Poly(Ethylene Glycol) Chemistry and Biological Applications* **1997**.

(103) Mellott, M. B.; Searcy, K.; Pishko, M. V. *Biomaterials* **2001**, *22*, 929-941.

(104) Russell, R. J.; Axel, A. C.; Shields, K. L.; Pishko, M. V. *Polymer* **2001**, *42*, 4893-4901.

(105) Rounds, R. M.; Ibey, B. L.; Beier, H. T.; Pishko, M. V.; Coté, G. L. *Journal of Fluorescence* **2007**, *17*, 57-63.

(106) Chang, E. P.; Holguin, D. *Journal of Adhesion* **2007**, *83*, 15-26.

(107) Mahmood Bin Mat Yunus, W.; Bin Abdul Rahman, A. *Appl. Opt.* **1988**, *27*, 3341-3343.

(108) McShane, M.; Stein, E. *In Vivo Glucose Sensing* **2010**.

(109) Dam, T. K.; Brewer, C. F. *Advances in carbohydrate chemistry and biochemistry* **2010**, *63*, 139-164.

(110) Olsen, L. R.; Dessen, A.; Gupta, D.; Sabesan, S.; Sacchettini, J. C.; Brewer, C. F. *Biochemistry* **1997**, *36*, 15073-15080.

(111) Filipe, V.; Hawe, A.; Jiskoot, W. *Pharmaceutical Research* **2010**, *27*, 796-810.

(112) Lim, J.; Simanek, E. E. *Advanced Drug Delivery Reviews* **2012**, *64*, 826-835.

(113) Lim, J.; Simanek, E. E. *Organic Letters* **2008**, *10*, 201-204.

(114) De Silva, A. P.; Moody, T. S.; Wright, G. D. *Analyst* **2009**, *134*, 2385-2393.

(115) Cakara, D.; Kleimann, J.; Borkovec, M. *Macromolecules* **2003**, *36*, 4201-4207.

(116) Jameson, D. M.; Ross, J. A. *Chemical Reviews* **2010**, *110*, 2685-2708.

(117) Jacob, G. S. *Biochemistry*® **1995**, *34*, 1210-1217.

(118) Oda, Y.; Nakayama, K.; Abdul-Rahman, B.; Kinoshita, M.; Hashimoto, O.; Kawasaki, N.; Hayakawa, T.; Kakehi, K.; Tomiya, N.; Lee, Y. C. *Journal of Biological Chemistry* **2000**, *275*, 26772-26779.

(119) Weatherman, R. V.; Kiessling, L. L. *Journal of Organic Chemistry* **1996**, *61*, 534-538.

(120) Oyelaran, O.; Gildersleeve, J. C. *Current Opinion in Chemical Biology* **2009**, *13*, 406-413.

(121) Song, X.; Xia, B.; Lasanajak, Y.; Smith, D. F.; Cummings, R. D. *Glycoconjugate Journal* **2008**, *25*, 15-25.

(122) Liu, Y.; Palma, A. S.; Feizi, T. *Biological Chemistry* **2009**, *390*, 647-656.

(123) Mandal, D. K.; Kishore, N.; Brewer, C. F. *Biochemistry* **1994**, *33*, 1149-1156.

(124) Wang, Z. X. *FEBS Letters* **1995**, *360*, 111-114.

(125) Kao, S.; Asanov, A. N.; Oldham, P. B. *Instrumentation Science and Technology* **1998**, *26*, 375-387.

(126) Cummings, R. D. In *Essentials of Glycobiology*, Varki A, C. R., Esko JD, Ed.; Cold Springs Harbor: New York, 2009.

(127) Findlay, J. W. A.; Dillard, R. F. *AAPS Journal* **2007**, *9*, E260-266.

(128) Jameson, D. M.; Seifried, S. E. *Methods: A Companion to Methods in Enzymology* **1999**, *19*, 222-233.

(129) Gestwicki, J. E.; Cairo, C. W.; Strong, L. E.; Oetjen, K. A.; Kiessling, L. L. *Journal of the American Chemical Society* **2002**, *124*, 14922-14933.

(130) Wilczewski, M.; Van Der Heyden, A.; Renaudet, O.; Dumy, P.; Coche-Guérente, L.; Labbé, P. *Organic and Biomolecular Chemistry* **2008**, *6*, 1114-1122.

(131) Naismith, J. H.; Field, R. A. *Journal of Biological Chemistry* **1996**, *271*, 972-976.

(132) Loris, R.; Maes, D.; Poortmans, F.; Wyns, L.; Bouckaert, J. *Journal of Biological Chemistry* **1996**, *271*, 30614-30618.

(133) Naismith, J. H.; Emmerich, C.; Habash, J.; Harrop, S. J.; Helliwell, J. R.; Hunter, W. N.; Raftery, J.; Kalb, A. J.; Yariv, J. *Acta Crystallographica Section D: Biological Crystallography* **1994**, *50*, 847-858.

(134) Bobbitt, J. M., 1956, pp 1-41.

(135) Bigge, J. C.; Patel, T. P.; Bruce, J. A.; Goulding, P. N.; Charles, S. M.; Parekh, R. B. *Analytical Biochemistry* **1995**, *230*, 229-238.

(136) Guttman, A.; Chen, F. T. A.; Evangelista, R. A.; Cooke, N. *Analytical Biochemistry* **1996**, *233*, 234-242.

(137) Harvey, D. J. *Journal of the American Society for Mass Spectrometry* **2000**, *11*, 900-915.

(138) Sato, K.; Okubo, A.; Yamazaki, S. *Analytical Biochemistry* **1998**, *262*, 195-197.

(139) Leteux, C.; Childs, R. A.; Chai, W.; Stoll, M. S.; Kogelberg, H.; Feizi, T. *Glycobiology* **1998**, *8*, 227-236.

(140) Ruhaak, L. R.; Steenvoorden, E.; Koeleman, C. A. M.; Deelder, A. M.; Wuhrer, M. *Proteomics* **2010**, *10*, 2330-2336.

(141) Zhang, Y.; Wang, Z.; Zhang, X.; Zhou, W.; Huang, L. *Carbohydrate Research* **2011**, *346*, 2156-2164.

(142) Reeves, P. J.; Callewaert, N.; Contreras, R.; Khorana, H. G. *Proceedings of the National Academy of Sciences of the United States of America* **2002**, *99*, 13419-13424.

(143) Yung-Chi, C.; Prusoff, W. H. *Biochemical Pharmacology* **1973**, *22*, 3099-3108.

(144) Huntington, J. A.; Stein, P. E. *Journal of Chromatography B: Biomedical Sciences and Applications* **2001**, *756*, 189-198.

(145) Laursen, B. W.; Krebs, F. C. *Angewandte Chemie - International Edition* **2000**, *39*, 3432-3434.

(146) Laursen, B. W., Krebs, F. C. *Chemistry - A European Journal* **2001**, *7*, 1773-1783.

(147) Dileesh, S.; Gopidas, K. R. *Journal of Photochemistry and Photobiology A: Chemistry* **2004**, *162*, 115-120.

(148) Thyrhaug, E.; Sørensen, T. J.; Gryczynski, I.; Gryczynski, Z.; Laursen, B. W. *Journal of Physical Chemistry A* **2013**, *117*, 2160-2168.

(149) Maliwal, B. P.; Fudala, R.; Raut, S.; Kokate, R.; Sørensen, T. J.; Laursen, B. W.; Gryczynski, Z.; Gryczynski, I. *PLoS ONE* **2013**, *8*.

(150) Sørensen, T. J.; Thyrhaug, E.; Szabelski, M.; Luchowski, R.; Gryczynski, I.; Gryczynski, Z.; Laursen, B. W. *Methods and Applications in Fluorescence* **2013**, *1*, 025001.

(151) Rich, R. M.; Stankowska, D. L.; Maliwal, B. P.; Sørensen, T. J.; Laursen, B. W.; Krishnamoorthy, R. R.; Gryczynski, Z.; Borejdo, J.; Gryczynski, I.; Fudala, R. *Analytical and Bioanalytical Chemistry* **2013**, *405*, 2065-2075.

(152) Kozlov, A. G.; Lohman, T. M. *Biochemistry* **2002**, *41*, 6032-6044.